Article

Conformational equilibria and intrinsic affinities define integrin activation

Jing Li[1,2,†], Yang Su[1,2,†], Wei Xia[1,2], Yan Qin[1,2], Martin J Humphries[3], Dietmar Vestweber[4], Carlos Cabañas[5] (iD) & Chafen Lu[1,2] & Timothy A Springer[1,2,*] (iD)

Abstract

We show that the three conformational states of integrin $\alpha_5\beta_1$ have discrete free energies and define activation by measuring intrinsic affinities for ligand of each state and the equilibria linking them. The 5,000-fold higher affinity of the extended-open state than the bent-closed and extended-closed states demonstrates profound regulation of affinity. Free energy requirements for activation are defined with protein fragments and intact $\alpha_5\beta_1$. On the surface of K562 cells, $\alpha_5\beta_1$ is 99.8% bent-closed. Stabilization of the bent conformation by integrin transmembrane and cytoplasmic domains must be overcome by cellular energy input to stabilize extension. Following extension, headpiece opening is energetically favored. N-glycans and leg domains in each subunit that connect the ligand-binding head to the membrane repel or crowd one another and regulate conformational equilibria in favor of headpiece opening. The results suggest new principles for regulating signaling in the large class of receptors built from extracellular domains in tandem with single-span transmembrane domains.

Introduction

To quantitatively relate the steps involved in signal transmission across the plasma membrane in cell surface receptors, an understanding of receptor energy landscapes is essential. The gaps in free energy between signal-competent and incompetent receptor conformational states are especially important. However, such understanding is currently limited to receptors with large lipid-embedded domains, such as G protein-coupled receptors and ion channels

(Ruiz & Karpen, 1997; Horrigan *et al*, 1999; Lape *et al*, 2008; Park *et al*, 2008; Cecchini & Changeux, 2015; Manglik *et al*, 2015). Much less is known about receptors that bind ligands through extracellular domains that are in tandem with single-span transmembrane domains, including integrins. Integrins are cell surface receptors that mediate cell-to-cell and cell-to-matrix adhesion. Integrins contain α-subunits and β-subunits that non-covalently associate into αβ heterodimers (Springer & Dustin, 2012) (Fig 1A). The β-propeller domain in α and the βI domain in β associate to form a ligand-binding head, which is linked to leg, transmembrane, and cytoplasmic domains in each subunit.

Integrins undergo large-scale conformational changes (Springer & Dustin, 2012). In the bent-closed (BC) conformation, the integrin ectodomain folds at knees in the α- and β-subunits so that the head and upper legs associate with the lower legs (Fig 1A). In two extended states, the extended-closed (EC) and extended-open (EO) conformations, extension of the α- and β-knees raises the headpiece above the lower legs on cell surfaces (Fig 1A). In transition from EC to EO, that is, headpiece opening, the ligand-binding metal ion-dependent adhesion site (MIDAS) in the β-subunit βI domain rearranges. This reshaping of the ligand-binding site is linked by α-helix pistoning within the βI domain to swing of the hybrid domain away from the integrin α-subunit (Fig 1A). Although the affinities of these states have not yet been measured, previous studies have correlated integrin adhesiveness and high affinity for ligand with the EO conformation (Takagi *et al*, 2002, 2003; Xiao *et al*, 2004; Chen *et al*, 2010; Schürpf & Springer, 2011; Zhu *et al*, 2013). Measurements of affinities on receptors with multiple conformational states yield an average affinity that is weighted according to the population of each conformation in the ensemble (Fig 1C). To understand biological function and its regulation, we need to know the affinity of specific receptor conformational states (intrinsic affinities, K_a), and the equilibrium constants (K_{conf}) linking inactive conformation(s) to active conformation(s). These quantities, to the best of our knowledge, remain undetermined for integrins and the large class of receptors with single-span transmembrane domains. In the absence of measurement of the intrinsic affinities of specific integrin

1 Program in Cellular and Molecular Medicine, Boston Children's Hospital, Boston, MA, USA
2 Department of Biological Chemistry and Molecular Pharmacology, Harvard Medical School, Boston, MA, USA
3 Wellcome Trust Centre for Cell-Matrix Research, University of Manchester, Manchester, UK
4 Max-Planck-Institute of Molecular Biomedicine, Münster, Germany
5 Centro de Biología Molecular Severo Ochoa (CSIC-UAM), and Departamento de Microbiología I, Facultad de Medicina, UCM, Madrid, Spain
*Corresponding author. Tel: +1 617 713 8200; E-mail: timothy.springer@childrens.harvard.edu
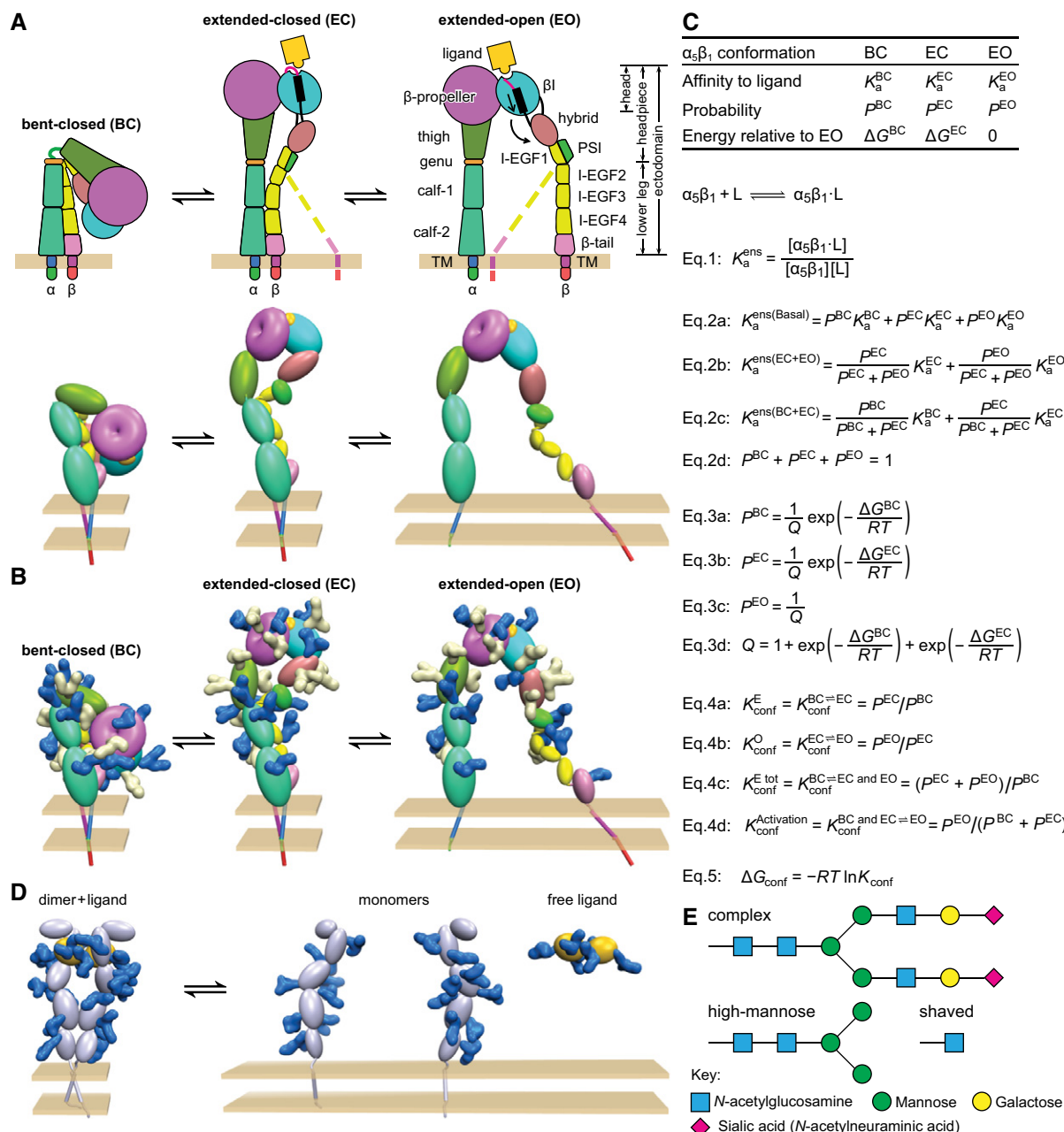†These authors contributed equally to this work

A

bent-closed (BC)   extended-closed (EC)   extended-open (EO)

ligand
β-propeller   βI
thigh   hybrid
genu   I-EGF1   PSI
calf-1   I-EGF2
I-EGF3
calf-2   I-EGF4
β-tail
TM   TM
α β   α β   α   β

head / headpiece / ectodomain / lower leg

B

bent-closed (BC)   extended-closed (EC)   extended-open (EO)

D

dimer+ligand   monomers   free ligand

C

$\alpha_5\beta_1$ conformation	BC	EC	EO
Affinity to ligand	K_a^{BC}	K_a^{EC}	K_a^{EO}
Probability	P^{BC}	P^{EC}	P^{EO}
Energy relative to EO	ΔG^{BC}	ΔG^{EC}	0

$$\alpha_5\beta_1 + L \rightleftharpoons \alpha_5\beta_1 \cdot L$$

Eq.1: $K_a^{ens} = \dfrac{[\alpha_5\beta_1 \cdot L]}{[\alpha_5\beta_1][L]}$

Eq.2a: $K_a^{ens(Basal)} = P^{BC}K_a^{BC} + P^{EC}K_a^{EC} + P^{EO}K_a^{EO}$

Eq.2b: $K_a^{ens(EC+EO)} = \dfrac{P^{EC}}{P^{EC}+P^{EO}}K_a^{EC} + \dfrac{P^{EO}}{P^{EC}+P^{EO}}K_a^{EO}$

Eq.2c: $K_a^{ens(BC+EC)} = \dfrac{P^{BC}}{P^{BC}+P^{EC}}K_a^{BC} + \dfrac{P^{EC}}{P^{BC}+P^{EC}}K_a^{EC}$

Eq.2d: $P^{BC} + P^{EC} + P^{EO} = 1$

Eq.3a: $P^{BC} = \dfrac{1}{Q}\exp\left(-\dfrac{\Delta G^{BC}}{RT}\right)$

Eq.3b: $P^{EC} = \dfrac{1}{Q}\exp\left(-\dfrac{\Delta G^{EC}}{RT}\right)$

Eq.3c: $P^{EO} = \dfrac{1}{Q}$

Eq.3d: $Q = 1 + \exp\left(-\dfrac{\Delta G^{BC}}{RT}\right) + \exp\left(-\dfrac{\Delta G^{EC}}{RT}\right)$

Eq.4a: $K_{conf}^{E} = K_{conf}^{BC \rightleftharpoons EC} = P^{EC}/P^{BC}$

Eq.4b: $K_{conf}^{O} = K_{conf}^{EC \rightleftharpoons EO} = P^{EO}/P^{EC}$

Eq.4c: $K_{conf}^{E\ tot} = K_{conf}^{BC \rightleftharpoons EC\ and\ EO} = (P^{EC}+P^{EO})/P^{BC}$

Eq.4d: $K_{conf}^{Activation} = K_{conf}^{BC\ and\ EC \rightleftharpoons EO} = P^{EO}/(P^{BC}+P^{EC})$

Eq.5: $\Delta G_{conf} = -RT \ln K_{conf}$

E complex

high-mannose   shaved

Key:
■ *N*-acetylglucosamine   ● Mannose   ● Galactose
◆ Sialic acid (*N*-acetylneuraminic acid)

Figure 1. Thermodynamic equilibria of integrin $\alpha_5\beta_1$ and relation to other receptors.

A–C   Integrins. (A) Integrin structure and arrangement of domains in the three overall states of the conformational ensemble (Luo *et al*, 2007), with dashed lines representing the flexibility of the lower β-leg in extended conformations (schematic, upper). In the Pymol representation (lower), structures based on intact, bent-closed integrin $\alpha_V\beta_3$ on the cell surface (Zhu *et al*, 2009), in the same integrin subfamily as $\alpha_5\beta_1$, are shown using an ellipsoid or torus for each extracellular domain. The extended-closed structure is made by rigid body movements at the knees. The extended-open structure is derived from extended-closed by superposition on the open headpiece of $\alpha_{IIb}\beta_3$ (Xiao *et al*, 2004). (B) Identical to (A, lower) except molecular surfaces are shown for N-glycans removed by mutation (Fig 6D–F, white) or not removed (blue). Glycans have the structure shown in (E). Glycans were added at all $\alpha_5\beta_1$ N-glycosylation sequons using $\alpha_5\beta_1$ headpiece structures (Xia & Springer, 2014) and an $\alpha_V\beta_3$ homology model. (C) Equations that describe the affinities and conformational equilibria of integrin ensembles.

D   Representative cytokine or growth factor receptor. The ligand-bound dimer is compact similarly to the bent-closed integrin conformation, whereas the unassociated monomers show no interaction with one another and thus separate from one another similarly to leg domains in the extended-open integrin structure. Therefore, inter-subunit crowding interactions may regulate ligand binding and dimerization in such receptors analogously to regulation of conformational transitions in integrins. Individual domains are shown as ellipses, and N-glycans are shown as blue molecular surfaces using the same chemical structures as in (B).

E   Representative N-glycan structures. The complex glycan is common among $\alpha_5\beta_1$ N-glycans (Sieber *et al*, 2007) and contains the average number of monosaccharide residues per N-glycosylation sequon found here for the complex glycoform of $\alpha_5\beta_1$. The high-mannose glycan contains the average number of monosaccharide residues in the high-mannose form of $\alpha_5\beta_1$. The shaved glycan is that after Endo H digestion; the mass estimated here for shaved $\alpha_5\beta_1$ suggests part of high-mannose glycans are shaved and the remainder are resistant to Endo H.

conformational states, the magnitude of the affinity increase is unknown (Zhu *et al*, 2013; Su *et al*, 2016). In the absence of knowledge of K_{conf}, we do not know which conformations predominate biologically, and how much energy is required to stabilize the active, high affinity state of integrins.

By measuring conformational equilibria here, we have also discovered that previously poorly appreciated components of surface receptors, such as their N-glycans and their leg domains that connect ligand-binding domains to the cell surface, can have important regulatory functions. Integrins, like most other cell surface receptors, are heavily glycosylated (Fig 1B). Glycans serve a variety of structural and functional roles (Stowell *et al*, 2015), but a compelling function is lacking in most receptors. The significance of the great variation in number of N-linked glycosylation sites among integrin subunits, ranging from 5 to 26 sites among the 18 human α-subunits and from 5 to 12 sites among the eight human β-subunits, is currently unknown. Moreover, during cell differentiation or transition from stasis to proliferation, alterations in glycosyl transferases cause substantial changes in N- and O-linked glycan processing, that is, in glycan branching and the number and nature of the monosaccharide residues in the glycan. Nonetheless, whether N-glycosylation regulates signaling by altering the equilibria between inactive and active receptor conformational states has been unknown.

Activation models in the integrin field have previously been discussed conceptually but not quantitatively. All integrin β-subunit cytoplasmic domains contain motifs that associate with cytoskeletal proteins. The β_1-subunit, among six of the eight mammalian integrin β-subunits, has binding sites for talins and kindlins, which link to the actin cytoskeleton (Calderwood *et al*, 2013). By an incompletely characterized process termed inside-out signaling, coupling through talin and kindlin to the actin cytoskeleton stabilizes the high affinity state of integrins (Springer & Dustin, 2012). In contrast, other proteins bind to integrin cytoplasmic domains and stabilize them in the inactive state (Bouvard *et al*, 2013). To quantitatively relate the steps involved in signal transmission across the plasma membrane in surface receptors, an understanding of the energy landscapes of their conformational ensembles is essential. The energy landscape, which dictates the fractional population of signaling competent and incompetent states of receptors on cell surfaces (Fig 1C), provides fundamental information including how much cellular energy is needed for integrin activation.

We use in our studies the model integrin $\alpha_5\beta_1$, a receptor for fibronectin that contributes to the assembly of fibronectin into fibrils (Schwarzbauer & DeSimone, 2011). Within fibronectin, $\alpha_5\beta_1$ recognizes an Arg-Gly-Asp (RGD) motif in a flexible loop in Fn3 domain 10 and a synergy site in Fn3 domain 9. We use allosteric, conformation-specific antibodies to convert the three overall conformational states basally present in the $\alpha_5\beta_1$ integrin ensemble into either one or two defined states. Measurements of the ligand-binding affinities of these ensembles enable calculation of intrinsic affinities and free energies of each state for both purified $\alpha_5\beta_1$ fragments and intact $\alpha_5\beta_1$ on cell surfaces. Antibodies that were originally selected to inhibit, activate, or report the activation status of the 12 different β_1 integrin αβ heterodimers are essential tools in this work (Byron *et al*, 2009; Su *et al*, 2016). Electron microscopy (EM) and functional comparisons among these antibodies have defined the $\alpha_5\beta_1$ conformational state(s) that they stabilize (Su *et al*, 2016).

Definition here of the energy landscape for a receptor with tandem extracellular, single-span transmembrane, and cytoplasmic domains reveals many features not previously anticipated.

Results

Principles for saturable stabilization of defined conformational states

Here, we describe the fluorescence polarization (FP) assay used in much of this work, and the methods required to establish that the measurements reflect values for the desired conformational states. FP is a rigorous, highly reproducible method for measuring binding of small fluorescent ligands to larger partners based on slowed tumbling and increased FP of the ligand-partner complex (Rossi & Taylor, 2011). Using fixed concentrations of integrin and fluorescein isothiocyanate (FITC)-labeled cyclic RGD peptide (cRGD) (Koivunen *et al*, 1995; Xia & Springer, 2014) and titrating in Fabs, we measured the ability of Fabs to increase or decrease ligand binding by altering integrin affinity for cRGD. We used Fabs (Fig 2A) to exclude complications from cross-linking by IgGs. Fab titrations showed that plateau values of FP were reached, reflecting saturable population of the desired conformations in the ensemble, and enabled calculation of Fab EC_{50} values (Fig 2B). The results were concordant with the effect of Fabs on $\alpha_5\beta_1$ conformation visualized by EM and on cell adhesion (Su *et al*, 2016). 12G10, HUTS4, and TS2/16 Fabs to β_1 increased FP to similarly high plateau values of 0.21–0.22 (Fig 2B), correlating with their stabilization of the open conformation of the βI domain (TS2/16) or the open conformation of the entire headpiece (12G10 and HUTS4) (Su *et al*, 2016). 8E3, 9EG7, and N29 Fabs to β_1 and SNAKA51 Fab to α_5 increased FP to lower plateau values of 0.14–0.16, consistent with the finding that they stabilize the extended conformation of $\alpha_5\beta_1$ and hence stabilize the EC and EO states (Su *et al*, 2016). In contrast, two inhibitory Fabs, SG/19 and mAb13, decreased FP from 0.12 to plateau values of 0.09 (Fig 2B), in agreement with findings that they stabilize the closed conformation of the headpiece and hence stabilize the BC and EC states (Su *et al*, 2016).

To saturarly populate desired conformations, Fabs must be used well above their EC_{50} values; furthermore, experimental design must take into account the principle that EC_{50} values are dependent on the population of the states in the pre-existing ensemble. We illustrate this by comparing EC_{50} values in Mg^{2+} to those in the presence of the integrin activator Mn^{2+} (Fig 2C). The higher FP basal values in Mn^{2+} (0.22) than in Mg^{2+} (0.12) suggested a higher proportion of the high affinity, EO state of $\alpha_5\beta_1$ in the conformational ensemble. Consistent with this higher proportion of the EO state in Mn^{2+}, EC_{50} values for the HUTS4 Fab specific for the EO state and 8E3 Fab specific for the EC and EO states were lower than in Mg^{2+}. Conversely, consistent with the lower proportion of the BC and EC states in Mn^{2+}, the EC_{50} value for SG/19 Fab specific for the EC and BC states was higher than in Mg^{2+} (Fig 2C). Accordingly, we have measured Fab EC_{50} values for each type of $\alpha_5\beta_1$ preparation studied in the experiments in this paper (Fig 2, and Appendix Fig S1 and Appendix Table S1). In all experiments, Fabs are used at concentrations well above their EC_{50}, such that the population of the state(s) they stabilize approaches 100% and apparent affinity
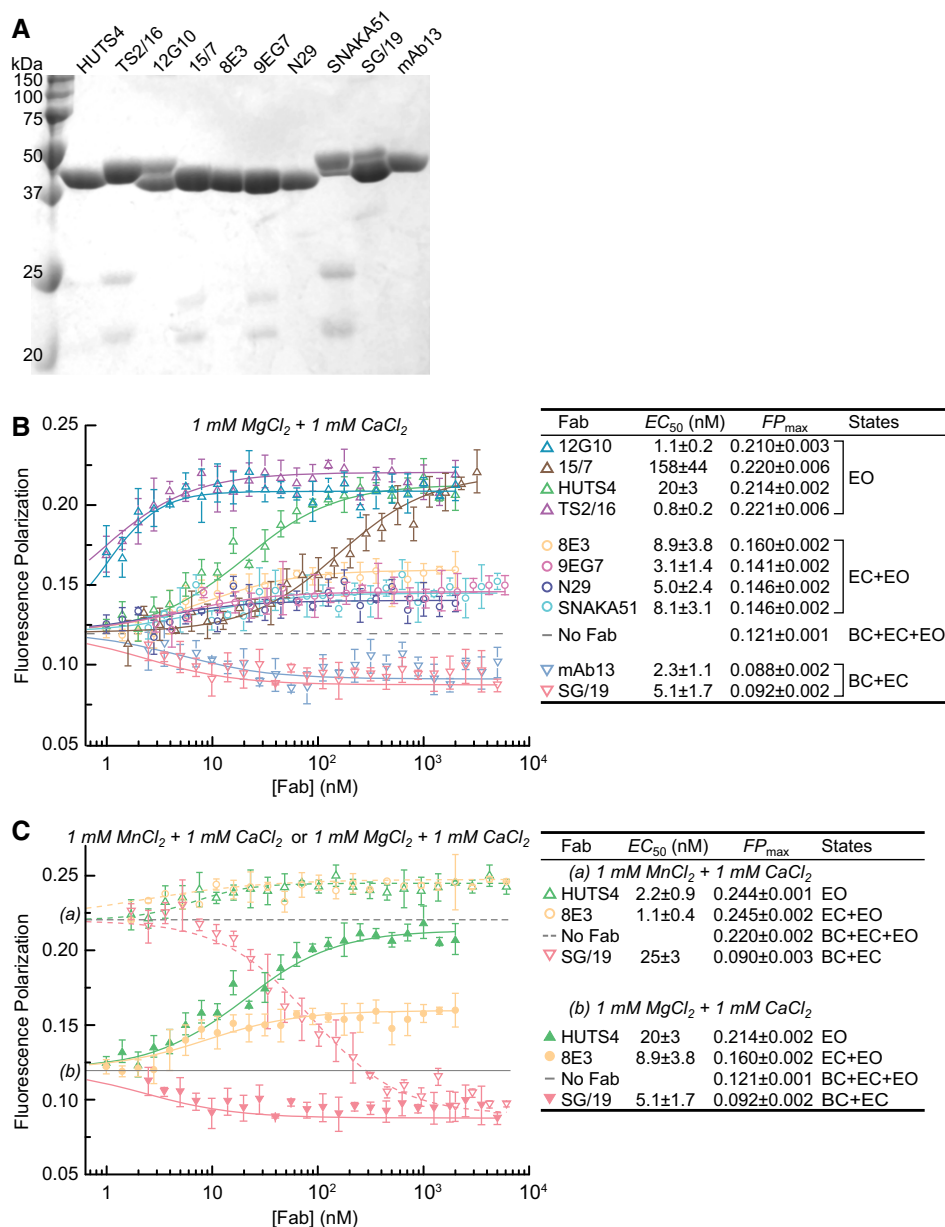
Figure 2.   Influence of conformation-selective Fabs and metal ions on ligand binding by the $\alpha_5\beta_1$ ectodomain.

A   Coomassie-stained, non-reducing SDS 12.5% PAGE of Fabs.

B, C   Dependence of unclasped, high-mannose $\alpha_5\beta_1$ ectodomain (20 nM) binding to FITC-cRGD (5 nM) in FP assays on Fab concentration in 1 mM Mg^{2+} & 1 mM Ca^{2+} (B) and in 1 mM Mg^{2+} & 1 mM Ca^{2+} compared to 1 mM Mn^{2+} & 1 mM Ca^{2+} (C). Values to the right of each plot are from nonlinear least square fits to Appendix Equation S1 (mean $\pm$ s.d. of triplicates).

(K_d^{app}) approaches true ensemble affinity (K_d^{ens}) (Appendix Table S1 and Appendix Fig S2).

A correction is required for measurements with Fabs that stabilize the closed conformations, because even a small amount of the much higher affinity open conformation makes a substantial contribution to measured apparent affinities. For these conditions, Fab K_d values or Fab EC_{50} values measured under conditions where they closely approximate K_d are used to convert measured K_d^{app} values to K_d^{ens} values (Appendix Figs S1 and S2, Appendix Table S1 and Appendix Equations S47–S55).

Finally, we evaluated the assumption that the intrinsic affinities of Fab-bound states measured here are close to the intrinsic affinity of that state in the absence of Fab. We tested a corollary: if Fabs stabilize states distinct from those in the absence of Fab, then states stabilized by distinct Fabs should also differ in ligand-binding affinity from one another. We therefore began our studies with an integrin ectodomain preparation in which ensembles containing the closed (BC+EC), extended (EC+EO), and EO conformations were well separated in affinity, enabling us to test the assumption that Fabs that stabilize the same states should give similar integrin

ligand-binding affinities. The $\alpha_5\beta_1$ ectodomain was purified from cells that secrete glycoproteins with high-mannose N-glycans. A clasp between the C-termini of the α_5 and β_1-subunits that facilitated high expression was proteolytically cleaved to yield the unclasped, high-mannose $\alpha_5\beta_1$ ectodomain. We used FP with a fixed concentration of FITC-cRGD in the absence or presence of Fabs at concentrations well above their EC_{50} values and measured integrin ligand-binding affinity by titrating in the integrin. The affinity for cRGD of the basal $\alpha_5\beta_1$ ensemble in the absence of Fab, that is, $K_d^{ens(Basal)}$, the population-weighted average affinity of all three states as shown in Eq. 2a in Fig 1C, was 47 nM (Fig 3A). Note that for concision, we use association constant K_a in equations and dissociation constant $K_d = 1/K_a$ for reporting affinities. The affinity intrinsic to the EO conformation was $K_d^{EO} = 2.0–2.6$ nM, measured in the presence of open-stabilizing Fabs TS2/16, 12G10, or HUTS4 (Fig 3A). The affinity intrinsic to the EC conformation was $K_d^{EC} = 6,500–9,200$ nM, measured in the presence of two sets of mutually compatible extension-stabilizing and closure-stabilizing Fabs (Su *et al*, 2016), SNAKA51 plus SG/19, or 9EG7 plus mAb13 (Fig 3A). The affinity of the ensemble comprising the two extended conformations, EC and EO (Eq. 2b in Fig 1C), was $K_d^{ens(EC+EO)} = 15–22$ nM (Fig 3A), measured in the presence of extension-stabilizing Fabs 8E3, N29, 9EG7, or SNAKA51. The affinity of an ensemble comprising the two closed conformations, BC and EC (Eq. 2c in Fig 1C), was $K_d^{ens(BC+EC)} = 4,600–9,400$ nM, measured in the presence of closure-stabilizing Fab SG/19 or mAb13 (Fig 3A). The similar affinities measured with independent Fabs stabilizing the same state, compared to the distinct affinities measured for the EO state, the closed states, and the extended states, support the assumption that these Fab-stabilized states are similar to the native states.

Affinities for cRGD in the absence or presence of Fabs were independently measured with the $\alpha_5\beta_1$ headpiece, which lacks the lower legs of the ectodomain (Fig 1A). $K_d^{ens(Basal)}$ was almost 100-fold lower for the headpiece than the ectodomain (Fig 3A and B). Nonetheless, the intrinsic affinity of the open headpiece, $K_d^O = 1.9 \pm 0.3$ nM (Fig 3B), was very similar to that of the extended-open ectodomain, $K_d^{EO} = 2.0–2.6$ nM (Fig 3A). The affinity of the closed headpiece, $K_d^C = 8,500–9,600$ nM, with SG/19 and mAb13 Fabs (Fig 3B) was in agreement with the lower estimate of 9,400 nM for closed ectodomain conformations (Fig 3A). Because
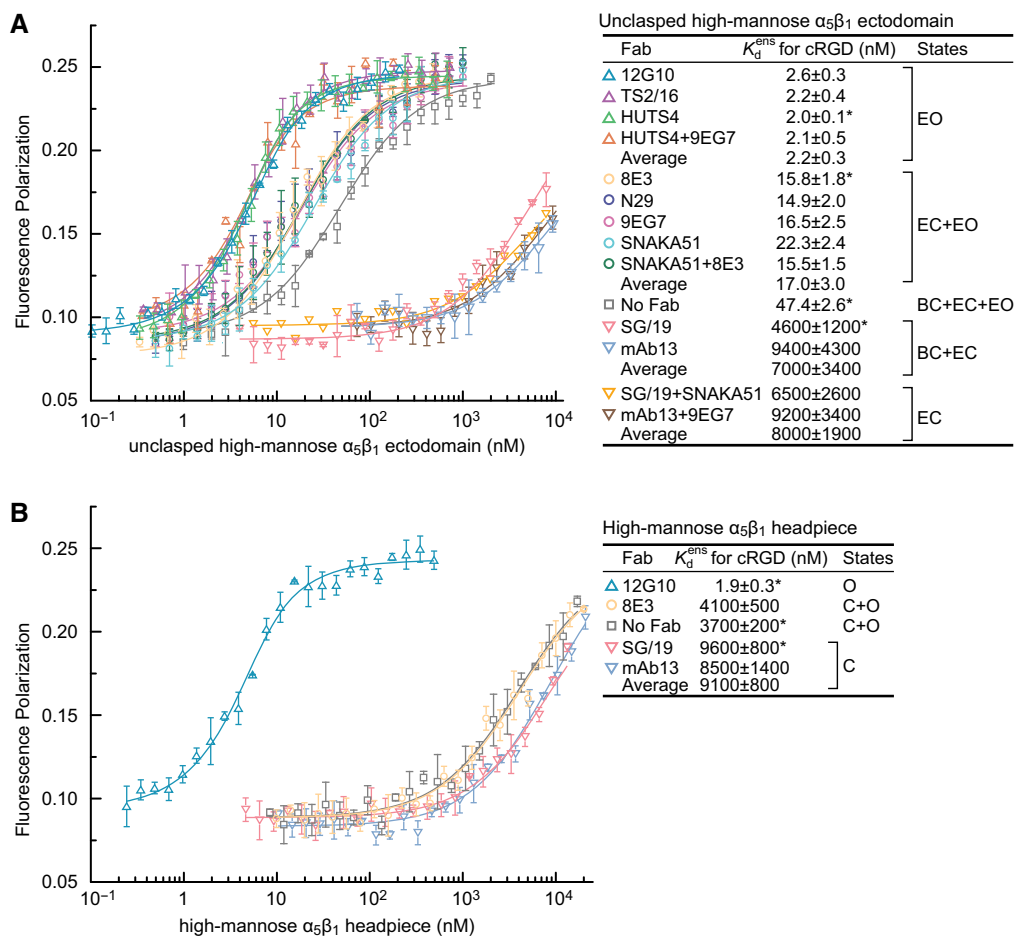

Figure 3. Intrinsic and ensemble affinities of $\alpha_5\beta_1$ ectodomain and headpiece preparations for cRGD.

A, B   Affinities of high-mannose glycoforms of the unclasped $\alpha_5\beta_1$ ectodomain (A) and headpiece (B) were measured using FP with FITC-cRGD in the presence of the indicated Fabs. Errors in the plotted datapoints are s.d. from average value of triplicate measurements. Errors for affinities in the inset table are s.d. from nonlinear least square fits of the average values from the triplicate measurements except values with "*" are s.d. from three experiments on different days.

the lower α- and β-legs are absent in the headpiece, Fabs that bind to the upper β-leg and stabilize extension (Fig 1A) should have no effect on headpiece affinity for ligand. Indeed, binding of extension-stabilizing Fab 8E3 to the PSI domain resulted in no change in headpiece affinity for cRGD (Fig 3B) in contrast to the threefold increase in affinity with the ectodomain (Fig 3A), even though 8E3 binds well to the headpiece as shown with ITC (Appendix Fig S3A).

Independent ligands and the free energy of each conformational state

Having established the validity of our use of conformation-specific Fabs to measure the properties of specific integrin conformational states, we went on to test further concepts and examine the molecular features that regulate integrin affinity and conformational equilibria. Distinct ligands are expected to have distinct affinities intrinsic to each integrin conformational state; however, the free energies of these states should be identical, if the ligands indeed bind to the same conformational states. We tested these ideas with two more ligands of $\alpha_5\beta_1$, the peptide GRGDSPK (RGD) and a fragment of fibronectin containing Fn3 domains 9 and 10 ($Fn3_{9-10}$). FP measurements with FITC-RGD showed K_d^{EO} of 71 nM, $K_d^{ens(EC+EO)}$ of 620 nM, and $K_d^{ens(Basal)}$ of 2,300 nM (Fig 4A). ITC measurements with RGD peptide showed K_d^{EO} of 68 nM and $K_d^{ens(Basal)}$ of 2,100 nM (Appendix Fig S3B and C). This excellent agreement in affinity between FP for FITC-RGD and ITC for RGD is more than sufficient to validate the energy landscape conclusions below. $Fn3_{9-10}$ affinity for $\alpha_5\beta_1$ was measured by competing FITC-cRGD binding in FP (Fig 4B and C). $Fn3_{9-10}$ showed K_d^{EO} of 0.44 nM, $K_d^{ens(EC+EO)}$ of 2.0 nM, $K_d^{ens(Basal)}$ of 5.2 nM, $K_d^{ens(BC+EC)}$ of 2,900 nM, and K_d^{EC} of 2,700 nM (Fig 4B–D). These measurements, and those in Fig 3, suggest that K_d^{EC} and $K_d^{ens(BC+EC)}$ are indistinguishable from one another, and by extension, that K_d^{EC} and K_d^{BC} are indistinguishable.

The population of each conformational state in the basal ensemble was calculated from $K_d^{ens(Basal)}$, $K_d^{ens(BC+EC)}$, $K_d^{ens(EC+EO)}$, and K_d^{EO} (Eq. 2a–d in Fig 1C) and was insensitive to the relatively large uncertainty in $K_d^{ens(BC+EC)}$ (Appendix Fig S2B). The population of each conformational state relates through the Boltzmann distribution to the relative free energy of each state and was thus used to calculate ΔG (Eq. 3a–d in Fig 1C). For each $\alpha_5\beta_1$ preparation, EO is used as the reference state ($\Delta G^{EO} = 0$). Despite use of three ligands varying more than 100-fold in affinity, saturation binding with cRGD and RGD, as well as competition with $Fn3_{9-10}$, yielded ΔG values that were within experimental error of one another, demonstrating the robustness of the results (Fig 4D and E). With all three ligands, the BC state was lowest in energy, and the EC state was intermediate in energy between the BC and EO states. The most accurately determined values, with cRGD, showed $\Delta G^{BC} = -1.5 \pm 0.1$ kcal/mol and $\Delta G^{EC} = -1.1 \pm 0.1$ kcal/mol with $\Delta G^{EO} = 0$ kcal/mol (Fig 4D and E).

Population of each conformational state also defined the conformational equilibria (K_{conf}) between the states (Eq. 4a–d in Fig 1C) and enabled calculation of the free energies associated with integrin conformational change (ΔG_{conf}) (Eq. 5 in Fig 1C). Thus, the extension step from BC to EC costs 0.4 kcal/mol (ΔG_{conf}^E) and the opening step from EC to EO costs 1.1 kcal/mol (ΔG_{conf}^O) (Fig 4D). Interconversion among the three integrin states does not necessarily happen

in a defined order (Takagi et al, 2002; Sen et al, 2013) (Movies EV1–EV3) and thus may also be conceptualized as interchange between one state and two other states. Thus, we may also consider extension as occurring from BC to either EC or EO (K_{conf}^{Etot} and ΔG_{conf}^{Etot}, Eq. 4c in Fig 1C). ΔG_{conf}^{Etot} (0.3 kcal/mol) was similar to ΔG_{conf}^E (0.4 kcal/mol) for unclasped, high-mannose $\alpha_5\beta_1$ (Fig 4D). Similarly, we may define $K_{conf}^{Actiation}$ and $\Delta G_{conf}^{Activation}$ for conversion from either BC or EC to EO (Eq. 4d in Figs 1C and 4D).
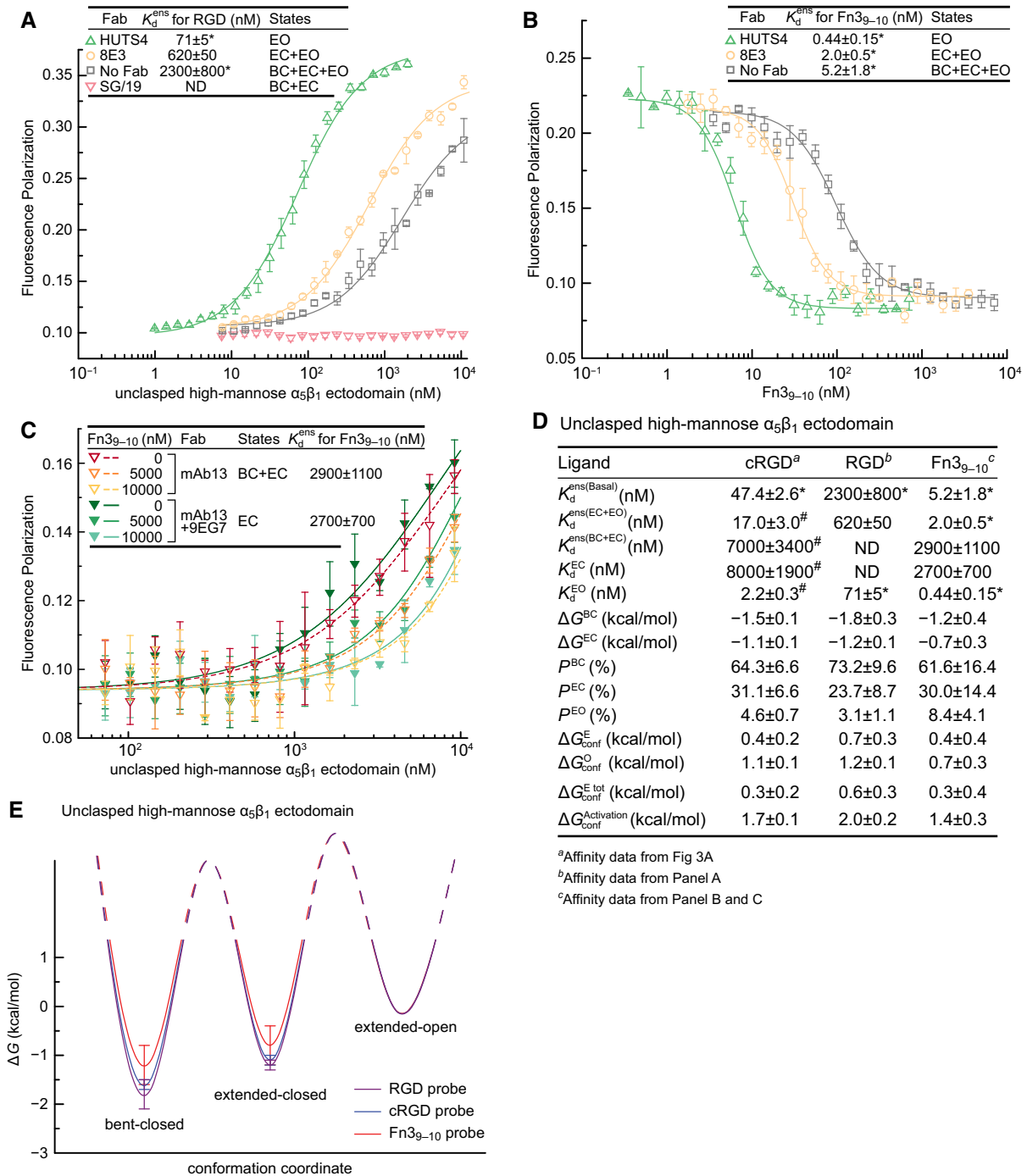
Regulation of conformational equilibria by C-terminal clasp and N-glycosylation

We next examined molecular features that regulate the populations (and relative free energies) of the three overall integrin conformational states. The C-termini of the integrin α- and β-subunit ectodomains are close to one another in bent ectodomain crystal structures and are followed in sequence by the α- and β-subunit transmembrane (TM) domains that associate with one another. Complementary α-helical sequences appended to the α and β ectodomains that associate as coiled-coils are frequently used to clasp the C-termini together in this region. The clasp can be released (unclasped) by protease digestion at a specific site included in the linker between the ectodomain and coiled-coils. EM of distinct integrin αβ heterodimers has shown that the clasp increases the proportion of particles in the bent conformation relative to extended conformations (Takagi et al, 2002; Nishida et al, 2006; Springer & Dustin, 2012).

We also tested whether N-glycans regulated integrin conformational equilibria by comparing $\alpha_5\beta_1$ with native, that is, complex N-glycans (Sieber et al, 2007), high-mannose N-glycans, and shaved N-glycans. Shaving with endoglycosidase H of integrins with high-mannose N-glycans leaves only a single monosaccharide residue attached to N-glycosylation sites, except for a minority of inaccessible sites (Xie et al, 2010). Testing clasped and unclasped $\alpha_5\beta_1$ ectodomains each with three types of N-glycans (Fig 5A), we obtained six cRGD binding datasets (Appendix Fig S4A–F) enabling intrinsic affinity and ΔG value determinations (Fig 5B and C) that are discussed as a whole.

The $K_d^{ens(Basal)}$ of the six preparations ranged from 12 to 200 nM, showing profound regulation of ensemble affinity by the clasp and N-glycans (Fig 5B). In contrast, the intrinsic affinities of the extended-open conformations in each preparation were very similar, with an average value of 2.4 nM (Fig 5B). Additionally, the affinities of the closed conformations, $K_d^{ens(BC+EC)}$, of each of the six preparations were similar to one another with an average value of 4,700 nM (Fig 5B). In agreement with the intrinsic affinities measured for headpiece and ectodomain constructs above, these results show that intrinsic affinities are properties of the ligand-binding site of specific integrin conformations and are influenced little, at least for peptide ligand and macromolecule fragments, by decorations at N-glycosylation sites or the distal clasp restraint.

The C-terminal clasp lowered $K_d^{ens(Basal)}$ of each integrin glycoform by several fold. The clasp markedly increased ΔG_{conf}^E by 1.1–1.5 kcal/mol (Fig 5B), showing that proximity of the α- and β-subunit C-termini as observed in bent ectodomain crystal structures indeed stabilizes the bent conformation. In contrast, the clasp had no consistent effect on the energy of headpiece opening (ΔG_{conf}^O, Fig 5B).

Figure 4. Intrinsic affinities and conformational equilibria of $\alpha_5\beta_1$ with three different ligands.

Data are for the unclasped, high-mannose $\alpha_5\beta_1$ ectodomain using the indicated Fabs.

A   Affinity for FITC-RGD measured with FP.

B   Affinity for Fn3$_{9-10}$ measured by inhibition of FITC-cRGD binding to 20 nM $\alpha_5\beta_1$ (with open-stabilizing Fab), 90 nM $\alpha_5\beta_1$ (with extension-stabilizing Fab), or 270 nM $\alpha_5\beta_1$ (with no Fab).

C   Affinity for Fn3$_{9-10}$ measured by inhibition of FITC-cRGD binding to a range of $\alpha_5\beta_1$ concentrations (with closure-stabilizing Fab) at three Fn3$_{9-10}$ concentrations.

D   Tabulation of results.

E   Energy landscape plots showing valleys for the ΔG values determined here as lines, and hills for the transition state ΔG values, which remain to be determined, as dashed lines.

Data information: (A–E) Errors in the plotted datapoints are s.d. from the average value of triplicate measurements. Errors in the affinity values are s.d. from nonlinear least square fits of the average value of triplicate measurements except values with "*" are s.d. from three experiments on different days and values with "#" represent s.d. of measurements with distinct Fabs stabilizing the same conformation. Errors for P and ΔG values are propagated from affinities values as described in the Materials and Methods.
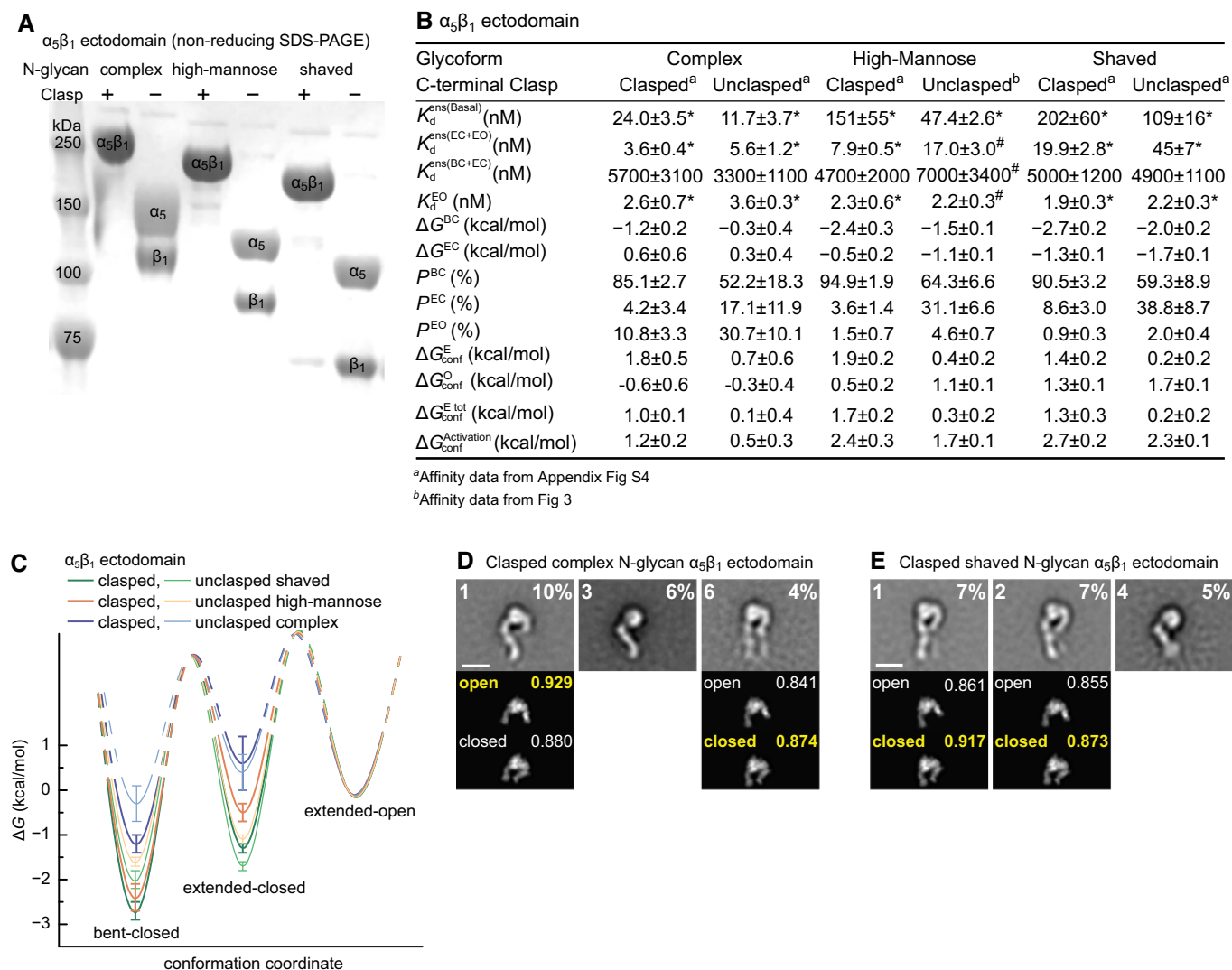
A

α$_5$β$_1$ ectodomain (non-reducing SDS–PAGE)

B α$_5$β$_1$ ectodomain

Glycoform	Complex		High-Mannose		Shaved	
C-terminal Clasp	Clasped[a]	Unclasped[a]	Clasped[a]	Unclasped[b]	Clasped[a]	Unclasped[a]
$K_d^{ens(Basal)}$ (nM)	24.0±3.5*	11.7±3.7*	151±55*	47.4±2.6*	202±60*	109±16*
$K_d^{ens(EC+EO)}$ (nM)	3.6±0.4*	5.6±1.2*	7.9±0.5*	17.0±3.0#	19.9±2.8*	45±7*
$K_d^{ens(BC+EC)}$ (nM)	5700±3100	3300±1100	4700±2000	7000±3400#	5000±1200	4900±1100
K_d^{EO} (nM)	2.6±0.7*	3.6±0.3*	2.3±0.6*	2.2±0.3#	1.9±0.3*	2.2±0.3*
ΔG^{BC} (kcal/mol)	−1.2±0.2	−0.3±0.4	−2.4±0.3	−1.5±0.1	−2.7±0.2	−2.0±0.2
ΔG^{EC} (kcal/mol)	0.6±0.6	0.3±0.4	−0.5±0.2	−1.1±0.1	−1.3±0.1	−1.7±0.1
P^{BC} (%)	85.1±2.7	52.2±18.3	94.9±1.9	64.3±6.6	90.5±3.2	59.3±8.9
P^{EC} (%)	4.2±3.4	17.1±11.9	3.6±1.4	31.1±6.6	8.6±3.0	38.8±8.7
P^{EO} (%)	10.8±3.3	30.7±10.1	1.5±0.7	4.6±0.7	0.9±0.3	2.0±0.4
ΔG_{conf}^{E} (kcal/mol)	1.8±0.5	0.7±0.6	1.9±0.2	0.4±0.2	1.4±0.2	0.2±0.2
ΔG_{conf}^{O} (kcal/mol)	-0.6±0.6	−0.3±0.4	0.5±0.2	1.1±0.1	1.3±0.1	1.7±0.1
$\Delta G_{conf}^{E\,tot}$ (kcal/mol)	1.0±0.1	0.1±0.4	1.7±0.2	0.3±0.2	1.3±0.3	0.2±0.2
$\Delta G_{conf}^{Activation}$ (kcal/mol)	1.2±0.2	0.5±0.3	2.4±0.3	1.7±0.1	2.7±0.2	2.3±0.1

[a]Affinity data from Appendix Fig S4
[b]Affinity data from Fig 3

C

α$_5$β$_1$ ectodomain

D Clasped complex N-glycan α$_5$β$_1$ ectodomain

E Clasped shaved N-glycan α$_5$β$_1$ ectodomain

Figure 5. Glycoform and C-terminal clasp regulate α$_5$β$_1$ ectodomain conformational equilibria and have little effect on intrinsic affinities.

A   SDS 7.5% PAGE of three α$_5$β$_1$ ectodomain glycoforms with or without C-terminal clasp stained with Coomassie blue.

B, C   Tabulation of results (B) and energy landscape plots (C). See Appendix Fig S4 for representative FP results. Error definitions and explanations of values marked with "*" and "#" are as in the Fig 4 legend.

D, E   Effect of complex (D) and shaved (E) N-glycans on clasped α$_5$β$_1$ ectodomain conformation in EM. Representative, well-resolved class averages are shown together with their rank among 35 class averages and the % of total particles in that class (inset, upper left and right, respectively). Below each *en face* class average are the best cross-correlating projections of open and closed headpiece crystal structures to the headpiece portion of the EM class average. Insets show correlation coefficients with the best correlating conformation in yellow. Scale bars are 10 nm. All class averages are shown in Appendix Fig S6.

N-linked glycoform type has a large influence on integrin α$_5$ and β$_1$-subunit migration in SDS–PAGE (Fig 5A). Multi-angle light scattering showed that complex, high-mannose, and shaved α$_5$β$_1$ ectodomain glycoprotein preparations are 21, 11, and 3% carbohydrate by mass, respectively (Appendix Fig S5). Moreover, N-glycoform has a surprisingly strong influence on conformational equilibria; free energies of the bent-closed and extended-closed conformations increase markedly with increasing % carbohydrate (Fig 5B). Compared to shaved N-glycans, complex N-glycans raised ΔG^{BC} by 1.5 kcal/mol for the clasped ectodomain and 1.7 kcal/mol for the unclasped ectodomain. Complex N-glycans also raised ΔG^{EC} by 1.9 kcal/mol (clasped) or 2.0 kcal/mol (unclasped) (Fig 5B). Remarkably, complex glycans reverse the relative stabilities of the two extended states so that the extended-open conformation is more stable than the extended-closed conformation (Fig 5C).

In negative stain EM, the high-mannose, clasped α$_5$β$_1$ ectodomain shows bent and extended-closed conformations (Su *et al*, 2016). Our findings on glycoforms led us to also examine the conformations of clasped α$_5$β$_1$ ectodomains with shaved and complex N-glycans (Fig 5D and E, and Appendix Fig S6). Both glycoforms exhibited bent and extended-closed α$_5$β$_1$ conformations; however, only α$_5$β$_1$ with complex N-glycans exhibited the extended-open conformation (Appendix Fig S5). Furthermore, the most populous class average of the clasped α$_5$β$_1$ ectodomain with complex N-glycans, representing 10% of all particles,

showed the extended-open conformation (Fig 5D panel 1). These EM results strongly support thermodynamic findings here that glycoforms regulate conformational equilibria and that complex N-glycans stabilize the EO state relative to the BC and EC states.

Regulation of conformational equilibria by integrin lower legs and the number of N-linked glycosylation sites

Why would the presence of the lower legs in the integrin ectodomain raise ensemble affinity for ligand by stabilizing the open headpiece as shown above in Fig 3? We tested the hypothesis that crowding or repulsive interactions between the lower legs would favor the greater separation between the knees that is present in the open compared to the closed conformation (Fig 1A and B). Integrin $\alpha_5\beta_1$ containing the lower leg of the β_1-subunit and not that of the α_5-subunit was well expressed and behaved during purification (Fig 6A). The $K_d^{ens(Basal)}$ of this semi-truncated integrin was identical to that of the headpiece, much lower than that of the ectodomain, and not affected by extension-stabilizing Fab (Fig 6B and C). Moreover, headpiece opening required 3.6 kcal/mol more energy for the semi-truncated ectodomain and headpiece constructs than for the unclasped ectodomain (Fig 6C).

The favoring of headpiece opening by increasing mass of N-glycans (Fig 5) might also suggest a role for crowding or repulsive interactions by glycans within the ectodomain. To test the corollary that the number of N-linked sites would similarly regulate headpiece opening, we mutated individual N-linked glycosylation sites in the integrin α_5 and β_1-subunits. N-linked site mutations were tested individually, and those with the least effect on $\alpha_5\beta_1$ expression were combined to create ΔN-α_5 with 6 of 14 N-linked sites removed and ΔN-β_1 with 5 of 12 sites removed. We then selected cell lines secreting all three possible combinations of mutant subunits with complex glycosylation (Fig 6D). $K_d^{ens(Basal)}$ of the ΔN-α_5/ΔN-β_1 mutant was decreased threefold, whereas the ΔN-α_5/β_1 and α_5/ΔN-β_1 heterodimers showed intermediate decreases in affinity, as predicted by the crowding/repulsion hypothesis (Fig 6E and Appendix Fig S4G–I). Nonetheless, the intrinsic affinities of the extended-open conformation K_d^{EO} stayed unchanged (Fig 6E and Appendix Fig S4). The bent-closed and extended-closed states were each stabilized by 0.8 kcal/mol in ΔN-α_5/ΔN-β_1 relative to wild-type $\alpha_5\beta_1$ (Fig 6E and F).

Conformational equilibria of cell surface $\alpha_5\beta_1$

We extended our measurements of affinities and conformational equilibria to native $\alpha_5\beta_1$ on the erythroleukemic cell line K562,

which expresses 200,000 $\alpha_5\beta_1$ molecules/cell (Faull *et al*, 1993), minimal levels of other integrin α-subunits (Appendix Fig S7), and is completely dependent on integrin $\alpha_5\beta_1$ for adhesion to fibronectin (Tsuchida *et al*, 1997). Saturation binding of Alexa488-labeled Fn3$_{9–10}$ to K562 cells was measured by fluorescence flow cytometry with no washing (Chigaev *et al*, 2001; Dong *et al*, 2014). Extension-stabilizing and open-stabilizing Fabs greatly increased Fn3$_{9–10}$ binding to K562 cells (Fig 7A). $K_d^{ens(EC+EO)}$ was 1.9–2.1 nM, and K_d^{EO} was 1.3–1.4 nM (Fig 7B), not far from values measured for the $\alpha_5\beta_1$ ectodomain in solution (Fig 4B). $K_d^{ens(Basal)}$ of K562 cells for Fn3$_{9–10}$ was too low to be measured by Alexa488-Fn3$_{9–10}$ saturation binding (Fig 7B). Therefore, we measured binding of Fn3$_{9–10}$ to K562 cells by enhancement of binding of open-stabilizing Alexa488-12G10 Fab, which yielded $K_d^{ens(Basal)}$ of 1,100 nM (Fig 7C).

Jurkat T lymphoblastoid cells express about eightfold less $\alpha_5\beta_1$ than K562 cells and higher levels of other β_1 integrins (Appendix Fig S8). Using the same methods as for K562 cells, we measured $\alpha_5\beta_1$-dependent binding affinities of Fn3$_{9–10}$ for Jurkat cells as $K_d^{ens(Basal)}$ = 750 ± 60 nM, $K_d^{ens(EC+EO)}$ = 1.7 ± 0.2 nM, and $K_d^{ens(EO)}$ = 1.6 ± 0.2 nM (Appendix Fig S8 and Fig 7E).

As a third, independent means of measuring the energy landscape of $\alpha_5\beta_1$ conformational states on cell surfaces, we measured the affinity of Alexa488-12G10 Fab for K562 cells. Use of 9EG7 Fab plus Fn3$_{9–10}$ to stabilize the extended-open conformation, or 9EG7 Fab plus SNAKA51 Fab to stabilize the ensemble with the two extended conformations, gave 12G10 Fab affinities of 0.4 and 0.7 nM, respectively (Fig 7D). In strong contrast, the affinity of 12G10 Fab for the basal ensemble of three states was 205 nM (Fig 7D).

The datasets on Fn3$_{9–10}$ and 12G10 Fab binding to K562 cells yield free energies of $\alpha_5\beta_1$ conformational states that are within experimental error of one another and similar to those on Jurkat cells (Fig 7E and F). On the cell surface, the BC state has a low free energy. ΔG^{BC} is −4.0 to −3.6 kcal/mol (Fig 7E). Thus, 99.7–99.8% of cell surface $\alpha_5\beta_1$ is in the bent-closed conformation. In contrast, the EC conformation is slightly higher in energy than the EO conformation, by 0.3–0.5 kcal/mol on K562 cells where it was much more accurately determined than on Jurkat cells. Thus, once $\alpha_5\beta_1$ extends on cell surfaces, it will predominantly populate the extended-open conformation, as found for the $\alpha_5\beta_1$ ectodomain with complex N-glycans with or without a clasp (Fig 5B). However, the bent-closed conformation is much more stable on cell surfaces than in clasped ectodomains (Fig 7F). Thus, the transmembrane and cytoplasmic domains of $\alpha_5\beta_1$, in the context of the plasma membrane and cytoplasmic environment, stabilize the bent-closed conformation much more than a coiled-coil clasp (Fig 7F and G).

Figure 6. Regulation of $\alpha_5\beta_1$ conformational equilibria by the lower legs and N-glycans.

A–C   The semi-truncated $\alpha_5\beta_1$ ectodomain. (A) Coomassie-stained SDS 7.5% PAGE. (B) Affinity of FITC-cRGD for the semi-truncated, high-mannose $\alpha_5\beta_1$ ectodomain in the presence of the indicated Fabs measured with FP. (C) Comparison of the semi-truncated ectodomain to the unclasped $\alpha_5\beta_1$ ectodomain and headpiece, all with high-mannose glycans.

D–F   Effect of N-glycosylation sequon mutation. The ΔN-α_5 and ΔN-β_1 mutants have 6 of 14 and 5 of 12 predicted N-glycosylation sites mutated, respectively. The indicated mutants were tested in the clasped $\alpha_5\beta_1$ ectodomain with complex N-glycosylation. (D) Coomassie-stained SDS 7.5% PAGE. (E) Tabulation of results. See Appendix Fig S4 for representative FP results. ND, not determined; limited solubility of the N-glycosylation sequon mutants prevented their use at the high concentrations required for intrinsic affinity measurements of the BC+EC ensemble. Therefore, thermodynamic parameters were calculated by assuming that the intrinsic affinities of the BC and EC conformations were identical to those determined for the WT ectodomain. (F) Energy landscape plots are as described in the Fig 4E legend.

Data information: (B, C, E, F) Error definitions are as described in the legend to Fig 4.
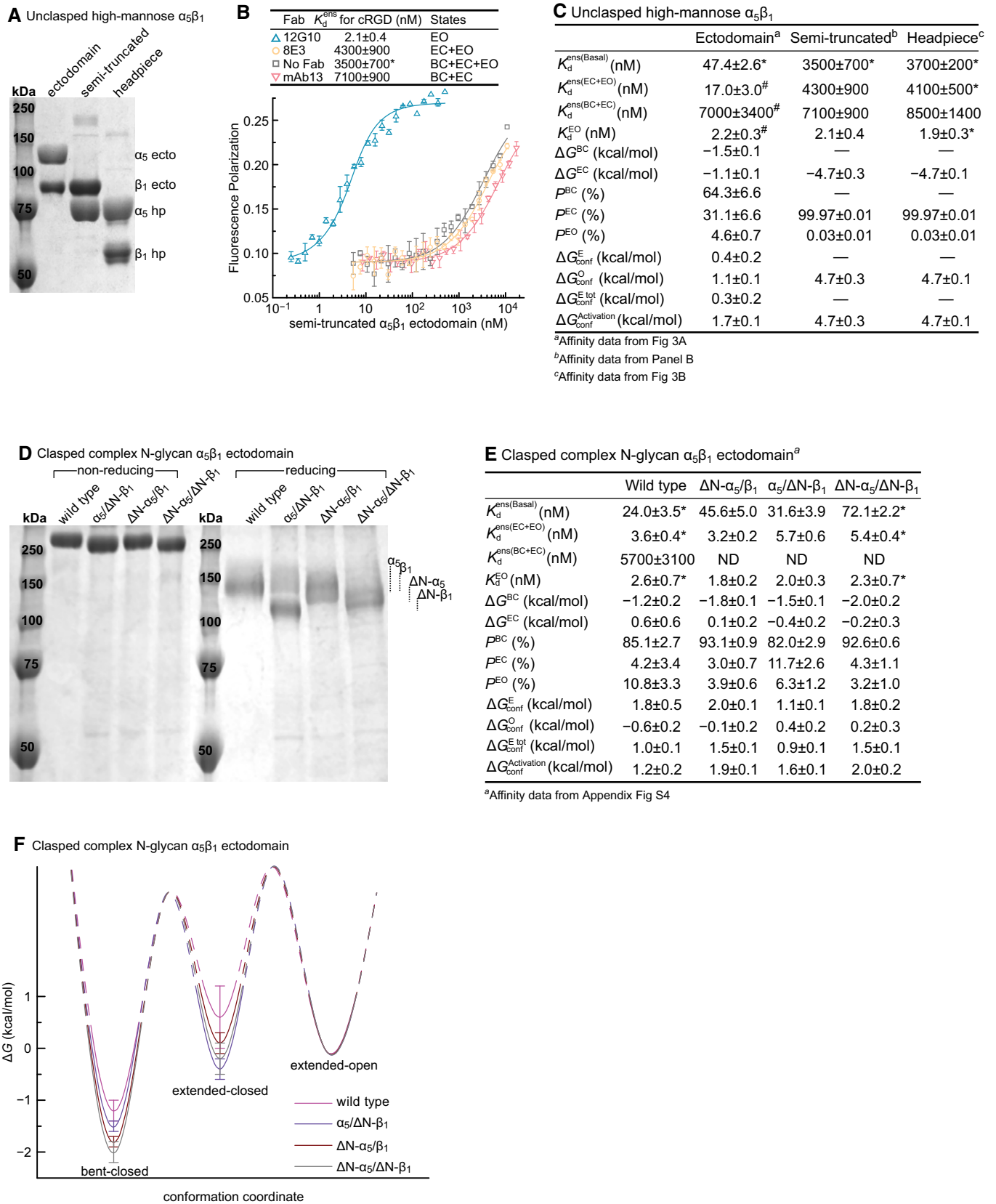
A Unclasped high-mannose $\alpha_5\beta_1$

B

Fab	K_d^{ens} for cRGD (nM)	States
△ 12G10	2.1±0.4	EO
○ 8E3	4300±900	EC+EO
□ No Fab	3500±700*	BC+EC+EO
▽ mAb13	7100±900	BC+EC

C Unclasped high-mannose $\alpha_5\beta_1$

	Ectodomain[a]	Semi-truncated[b]	Headpiece[c]
$K_d^{ens(Basal)}$ (nM)	47.4±2.6*	3500±700*	3700±200*
$K_d^{ens(EC+EO)}$ (nM)	17.0±3.0#	4300±900	4100±500*
$K_d^{ens(BC+EC)}$ (nM)	7000±3400#	7100±900	8500±1400
K_d^{EO} (nM)	2.2±0.3#	2.1±0.4	1.9±0.3*
ΔG^{BC} (kcal/mol)	−1.5±0.1	—	—
ΔG^{EC} (kcal/mol)	−1.1±0.1	−4.7±0.3	−4.7±0.1
P^{BC} (%)	64.3±6.6	—	—
P^{EC} (%)	31.1±6.6	99.97±0.01	99.97±0.01
P^{EO} (%)	4.6±0.7	0.03±0.01	0.03±0.01
ΔG_{conf}^{E} (kcal/mol)	0.4±0.2	—	—
ΔG_{conf}^{O} (kcal/mol)	1.1±0.1	4.7±0.3	4.7±0.1
$\Delta G_{conf}^{E\,tot}$ (kcal/mol)	0.3±0.2	—	—
$\Delta G_{conf}^{Activation}$ (kcal/mol)	1.7±0.1	4.7±0.3	4.7±0.1

[a]Affinity data from Fig 3A
[b]Affinity data from Panel B
[c]Affinity data from Fig 3B

D Clasped complex N-glycan $\alpha_5\beta_1$ ectodomain

E Clasped complex N-glycan $\alpha_5\beta_1$ ectodomain[a]

	Wild type	ΔN-α_5/β_1	α_5/ΔN-β_1	ΔN-α_5/ΔN-β_1
$K_d^{ens(Basal)}$ (nM)	24.0±3.5*	45.6±5.0	31.6±3.9	72.1±2.2*
$K_d^{ens(EC+EO)}$ (nM)	3.6±0.4*	3.2±0.2	5.7±0.6	5.4±0.4*
$K_d^{ens(BC+EC)}$ (nM)	5700±3100	ND	ND	ND
K_d^{EO} (nM)	2.6±0.7*	1.8±0.2	2.0±0.3	2.3±0.7*
ΔG^{BC} (kcal/mol)	−1.2±0.2	−1.8±0.1	−1.5±0.1	−2.0±0.2
ΔG^{EC} (kcal/mol)	0.6±0.6	0.1±0.2	−0.4±0.2	−0.2±0.3
P^{BC} (%)	85.1±2.7	93.1±0.9	82.0±2.9	92.6±0.6
P^{EC} (%)	4.2±3.4	3.0±0.7	11.7±2.6	4.3±1.1
P^{EO} (%)	10.8±3.3	3.9±0.6	6.3±1.2	3.2±1.0
ΔG_{conf}^{E} (kcal/mol)	1.8±0.5	2.0±0.1	1.1±0.1	1.8±0.2
ΔG_{conf}^{O} (kcal/mol)	−0.6±0.2	−0.1±0.2	0.4±0.2	0.2±0.3
$\Delta G_{conf}^{E\,tot}$ (kcal/mol)	1.0±0.1	1.5±0.1	0.9±0.1	1.5±0.1
$\Delta G_{conf}^{Activation}$ (kcal/mol)	1.2±0.2	1.9±0.1	1.6±0.1	2.0±0.2

[a]Affinity data from Appendix Fig S4

F Clasped complex N-glycan $\alpha_5\beta_1$ ectodomain

Figure 6.

Discussion

Methodologies for measuring intrinsic affinities and conformational equilibria of cell surface receptors

We have advanced here an approach to measuring conformational equilibria of multi-domain, multi-subunit receptors that should be extendible to many other cell surface receptors. Using antibodies to stabilize the same conformational states that proteins exhibit in the absence of antibodies is supported by the finding that antibodies usually stabilize proteins in conformations near energy minima (Kastritis *et al*, 2011). Indeed, one of the antibodies studied here, SG/19, binds to a closed headpiece conformation indistinguishable in atomic structures from that in the absence of Fab (Nagae *et al*, 2012; Xia & Springer, 2014). Thermodynamic studies using Fabs were validated here in a study without Fabs; complex N-glycans were shown with EM to stabilize the EO conformation. However, great care needs to be taken to validate the assumption that Fab-stabilized states resemble those in native proteins, and we have already found one exception, with TS2/16 Fab (Su *et al*, 2016). Here we have used between two to four independent antibodies or antibody combinations, often binding to distinct domains, to stabilize ensembles containing the EO, EC, EO+EC, and EC+BC states. In all cases, independent antibodies that stabilized the same conformational state(s) as determined by EM yielded similar ensemble K_d values, validating stabilization of the same state(s), and supporting the assumption that these states resembled those in the absence of Fab. Quantitatively, the antibodies must be highly state-specific in order to give large shifts in affinities, to give consistent intrinsic affinities on constructs with large differences in basal affinities, and to give similar intrinsic affinities using Fabs to distinct epitopes. Exceptions to the rule that antibodies stabilize native states might occur when a non-native Fab-bound state can be reached that is lower in energy than the Fab-bound native state. This appeared to occur with the ΔN-α_5/ΔN-β_1 mutant in the presence of SG/19 Fab and ligand. Increasing concentrations of SG/19 Fab lowered affinity to a plateau value, but not to the same value as for wild-type $\alpha_5\beta_1$ or ΔN-α_5/ΔN-β_1 with mAb 13. Our interpretation is that removal of N-linked sites nearby the SG/19 binding site enabled a non-native state in which the βI domain was not fully in the closed conformation and could bind ligand. This emphasizes the importance of the use of independent Fabs to stabilize the same state. We also re-iterate the importance of using monovalent Fabs rather than bivalent IgGs and of using Fabs at concentrations well above their EC_{50} values to ensure saturation of the ensemble with the desired conformation(s).

In passing, we mention two common fallacies in the integrin field. On "resting" cells or in the case of purified integrins in the absence of activation, the low-affinity conformation is not uniformly adopted, as shown by our ensemble measurements. Furthermore, Mn^{2+} does not "maximally" activate integrins, as shown by their increased affinity in the presence of Fabs that stabilize the EO state. In the absence of stabilizing Fabs, integrins are present in all three conformations in all conditions we examined. The ensemble may contain all three conformations in similar amounts, as for the unclasped ectodomain with complex glycosylation, or one conformation in great excess over the others, as for the BC conformation on cell surfaces.

Intrinsic affinities of integrin states

A key question in the integrin field has been how adhesiveness and affinity are regulated. However, elucidation of integrin affinity regulation has been elusive (Schürpf & Springer, 2011; Zhu *et al*, 2013). Understanding how integrins bind ligand and connect to the cytoskeleton to mediate adhesion and cell migration requires not only the parts list and how the parts fit together, but also quantitative understanding of the binding affinities of those parts and the equilibria that regulate integrin conformation and affinity. Here, we have achieved such an understanding for an integrin of central importance in cell migration, signaling, adhesion, and assembly of fibronectin into the fibrils characteristic of the chordate extracellular matrix (Schwarzbauer & DeSimone, 2011). Our studies now make the biological processes in which integrin $\alpha_5\beta_1$ participates accessible to quantitative methods that seek to relate biological inputs to biological outputs in living cells.

Previous studies have correlated integrin adhesiveness and high affinity for ligand with the open conformation of the headpiece (Takagi *et al*, 2002, 2003; Xiao *et al*, 2004; Chen *et al*, 2010; Schürpf & Springer, 2011; Zhu *et al*, 2013). However, neither the affinities for ligand intrinsic to the closed and open headpiece conformations nor the magnitude of the affinity increase were previously measured. Here, we have measured intrinsic affinities of extended-open $\alpha_5\beta_1$ for RGD peptide, cRGD, and $Fn3_{9-10}$ as 71, 2.2, and 0.44 nM, respectively. We further determined the intrinsic affinity of closed $\alpha_5\beta_1$ for cRGD as 7,000–8,000 nM, and for $Fn3_{9-10}$ as 2,700–2,900 nM. The large magnitude of the affinity increase of

---

Figure 7. Conformational equilibria and intrinsic affinity of intact $\alpha_5\beta_1$ on cell surfaces.

Mean fluorescence intensity (MFI) after background subtraction is from quantitative fluorescence flow cytometry of K562 cells without washing.

A   Determination of EC_{50} values for conformation-selective Fabs from enhancement of 10 nM Alexa488-$Fn3_{9-10}$ binding and fitting to Appendix Equation S2. Mean ± s.d. of least square fits to triplicates.

B   Affinity of $\alpha_5\beta_1$ for Alexa488-$Fn3_{9-10}$ in the presence of indicated Fabs.

C   Affinity of $\alpha_5\beta_1$ for $Fn3_{9-10}$ by enhancement of 0.4 nM Alexa488-12G10 Fab binding.

D   Affinities of $\alpha_5\beta_1$ for Alexa488-12G10 Fab in the presence of indicated Fabs.

E   Thermodynamics and intrinsic affinities of $\alpha_5\beta_1$ conformational states on K562 cells and Jurkat cells (Appendix Fig S8). Affinity for $Fn3_{9-10}$ of the closed conformations of $\alpha_5\beta_1$ on K562 cells was estimated from K_d^{EO} using the same fold-difference as found with $Fn3_{9-10}$ for the $\alpha_5\beta_1$ ectodomain (Fig 4D). Since 12G10 stabilizes the open conformation only, thermodynamic calculations use $K_a = 0$ for the closed conformations.

F   Energy landscape plots, as described in the Fig 4E legend, comparing K562 $\alpha_5\beta_1$ to the clasped and unclasped $\alpha_5\beta_1$ ectodomain with complex glycosylation (Fig 5B).

G   Summary of the intrinsic affinities of $\alpha_5\beta_1$ conformational states on K562 cells and comparison of the conformational equilibria for $\alpha_5\beta_1$ on K562 cells and for the unclasped $\alpha_5\beta_1$ ectodomain with complex glycosylation.

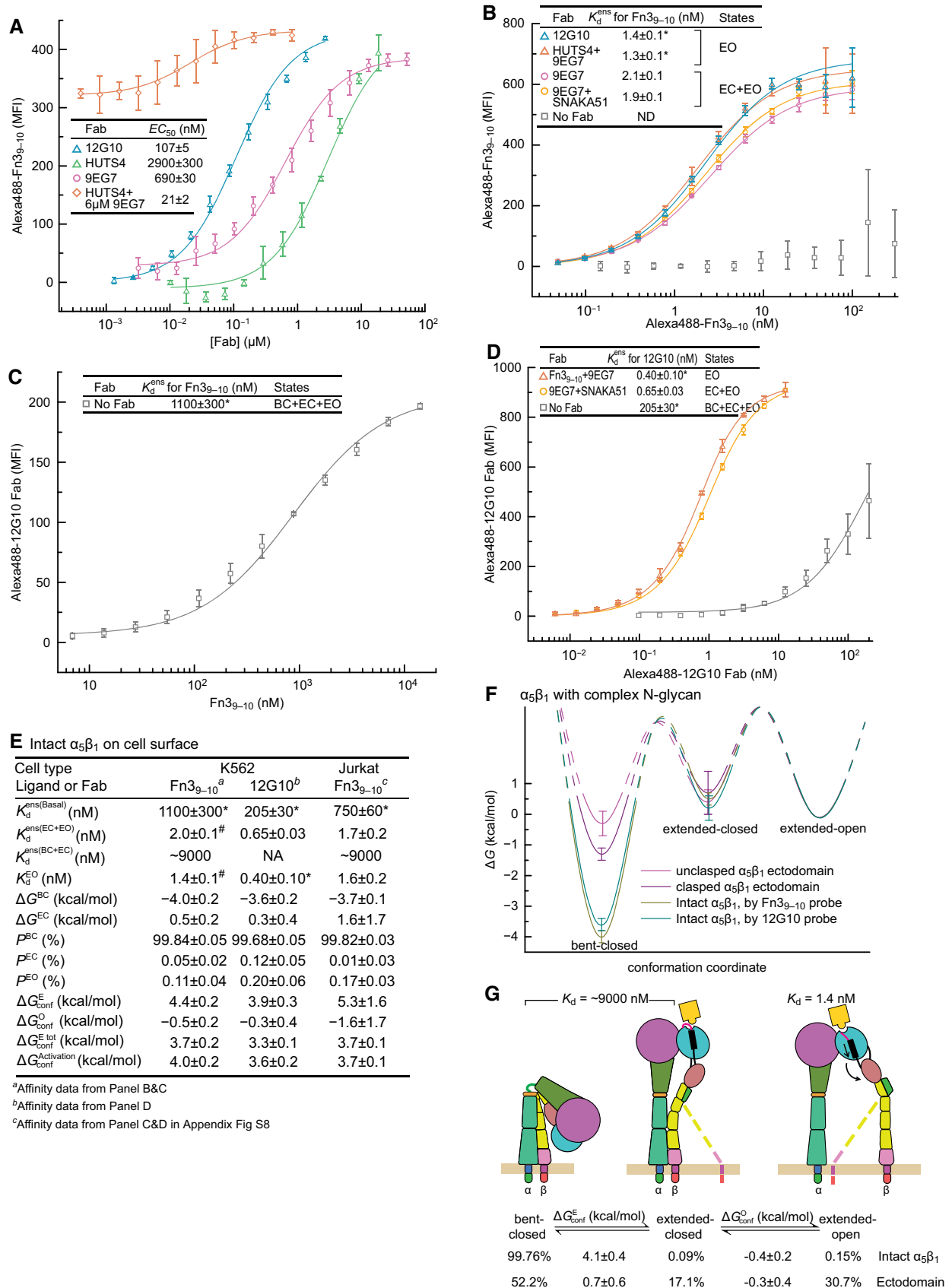Data information: (B–F) Error definitions are as described in the legend to Fig 4.

A

Fab	EC_{50} (nM)
12G10	107±5
HUTS4	2900±300
9EG7	690±30
HUTS4+ 6μM 9EG7	21±2

B

Fab	K_d^{ens} for Fn3$_{9-10}$ (nM)	States
12G10	1.4±0.1*	EO
HUTS4+ 9EG7	1.3±0.1*	EO
9EG7	2.1±0.1	EC+EO
9EG7+ SNAKA51	1.9±0.1	EC+EO
No Fab	ND	

C

Fab	K_d^{ens} for Fn3$_{9-10}$ (nM)	States
No Fab	1100±300*	BC+EC+EO

D

Fab	K_d^{ens} for 12G10 (nM)	States
Fn3$_{9-10}$+9EG7	0.40±0.10*	EO
9EG7+SNAKA51	0.65±0.03	EC+EO
No Fab	205±30*	BC+EC+EO

E Intact α$_5$β$_1$ on cell surface

Cell type	K562		Jurkat
Ligand or Fab	Fn3$_{9-10}$[a]	12G10[b]	Fn3$_{9-10}$[c]
$K_d^{ens(Basal)}$ (nM)	1100±300*	205±30*	750±60*
$K_d^{ens(EC+EO)}$ (nM)	2.0±0.1#	0.65±0.03	1.7±0.2
$K_d^{ens(BC+EC)}$ (nM)	~9000	NA	~9000
K_d^{EO} (nM)	1.4±0.1#	0.40±0.10*	1.6±0.2
ΔG^{BC} (kcal/mol)	−4.0±0.2	−3.6±0.2	−3.7±0.1
ΔG^{EC} (kcal/mol)	0.5±0.2	0.3±0.4	1.6±1.7
P^{BC} (%)	99.84±0.05	99.68±0.05	99.82±0.03
P^{EC} (%)	0.05±0.02	0.12±0.05	0.01±0.03
P^{EO} (%)	0.11±0.04	0.20±0.06	0.17±0.03
ΔG_{conf}^{E} (kcal/mol)	4.4±0.2	3.9±0.3	5.3±1.6
ΔG_{conf}^{O} (kcal/mol)	−0.5±0.2	−0.3±0.4	−1.6±1.7
$\Delta G_{conf}^{E,tot}$ (kcal/mol)	3.7±0.2	3.3±0.1	3.7±0.1
$\Delta G_{conf}^{Activation}$ (kcal/mol)	4.0±0.2	3.6±0.2	3.7±0.1

[a]Affinity data from Panel B&C

[b]Affinity data from Panel D

[c]Affinity data from Panel C&D in Appendix Fig S8

F α$_5$β$_1$ with complex N-glycan

unclasped α$_5$β$_1$ ectodomain
clasped α$_5$β$_1$ ectodomain
Intact α$_5$β$_1$, by Fn3$_{9-10}$ probe
Intact α$_5$β$_1$, by 12G10 probe

G

bent-closed	ΔG_{conf}^{E} (kcal/mol)	extended-closed	ΔG_{conf}^{O} (kcal/mol)	extended-open	
99.76%	4.1±0.4	0.09%	−0.4±0.2	0.15%	Intact α$_5$β$_1$
52.2%	0.7±0.6	17.1%	−0.3±0.4	30.7%	Ectodomain

Figure 7.

4,000-fold to 6,000-fold should put to rest any lingering doubt in the integrin community about the relevance of changes in conformation and affinity to the regulation of integrin function and adhesiveness (Zhu *et al*, 2013).

Conformational equilibria in integrin allostery

Our studies extend structural observations on the three overall integrin states in EM (Takagi *et al*, 2002, 2003; Zhu *et al*, 2008; Chen *et al*, 2010; Su *et al*, 2016) by showing that these correspond to three states with discrete free energies. The bent-closed conformation of integrins is compact, well defined, and amenable to crystallography as shown with integrins $\alpha_V\beta_3$, $\alpha_{IIb}\beta_3$, and $\alpha_X\beta_2$ (Xiong *et al*, 2001; Zhu *et al*, 2008; Xie *et al*, 2010). However, extended-closed and extended-open conformations show flexible lower legs and have thus far been amenable to EM and small-angle X-ray scattering but not crystallography; atomic understanding of the headpiece and β-legs outside of the bent conformation comes from crystallization of ectodomain fragments (Springer & Dustin, 2012). EM and crystal structures show that the β-leg is flexible, particularly at the knee between EGF1 in the upper leg and EGF2 in the lower leg (Shi *et al*, 2007). Flexion of the α-subunit occurs at its knee between thigh and calf-1 and also at the β-propeller interface with thigh (Xie *et al*, 2010). Because of the considerable flexibility of the integrin legs when extended, the extended-closed and extended-open states should be considered not single but overall states, each with a large number of microstates that vary in leg domain orientation (Takagi *et al*, 2002).

With this heterogeneity among microstates in mind, it is gratifying that the studies here show that the bent-closed, extended-closed, and extended-open states defined structurally are also distinct in free energy. Thus, Fabs that induced extension by binding to the interface in the α-subunit lower leg between the calf-1 and calf-2 domains, to the PSI domain in the upper β-leg, or to the I-EGF2 domain in the lower β-leg, induced extended states indistinguishable in free energy. The difference in energy between the BC and EC states may relate to breakage of the large interfaces in the BC conformation between the headpiece and lower legs and between the α-subunit and β-subunit legs (Takagi *et al*, 2002), the replacement of these interfaces by solvent in the extended-closed conformation, and the large number of leg conformations accessible after extension. By contrast, differences between interfaces to which Fabs bind and among the conformational microstates accessible in the two extended overall states with different bound Fab must be minor in comparison.

Headpiece opening involves highly discrete βI domain α7-helix pistoning and remodeling of a large βI/hybrid domain interface in the closed conformation to a smaller interface in the open conformation (Xiao *et al*, 2004). Again, binding of Fabs to distinct epitopes in the βI and hybrid domains suggested an extended-open state with discrete ΔG despite evidence for leg flexibility in this state. Furthermore, the combined use of two Fabs to induce extension and opening compared to the use of one open-stabilizing Fab resulted in no significant affinity differences compared to the scale of the affinity differences between states.

Measurements of $\alpha_5\beta_1$ conformational equilibria on the K562 erythroleukemia cell line quantify the energy requirements in the pathway of integrin activation from the bent-closed to the extended-open conformation. Surprisingly, energy is only required for extension; once the integrin extends, the open headpiece is slightly energetically favored over the closed headpiece. Furthermore, in the absence of ligand the basal integrin ensemble on K562 cells is $99.76 \pm 0.08\%$ bent-closed, $0.09 \pm 0.04\%$ extended-closed, and $0.15 \pm 0.03\%$ extended-open. In K562 cells, the energy input required to stabilize integrin extension and headpiece opening of ~4 kcal/mol may come from the ATP hydrolysis required to drive actin polymerization into filaments and myosin-dependent actin filament contraction, and be coupled to integrin conformational change through the cytoskeletal force model of integrin activation (Zhu *et al*, 2008).

$\alpha_5\beta_1$ energy landscape on the cell surface

Comparisons among intact $\alpha_5\beta_1$ on K562 cells and soluble fragments provide insights into the molecular components that contribute to the energy landscape. On K562 cells, extension requires a large energy input; in contrast, headpiece opening spontaneously follows extension because the EO conformation is lower in energy than the EC conformation. To estimate the contribution to energetics of the TM and cytoplasmic domains, as a first approximation the energy required for extension of the ectodomain portion of $\alpha_5\beta_1$ on the cell surface and the unclasped $\alpha_5\beta_1$ ectodomain with complex N-glycans in solution may be compared. This comparison suggests that a substantial amount of energy is required for alterations in the TM and cytoplasmic domains that are associated with extension. Thus, inside-out signaling must input, through alterations in TM/cytoplasmic domains, about 3.5 kcal/mol ($\Delta G_{conf}^{E\,tot}$) to convert the EC+EO conformations from a population of 0.2% in the basal ensemble to a population of 50% in an active ensemble. Considerable evidence shows that both the α- and β-subunit cytoplasmic domains and transmembrane domains separate upon integrin activation (Kim *et al*, 2003; Luo *et al*, 2004a, 2005; Zhu *et al*, 2009). Structures determined for the TM domains in intact integrins on cell surfaces and for TM domain peptides in bicelles show an interface between the TM domains that extends through the bilayer and is enhanced by a reverse-turn at a GFFKR motif at the cytoplasmic face (Lau *et al*, 2009; Zhu *et al*, 2009). The current study has not probed the energetics of integrin TM and cytoplasmic domain association; however, the large contribution to the energetics of extension (ΔG_{conf}^{E}) by the TM and cytoplasmic domains suggests that on cell surfaces, a higher proportion of EC state than BC state integrins may have their α- and β-subunit TM and cytoplasmic domains dissociated from one another. On cells, integrins associate with cytoplasmic proteins that stabilize activation or inactivation (Bouvard *et al*, 2013; Calderwood *et al*, 2013), and these interactions will also contribute to the free energies we measure at 20–25°C where the membrane bilayer is fluid. We found no difference in conformational state free energy between $\alpha_5\beta_1$ on two different cell types; however, such differences may be found for other cell types or other integrins.

Relief of crowding or repulsive interactions between the lower α- and β-subunit legs is an important driver of headpiece opening and may also drive TM domain separation. Compared to the ectodomain construct, much more energy is required for headpiece opening in protein constructs lacking one or both lower legs. In the bent-closed conformation on cell surfaces, the lower legs meet the upper legs at

a point where the integrin α and β knees are close together. The lower legs also meet, through short linkers of ~8 residues in α_5 and ~4 residues in β_1, at the α and β TM domains where they are close together (Zhu *et al*, 2009). Therefore, crowding interactions between the lower α and β legs may drive TM/cytoplasmic domain separation similarly to headpiece opening.

Measurements of equilibria provide insights into integrin structure and function orthogonal but complementary to insights from structural biology

Our findings that the extended-open conformation of the ectodomain is stabilized by (i) the presence of the lower legs and (ii) large N-glycans suggest the hypothesis that in multi-domain receptors, non-ligand-binding (leg) domains and N-glycans may have previously unappreciated roles in regulating affinity for ligands and conformational equilibria. In the case of integrins, the α- and β-subunit knees are 10 Å apart in the bent-closed conformation and 100 Å apart in the extended-open conformation (Springer *et al*, 2008; Zhu *et al*, 2008). Thus, in the extended-closed conformation, the lower integrin α- and β-legs are very close at the knees and will crowd or repel one another. This hypothesis predicts that both integrin lower legs must be present to obtain crowding or repulsion and relief by opening, as we experimentally verified.

Conformational equilibria and allosteric regulation were elegantly described decades ago for membrane channels using measurements of their opening and closing, and more recently measured for G protein-coupled receptors (Ruiz & Karpen, 1997; Horrigan *et al*, 1999; Lape *et al*, 2008; Park *et al*, 2008; Cecchini & Changeux, 2015; Manglik *et al*, 2015). All of these receptors have a large domain composed of multiple TM domains embedded in the membrane and have N-glycosylated extracellular loops or domains. Another large class of glycosylated receptors to which integrins belong have extracellular domains in tandem with single-span TM domains. Many of these receptors bind ligands in membrane distal domains and have a larger number of domains, often cysteine-rich, immunoglobulin-like or fibronectin type 3-like, that link the ligand-binding domain(s) to single TM domains (Fig 1D). We propose that the glycosylated tandem domains that link ligand-binding and TM domains in such receptors are analogous to the leg domains of integrins. The active states of integrins and these receptors have an inverse relationship, such that the active, open, TM domain-apart integrin state corresponds to the monomeric, inactive state of cytokine and growth factor receptors, whereas the inactive, bent-closed, TM domain-together state of integrins corresponds to the active, multimeric, ligand-bound, TM domain-together state of such receptors (Fig 1D). Such receptors do not signal in the absence of cross-linking by ligand, and it will be interesting to investigate whether inter-monomer crowding or repulsive interactions between leg domains are also present in cytokine and growth factor receptors and function to prevent multimerization and signaling in the absence of ligand. We propose that glycans and leg domains may regulate monomer-dimer equilibria in such receptors similarly to their regulation of $K_{\text{conf}}^{\text{Activation}}$ in integrins (Fig 1).

The large amount of space that N-glycans occupy on the surface of receptors (Fig 1B and D) is often not recognized. N-glycans are often removed prior to crystallization. Moreover, glycosidic bonds are typically free to rotate, both at linkages to Asn and

monosaccharide-monosaccharide linkages, and thus, glycan residues are usually difficult to visualize in crystal structures even when present. This flexibility enables N-glycans on one domain to sweep out a large hydrodynamic radius and to crowd or repel with their sialic acid residues other protein domains or N-glycans linked to other sites. The composition and chemical structures of the N-glycans in native integrin $\alpha_5\beta_1$ are well defined (Sieber *et al*, 2007), enabling us to create a scale model comparing the size of the protein and carbohydrate components of $\alpha_5\beta_1$ (Fig 1B). Building a natively glycosylated model of $\alpha_5\beta_1$ BC was challenged by the difficulty of obtaining orientations of glycosidic linkages that prevented N-glycans from clashing with protein or nearby N-glycans. Much of the protein surface in integrins (Fig 1A, lower) is obscured by N-glycans (Fig 1B). Once an integrin extends, the size, flexibility, and hydration of N-glycans creates potential overlap or repulsion between N-glycans attached to different domains, and the protein domains in the lower legs have the potential themselves to also sterically overlap. Such interactions might explain the contribution of the N-glycans and lower leg domains to favoring the less compact EO state over the more compact BC and EC states in integrins. We believe that the effects of glycan shortening and N-linked site removal are general rather than associated with specific N-linked sites. We have used no structural information to guide removal of N-linked sites in α_5 and β_1, and the sites removed (white glycans, Fig 1B) have a similar distribution to sites that remained (blue glycans, Fig 1B).

We were surprised by the large effect of N-glycans and leg domains on conformational equilibria. Compared to shaved glycans, complex glycans raise affinity for ligand of the basal $\alpha_5\beta_1$ ectodomain ensemble by 8- to 10-fold, much more than clasp removal. Furthermore, the presence of both lower legs raises ensemble affinity of the ectodomain by 80-fold compared to the headpiece.

Thus, N-glycans and the lower integrin legs each have major roles in regulating integrin allostery. Although the βI/hybrid and I-EGF1/I-EGF2 interfaces also may regulate integrin allostery (Xiao *et al*, 2004; Smagghe *et al*, 2010), domains in proteins and their interfaces have many evolutionary constraints. The identity and number of upper and lower leg domains in integrin α- and β-subunits are invariant in multi-cellular animals from sponges to chordates and thus have been fixed in evolutionary history for ~600 million years. This invariance likely reflects how closely the legs pack in the bent conformation and the precise requirements of integrins as molecular machines (Takagi *et al*, 2002). While integrin legs have previously been viewed largely as passive conduits for transmission of signals between the ligand-binding head and the plasma membrane, our study demonstrates that the lower legs have a key role in regulating integrin allostery, and thus activation.

Our results establish the principle that variation in N-glycosylation site number can regulate conformational equilibria of multi-domain receptors. N-glycosylation is not only a previously unrecognized mechanism for regulating conformational equilibria but is also evolutionarily facile. We have shown that a decrease in the number of N-glycosylation sites on integrin $\alpha_5\beta_1$ stabilizes its bent-closed and extended-closed conformations and lowers the ligand-binding affinity of its basal ensemble; decreases in the number and complexity of carbohydrate residues at each N-linked site had a similar effect. Among integrins, β_1 integrins are widely expressed

in extravascular environments and are considered to be basally active, whereas β_2 and β_3 integrins are expressed in vascular environments and are considered basally inactive. Our study opens up testing the hypothesis that integrins differ in their activation set points, and provides benchmark measurements on $\alpha_5\beta_1$. It is interesting that among integrin β-subunits, β_1 has the most N-glycosylation sequons (12), β_4 has the least (5), and β_2 and β_3 are tied for next least (6). Variation in the number of N-glycans is also great among integrin α-subunits and ranges from 26 on α_1 to 5 on α_7 and α_{IIb}. Further study is required to determine the molecular basis for apparently markedly different set points among integrins in their basal activity on cells (Bazzoni *et al*, 1998). However, our studies raise the possibility that N-glycosylation site number may be among the mechanisms that regulate integrin basal activity and that N-glycosylation may play a wide role in regulating conformational equilibria of extracellular and membrane proteins.

Materials and Methods

Fabs

Briefly, sources of hybridomas for 12G10, HUTS4, 8E3, 9EG7 and SNAKA51 (Askari *et al*, 2010), and SG/19 and TS2/16 (Luo *et al*, 2004b) were as described in the citations. N29 (Ni *et al*, 1998) and mAb13 (Akiyama *et al*, 1989) hybridomas were kind gifts of J. Wilkins (U. Manitoba, Canada) and K. Yamada (NIH, USA), respectively. Anti-$\alpha_5\beta_1$ hybridoma sources and details of purification of IgG by protein G affinity and preparation of Fab fragments with papain digestion and purification of Fabs by Hi-Trap Q chromatography were as described in detail (Su *et al*, 2016).

Integrin $\alpha_5\beta_1$ constructs

DNA constructs, stable HEK 293S GnTI$^{-/-}$ cell lines (*N*-acetylglucosaminyltransferase I deficient), and high-mannose $\alpha_5\beta_1$ ectodomain (α_5 F1 to Y954 and β_1 Q1 to D708), headpiece (α_5 F1 to L609 and β_1 Q1 to E481), and semi-truncated (α_5 F1 to L609 and β_1 Q1 to D708) fragments were prepared as described (Takagi *et al*, 2001; Xia & Springer, 2014). High-mannose glycoforms were shaved with endoglycosidase H in 50 mM MES buffer (pH 5.6), 100 mM NaCl, 1 mM CaCl$_2$, and 1 mM MgCl$_2$, at an equal protein and enzyme mass ratio, for 12 h at room temperature, followed by gel filtration purification.

The complex glycoform of the $\alpha_5\beta_1$ ectodomain and its N-linked glycosylation site mutants with mature Asn residues at 256, 266, 483, 489, 568, and 634 in α_5 (ΔN-α_5), or 74, 77, 343, 386, and 500 in β_1 (ΔN-β_1) mutated to Arg were produced by co-transfecting HEK 293 cells with codon-optimized α_5 and β_1 cDNAs with secretion peptide, purification tags, and C-terminal clasp (Takagi *et al*, 2001; Xia & Springer, 2014) in pcDNA3.1/Hygro(−) and pIRES vectors. Stable transfectants were selected with hygromycin (100 μg/ml) and G418 (1 mg/ml), and $\alpha_5\beta_1$ glycoproteins were purified as for the high-mannose glycoform.

Peptide ligands and Fn3$_{9-10}$

Cyclic RGD peptide (ACRGDGWCG) and RGD peptide (GRGDSPK) (> 95% pure) were synthesized and labeled with FITC at the

N-terminus via a 6-aminohexanoic acid spacer by GenScript (Piscataway, NJ). Human Fn3$_{9-10}$ (mature residues G1326 to T1509) and its S1417C mutant were expressed in *Escherichia coli* and purified as described (Takagi *et al*, 2001). The mutant was fluorescently labeled with Alexa Fluor 488 C5 maleimide (ThermoFisher Scientific) in PBS.

Fluorescence polarization

Each sample (10 μl) contained 150 mM NaCl, 1 mM CaCl$_2$, 1 mM MgCl$_2$, 5 nM FITC-cRGD or FITC-RGD, $\alpha_5\beta_1$, and indicated Fabs and/or Fn3$_{9-10}$ in 20 mM Tris buffer (pH 7.4). For competitive binding, $\alpha_5\beta_1$ was pre-equilibrated with Fn3$_{9-10}$ for 2 h before mixing with FITC-cRGD. The mixture was allowed to equilibrate for 2 h (24 h with 12G10 Fab to reach equilibrium) before recording FP on a Synergy NEO HTS multi-mode microplate reader (Biotek).

Quantitative fluorescent flow cytometry

K562 and Jurkat cells (10^6 cells/ml in RPMI-1640 medium, 10% FBS) were washed twice with assay medium (Leibovitz's L-15 medium, 10 mg/ml BSA) containing 5 mM EDTA, twice with assay medium, and resuspended in assay medium. Each sample (50 μl) contained cells (2 × 10^6 cells/ml), Alexa488-Fn3$_{9-10}$ or Alexa488-12G10, and indicated Fabs or Fn3$_{9-10}$ in assay medium. The mixture was allowed to equilibrate for 1.5 h before flow cytometry (BD FACSCanto II) without washing (Chigaev *et al*, 2001; Dong *et al*, 2014). Alexa488-Fn3$_{9-10}$ or Alexa488-12G10 binding was measured as mean fluorescence intensity (MFI); background MFI was subtracted and was measured by the same method in the presence of 10 mM EDTA (K562) or 100-fold excess of α_5-specific, ligand-blocking antibody mAb16 (Burrows *et al*, 1999) over Fn3$_{9-10}$ (Jurkat).

Thermodynamic properties

Ligand-binding affinities of $\alpha_5\beta_1$ ensembles in the absence or presence of Fabs were measured by saturation binding or competitive binding using FP or flow cytometry. Probabilities of each $\alpha_5\beta_1$ conformation in the basal ensemble and their free energies relative to that of the extended-open conformation (ΔG^{BC} and ΔG^{EC}; $\Delta G^{EO} = 0$) were calculated from intrinsic and ensemble affinities (Fig 1C). Appendix Equations S1–S94 used to obtain reported values are described in Appendix Supplementary Materials and Methods. Briefly, K_d^{app} values were obtained from fits to Appendix Equations S16, S17, S26, and S28; K_d^{ens} values in the presence of closure-stabilizing Fabs were calculated using Appendix Equation S64; in all other conditions, $K_d^{ens} = K_d^{app}$ (Appendix Fig S2); P and ΔG values are calculated from K_d^{ens} values with Appendix Equations S73–S77 and S82–S84, respectively, and their errors are calculated by propagation from K_d^{ens} errors.

Expanded View for this article is available online.

Author contributions

JL, CL, and TAS designed research; JL, YS, WX, and YQ performed research; JL, YS, and TAS analyzed data and wrote the manuscript; MJH, DV, and CC provided reagents and aided in interpretation of results.

Conflict of interest

The authors declare that they have no conflict of interest.

References

Akiyama SK, Yamada SS, Chen WT, Yamada KM (1989) Analysis of fibronectin receptor function with monoclonal antibodies: roles in cell adhesion, migration, matrix assembly, and cytoskeletal organization. *J Cell Biol* 109: 863−875

Askari JA, Tynan CJ, Webb SE, Martin-Fernandez ML, Ballestrem C, Humphries MJ (2010) Focal adhesions are sites of integrin extension. *J Cell Biol* 188: 891−903

Bazzoni G, Ma L, Blue M-L, Hemler ME (1998) Divalent cations and ligands induce conformational changes that are highly divergent among β1 integrins. *J Biol Chem* 273: 6670−6678

Bouvard D, Pouwels J, De Franceschi N, Ivaska J (2013) Integrin inactivators: balancing cellular functions in vitro and in vivo. *Nat Rev Mol Cell Biol* 14: 430−442

Burrows L, Clark K, Mould AP, Humphries MJ (1999) Fine mapping of inhibitory anti-a 5 monoclonal antibody epitopes that differentially affect integrin-ligand binding. *Biochem J* 344(Pt 2): 527−533

Byron A, Humphries J, Askari JA, Craig SE, Mould AP, Humphries M (2009) Anti-integrin monoclonal antibodies. *J Cell Sci* 122: 4009−4011

Calderwood DA, Campbell ID, Critchley DR (2013) Talins and kindlins: partners in integrin-mediated adhesion. *Nat Rev Mol Cell Biol* 14: 503−517

Cecchini M, Changeux JP (2015) The nicotinic acetylcholine receptor and its prokaryotic homologues: structure, conformational transitions & allosteric modulation. *Neuropharmacology* 96: 137−149

Chen X, Xie C, Nishida N, Li Z, Walz T, Springer TA (2010) Requirement of open headpiece conformation for activation of leukocyte integrin αXβ2. *Proc Natl Acad Sci USA* 107: 14727−14732

Chigaev A, Blenc AM, Braaten JV, Kumaraswamy N, Kepley CL, Andrews RP, Oliver JM, Edwards BS, Prossnitz ER, Larson RS, Sklar LA (2001) Real-time analysis of the affinity regulation of α4-integrin: the physiologically activated receptor is intermediate in affinity between resting and Mn^{2+} or antibody activation. *J Biol Chem* 276: 48670−48678

Dong X, Hudson NE, Lu C, Springer TA (2014) Structural determinants of integrin β-subunit specificity for latent TGF-β. *Nat Struct Mol Biol* 21: 1091−1096

Faull RJ, Kovach NL, Harlan JM, Ginsberg MH (1993) Affinity modulation of integrin α5β1: regulation of the functional response by soluble fibronectin. *J Cell Biol* 121: 155−162

Horrigan FT, Cui J, Aldrich RW (1999) Allosteric voltage gating of potassium channels I. Mslo ionic currents in the absence of Ca(2+). *J Gen Physiol* 114: 277−304

Kastritis PL, Moal IH, Hwang H, Weng Z, Bates PA, Bonvin AM, Janin J (2011) A structure-based benchmark for protein-protein binding affinity. *Protein Sci* 20: 482−491

Kim M, Carman CV, Springer TA (2003) Bidirectional transmembrane signaling by cytoplasmic domain separation in integrins. *Science* 301: 1720−1725

Koivunen E, Wang B, Ruoslahti E (1995) Phage libraries displaying cyclic peptides with different ring sizes: ligand specificities of the RGD-directed integrins. *Biotechnology (N Y)* 13: 265−270

Lape R, Colquhoun D, Sivilotti LG (2008) On the nature of partial agonism in the nicotinic receptor superfamily. *Nature* 454: 722−727

Lau TL, Kim C, Ginsberg MH, Ulmer TS (2009) The structure of the integrin αIIbβ3 transmembrane complex explains integrin transmembrane signalling. *EMBO J* 9: 1351−1361

Luo B-H, Springer TA, Takagi J (2004a) A specific interface between integrin transmembrane helices and affinity for ligand. *PLoS Biol* 2: 776−786

Luo B-H, Strokovich K, Walz T, Springer TA, Takagi J (2004b) Allosteric β1 integrin antibodies that stabilize the low affinity state by preventing the swing-out of the hybrid domain. *J Biol Chem* 279: 27466−27471

Luo B-H, Carman CV, Takagi J, Springer TA (2005) Disrupting integrin transmembrane domain heterodimerization increases ligand binding affinity, not valency or clustering. *Proc Natl Acad Sci USA* 102: 3679−3684

Luo B-H, Carman CV, Springer TA (2007) Structural basis of integrin regulation and signaling. *Annu Rev Immunol* 25: 619−647

Manglik A, Kim TH, Masureel M, Altenbach C, Yang Z, Hilger D, Lerch MT, Kobilka TS, Thian FS, Hubbell WL, Prosser RS, Kobilka BK (2015) Structural insights into the dynamic process of β2-adrenergic receptor signaling. *Cell* 161: 1101−1111

Nagae M, Re S, Mihara E, Nogi T, Sugita Y, Takagi J (2012) Crystal structure of α5β1 integrin ectodomain: atomic details of the fibronectin receptor. *J Cell Biol* 197: 131−140

Ni H, Li A, Simonsen N, Wilkins JA (1998) Integrin activation by dithiothreitol or Mn^{2+} induces a ligand-occupied conformation and exposure of a novel NH2-terminal regulatory site on the b1 integrin chain. *J Biol Chem* 273: 7981−7987

Nishida N, Xie C, Shimaoka M, Cheng Y, Walz T, Springer TA (2006) Activation of leukocyte β2 integrins by conversion from bent to extended conformations. *Immunity* 25: 583−594

Park PL, Lodowski DT, Palczewski K (2008) Activation of G protein-coupled receptors: beyond two-state models and tertiary conformational changes. *Annu Rev Pharmacol Toxicol* 48: 107−141

Rossi AM, Taylor CW (2011) Analysis of protein-ligand interactions by fluorescence polarization. *Nat Protoc* 6: 365−387

Ruiz ML, Karpen JW (1997) Single cyclic nucleotide-gated channels locked in different ligand-bound states. *Nature* 389: 389−392

Schürpf T, Springer TA (2011) Regulation of integrin affinity on cell surfaces. *EMBO J* 30: 4712−4727

Schwarzbauer JE, DeSimone DW (2011) Fibronectins, their fibrillogenesis, and in vivo functions. *Cold Spring Harb Perspect Biol* 3: 1−19

Sen M, Yuki K, Springer TA (2013) An internal ligand-bound, metastable state of a leukocyte integrin, αXβ2. *J Cell Biol* 203: 629−642

Shi M, Foo SY, Tan SM, Mitchell EP, Law SK, Lescar J (2007) A structural hypothesis for the transition between bent and extended conformations of the leukocyte β2 integrins. *J Biol Chem* 282: 30198−30206

Sieber JW, Willig KI, Kutzner C, Gerding-Reimers C, Harke B, Donnert G, Rammner B, Eggeling C, Hell SW, Grubmüller H, Lang T (2007) Anatomy and dynamics of a supramolecular membrane protein cluster. *Science* 317: 1072−1076

Smagghe B, Huang P, Ban Y-E, Baker D, Springer TA (2010) Modulation of integrin activation by an entropic spring in the β-knee. *J Biol Chem* 285: 32954−32966

Springer TA, Zhu J, Xiao T (2008) Structural basis for distinctive recognition of fibrinogen γC peptide by the platelet integrin αIIbβ3. *J Cell Biol* 182: 791−800

Springer TA, Dustin ML (2012) Integrin inside-out signaling and the immunological synapse. *Curr Opin Cell Biol* 24: 107−115

Stowell SR, Ju T, Cummings RD (2015) Protein glycosylation in cancer. *Annu Rev Pathol* 10: 473−510

Su Y, Xia W, Li J, Walz T, Humphries MJ, Vestweber D, Cabañas C, Lu C, Springer TA (2016) Relating conformation to function in integrin α5β1. *Proc Natl Acad Sci USA* 113: E3872−E3881

Takagi J, Erickson HP, Springer TA (2001) C-terminal opening mimics "inside-out" activation of integrin α5β1. *Nat Struct Biol* 8: 412−416

Takagi J, Petre BM, Walz T, Springer TA (2002) Global conformational rearrangements in integrin extracellular domains in outside-in and inside-out signaling. *Cell* 110: 599−611

Takagi J, Strokovich K, Springer TA, Walz T (2003) Structure of integrin α5β1 in complex with fibronectin. *EMBO J* 22: 4607−4615

Tsuchida J, Ueki S, Saito Y, Takagi J (1997) Classification of 'activation' antibodies against integrin β1 chain. *FEBS Lett* 416: 212−216

Xia W, Springer TA (2014) Metal ion and ligand binding of integrin α5β1. *Proc Natl Acad Sci USA* 111: 17863−17868

Xiao T, Takagi J, Wang J-H, Coller BS, Springer TA (2004) Structural basis for allostery in integrins and binding of fibrinogen-mimetic therapeutics. *Nature* 432: 59−67

Xie C, Zhu J, Chen X, Mi L, Nishida N, Springer TA (2010) Structure of an integrin with an αI domain, complement receptor type 4. *EMBO J* 29: 666−679

Xiong J-P, Stehle T, Diefenbach B, Zhang R, Dunker R, Scott DL, Joachimiak A, Goodman SL, Arnaout MA (2001) Crystal structure of the extracellular segment of integrin αVβ3. *Science* 294: 339−345

Zhu J, Luo BH, Xiao T, Zhang C, Nishida N, Springer TA (2008) Structure of a complete integrin ectodomain in a physiologic resting state and activation and deactivation by applied forces. *Mol Cell* 32: 849−861

Zhu J, Luo BH, Barth P, Schonbrun J, Baker D, Springer TA (2009) The structure of a receptor with two associating transmembrane domains on the cell surface: integrin αIIbβ3. *Mol Cell* 34: 234−249

Zhu J, Zhu J, Springer TA (2013) Complete integrin headpiece opening in eight steps. *J Cell Biol* 201: 1053−1068

Conformational Equilibria and Intrinsic Affinities Define Integrin Activation

Jing Li[1*], Yang Su[1*], Wei Xia[1], Yan Qin[1], Martin Humphries[2], Dietmar Vestweber[3], Carlos Cabañas[4], Chafen Lu[1] and Timothy A. Springer[1]

[1]Program in Cellular and Molecular Medicine, Boston Children's Hospital and Department of Biological Chemistry and Molecular Pharmacology, Harvard Medical School, 3 Blackfan Circle, Boston, MA 02115

[2]Wellcome Trust Centre for Cell-Matrix Research, Faculty of Life Sciences, University of Manchester, M13 9PT, United Kingdom

[3]Max-Planck-Institute of Molecular Biomedicine, Germany

[4]Centro de Biología Molecular Severo Ochoa (CSIC-UAM), 28049 Madrid, Spain

Corresponding author:

Dr. Timothy A. Springer, Program in Cellular and Molecular Medicine at Boston Children's Hospital

Department of Biological Chemistry and Molecular Pharmacology, Harvard Medical School

3 Blackfan Circle, 3rd Floor, Room 3103, Boston, MA 02115

(617) 713-8200, Fax: (617) 713-8232

timothy.springer@childrens.harvard.edu

[*]Equal contribution

Contents

Materials and Methods

Materials

hTERT-BJ cells were a gift from Dr. Robert A. Weinberg (Whitehead Institute for Biomedical Research). Mouse anti-human antibodies J143 (4th International Workshop on Leukocytes), SAM-1 (5th International Workshop on Leukocytes), #481709 (R&D Systems), LM142 (EMD Millipore) and TS2/4 [1] were from the indicated sources. FITC-conjugated goat anti-mouse IgG was purchased from Sigma. α_5 specific blocking antibody mAb16 was purified from hybridoma provided to us by Dr. Kenneth M. Yamada. α_4 specific antibody Natalizumab was from commercial source.

Negative stain electron microscopy (EM)

EM specimen preparation, data collection and processing were as described [2].

Isothermal titration calorimetry (ITC)

ITC was performed in buffer containing 20 mM Tris (pH 7.4), 150 mM NaCl, 1 mM $CaCl_2$ and 1 mM $MgCl_2$ at 25 °C with 20 injections (2 μL each) on MicroCal iTC200. Data were fit to the one-site binding model [3] in OriginPro 7.

Protein and carbohydrate composition

Unclasped $\alpha_5\beta_1$ ectodomain with shaved (30 μg), high-mannose (60 μg), and complex (30 μg) N-glycans were separately loaded on an Agilent liquid chromatography system equipped with a TSKgel BioAssist G4SWXL analytical size exclusion column (Tosoh Bioscience), a DAWN HELEOS II multi-angle light scattering detector, an Optilab T-rEX refractive index detector and a variable wavelength UV detector (Wyatt Technology Corporation). Data were processed in ASTRA 6 using the protein conjugate model ($dn/dc = 0.185$ and 0.145 for protein and carbohydrate components, respectively) [4].

Staining integrin subunits on cell surface

Surface expression of integrin α_3-, α_5-, α_8- and α_V-subunits on K562, HEK293 and hTERT-BJ cells was quantified by immuno-staining. β_1 integrins with the latter three α-subunits bind ligands containing the Arg-Gly-Asp (RGD) motif [5]. Cells (10^6/mL in PBS supplemented with 50 mg/mL BSA and 1 mg/mL Na_3N) were incubated on ice with 50 μg/mL human IgG for 20 min to block Fc-receptors, then incubated with 2.5 μg/mL primary antibodies J143 (anti-α_3), SAM-1 (anti-α_5), #481709 (anti-α_8), LM142 (anti-α_V) or TS2/4 (anti-α_L) for 30 min, followed by 3 washes. Cells were then incubated with 2 μg/mL FITC-conjugated goat anti-mouse IgG for 30 min, followed by 3 washes, and subjected to flow cytometry (BD FACSCanto II). Staining lymphocyte integrin subunit α_L was a negative control.

Quantitative comparison of α_5-, α_4- and β_1 subunit expression levels on K562 and Jurkat cells was the same as described about except that cells were only incubated with 3.75 μg/mL Alexa647-conjugated primary antibodies before subject to washing and flow cytometry.

Supplementary Text

EC_{50} or affinity of Fabs for $\alpha_5\beta_1$ and Eqs. S1–S11

For soluble $\alpha_5\beta_1$ ectodomain or headpiece proteins, 20 nM $\alpha_5\beta_1$ (or 100 nM $\alpha_5\beta_1$ with closure-stabilizing Fabs) were equilibrated with 0–10,000 nM of Fabs for 2 hr. The mixture was then incubated with 5 nM

FITC-cRGD for 2 hr, and FP was measured. Fab-binding was reported by changes in FP. For intact $\alpha_5\beta_1$, K562 cells (2×10^6 cells/mL) were incubated with 10 nM Alexa488-Fn$_{9-10}$ and 0–100,000 nM of Fabs for 1.5 hr and subjecting to flow cytometry. Fab-binding was reported by changes in mean fluorescence intensity (MFI).

For determining EC_{50} values for extension-stabilizing and open-stabilizing Fabs, we made the assumption that the increase in FP was directly proportional to the increase in concentration of Fab-bound open $\alpha_5\beta_1$. This assumption is reasonable because the affinity of the EO conformation is so much higher than that of the BC and EC conformations for cRGD. Therefore, data were fit to a dose response curve:

$$FP_{\text{obs}} = FP_0 + \frac{FP_{\text{sat}} - FP_0}{EC_{50}/[\text{Fab}]_{\text{tot}} + 1} \tag{S1}$$

$$MFI_{\text{obs}} = \frac{MFI_{\text{sat}}}{EC_{50}/[\text{Fab}]_{\text{tot}} + 1} \tag{S2}$$

where FP_0 is the FP without added Fab, FP_{sat} and MFI_{sat} are plateau values of FP and MFI, respectively, at high Fab concentration, and EC_{50} is the Fab concentration at the inflection point where half-maximum change in FP or MFI was observed. The Fab's K_d for $\alpha_5\beta_1$ is approximated by EC_{50}.

In the case of closure-stabilizing Fabs where $\alpha_5\beta_1$ was used at a high concentration in the assay, EC_{50} significantly deviates from K_d due to depletion of Fab and FITC-cRGD. Therefore, we wrote equations S3-S10 as described below, and fit data to Eq. S11 below. In the assay, FITC-cRGD and its complex with $\alpha_5\beta_1$ free of Fab were the major sources of FP_{obs}; the $\alpha_5\beta_1$·Fab complex essentially does not bind FITC-cRGD due to its extremely low affinity, which was evident in Fig. 2 and Fig. S1 where at high concentrations of closure-stabilizing Fab, FP_{obs} dropped to the value of free FITC-cRGD (0.09). Experimentally, $\alpha_5\beta_1$ was at 100 nM and cRGD was at 5 nM; in experiments to determine Fab K_d (Fig. S1) most of the FP signal was due to cRGD bound to the open $\alpha_5\beta_1$ conformation. Because the observed decrease in FP was due to Fab-binding to $\alpha_5\beta_1$ and stabilizing it in the closed conformation, we first wrote the equations for Fab-binding to $\alpha_5\beta_1$ and then considered the effect on $\alpha_5\beta_1$ binding to cRGD:

$$\alpha_5\beta_1 + \text{Fab} \rightleftharpoons \alpha_5\beta_1\text{·Fab} \qquad K_d^{\text{ens(Basal):Fab}} = \frac{[\alpha_5\beta_1]'[\text{Fab}]}{[\alpha_5\beta_1\text{·Fab}]} \tag{S3}$$

$$[\alpha_5\beta_1]_{\text{tot}} = [\alpha_5\beta_1]' + [\alpha_5\beta_1\text{·Fab}] \tag{S4}$$

$$[\text{Fab}]_{\text{tot}} = [\text{Fab}] + [\alpha_5\beta_1\text{·Fab}] \tag{S5}$$

where $K_d^{\text{ens(Basal):Fab}}$ is Fab's K_d for $\alpha_5\beta_1$, $[\alpha_5\beta_1]_{\text{tot}}$ and $[\text{Fab}]_{\text{tot}}$ are total concentrations of $\alpha_5\beta_1$ (100 nM) and closure-stabilizing Fab in the assay, respectively; $[\alpha_5\beta_1]'$ is the concentration of Fab-free $\alpha_5\beta_1$ at equilibrium. In the following equations, we make the reasonable assumption that only Fab-free $\alpha_5\beta_1$ contributes to the FP signal:

$$\alpha_5\beta_1 + \text{L} \rightleftharpoons \alpha_5\beta_1\text{·L} \qquad K_d^{\text{ens(Basal):L}} = \frac{[\alpha_5\beta_1][\text{L}]}{[\alpha_5\beta_1\text{·L}]} \tag{S6}$$

3

$$[\alpha_5\beta_1]' = [\alpha_5\beta_1] + [\alpha_5\beta_1 \cdot L] \tag{S7}$$

$$[L]_{tot} = [L] + [\alpha_5\beta_1 \cdot L] \tag{S8}$$

where $[L]_{tot}$ is the total concentration of FITC-cRGD (5 nM); $[\alpha_5\beta_1]$ is the concentration of free $\alpha_5\beta_1$ in the final mixture, and $K_d^{ens(Basal):L}$ is the affinity of $\alpha_5\beta_1$ for FITC-cRGD in the absence of Fabs, which was measured separately in a saturation binding assay (next section).

Solve Eq. S3–S8 for $[\alpha_5\beta_1 \cdot L]$:

$$[\alpha_5\beta_1]' = \frac{[\alpha_5\beta_1]_{tot} - [Fab]_{tot} - K_d^{ens(Basal):Fab} + \sqrt{\left([\alpha_5\beta_1]_{tot} + [Fab]_{tot} + K_d^{ens(Basal):Fab}\right)^2 - 4[\alpha_5\beta_1]_{tot}[Fab]_{tot}}}{2} \tag{S9}$$

$$[\alpha_5\beta_1 \cdot L] = \frac{[\alpha_5\beta_1]' + [L]_{tot} + K_d^{ens(Basal):L} - \sqrt{\left([\alpha_5\beta_1]' + [L]_{tot} + K_d^{ens(Basal):L}\right)^2 - 4[\alpha_5\beta_1]'[L]_{tot}}}{2} \tag{S10}$$

Therefore

$$FP_{obs} = \frac{[L]}{[L]_{tot}} \cdot FP_L + \frac{[\alpha_5\beta_1 \cdot L]}{[L]_{tot}} \cdot FP_{\alpha_5\beta_1 \cdot L} \tag{6}$$

$$= \frac{[L]_{tot} - [\alpha_5\beta_1 \cdot L]}{[L]_{tot}} \cdot FP_L + \frac{[\alpha_5\beta_1 \cdot L]}{[L]_{tot}} \cdot FP_{\alpha_5\beta_1 \cdot L} = FP_L + \frac{[\alpha_5\beta_1 \cdot L]}{[L]_{tot}} \cdot \left(FP_{\alpha_5\beta_1 \cdot L} - FP_L\right)$$

$$= FP_L + \frac{[\alpha_5\beta_1]' + [L]_{tot} + K_d^{ens(Basal):L} - \sqrt{\left([\alpha_5\beta_1]' + [L]_{tot} + K_d^{ens(Basal):L}\right)^2 - 4[\alpha_5\beta_1]'[L]_{tot}}}{2[L]_{tot}} \cdot \left(FP_{\alpha_5\beta_1 \cdot L} - FP_L\right)$$

$$\tag{S11}$$

where FP_L and $FP_{\alpha_5\beta_1 \cdot L}$ are FP of free FITC-cRGD and $\alpha_5\beta_1 \cdot$FITC-cRGD complex, respectively; $[\alpha_5\beta_1]'$ is defined in Eq. S9. Fitting the FP_{obs} and $[Fab]_{tot}$ data to Eq. S11 yielded $K_d^{ens(Basal):Fab}$, FP_L and $FP_{\alpha_5\beta_1 \cdot L}$.

Affinity of $\alpha_5\beta_1$ for ligand or for 12G10 Fab from saturation binding and Eqs. S12–S17

For soluble $\alpha_5\beta_1$ ectodomain or headpiece proteins, 0.1–10,000 nM $\alpha_5\beta_1$ were incubated with 5 nM FITC-cRGD or FITC-RGD ligand for 2 hr (24 hr in the presence of 12G10 Fab to reach equilibrium). Binding of FITC-cRGD or FITC-RGD was measured as FP. For intact $\alpha_5\beta_1$, K562 cells (2×10^6 cells/mL) were incubated with 0.1–100 nM Alexa488-Fn$_{9-10}$ or Alexa488-12G10 Fab for 1.5 hr and subjected to flow cytometry. Binding of Alexa488-Fn$_{9-10}$ or Alexa488-12G10 was measured as mean fluorescence intensity (MFI). Using L to denote the fluorescent ligand or 12G10 Fab, at equilibrium:

$$\alpha_5\beta_1 + L \rightleftharpoons \alpha_5\beta_1 \cdot L \qquad K_d^{app} = \frac{[\alpha_5\beta_1][L]}{[\alpha_5\beta_1 \cdot L]} \tag{S12}$$

$$[\alpha_5\beta_1]_{tot} = [\alpha_5\beta_1] + [\alpha_5\beta_1 \cdot L] \tag{S13}$$

$$[L]_{tot} = [L] + [\alpha_5\beta_1 \cdot L] \tag{S14}$$

where $[\alpha_5\beta_1]_{tot}$ is the total concentration of soluble $\alpha_5\beta_1$ in solution or total amount of $\alpha_5\beta_1$ on cell surface, $[L]_{tot}$ is the total concentration of the fluorescent ligand or 12G10 Fab, and K_d^{app} is the apparent binding affinity of $\alpha_5\beta_1$ for ligand or 12G10 (defined in Eq. S47).

4

Solve Eq. S12–S14 for $[\alpha_5\beta_1\cdot L]$:

$$[\alpha_5\beta_1\cdot L] = \frac{[L]_{tot} + K_d^{app} + [\alpha_5\beta_1]_{tot} - \sqrt{\left([L]_{tot} + K_d^{app} + [\alpha_5\beta_1]_{tot}\right)^2 - 4[L]_{tot}[\alpha_5\beta_1]_{tot}}}{2} \tag{S15}$$

Therefore, the measured FP (FP_{obs}) or MFI (MFI_{obs}) are

$$FP_{obs} = \frac{[L]}{[L]_{tot}} \cdot FP_L + \frac{[\alpha_5\beta_1\cdot L]}{[L]_{tot}} \cdot FP_{\alpha_5\beta_1\cdot L} \tag{6}$$

$$= \frac{[L]_{tot} - [\alpha_5\beta_1\cdot L]}{[L]_{tot}} \cdot FP_L + \frac{[\alpha_5\beta_1\cdot L]}{[L]_{tot}} \cdot FP_{\alpha_5\beta_1\cdot L} = FP_L + \frac{[\alpha_5\beta_1\cdot L]}{[L]_{tot}} \cdot \left(FP_{\alpha_5\beta_1\cdot L} - FP_L\right)$$

$$= FP_L + \frac{[L]_{tot} + K_d^{app} + [\alpha_5\beta_1]_{tot} - \sqrt{\left([L]_{tot} + K_d^{app} + [\alpha_5\beta_1]_{tot}\right)^2 - 4[L]_{tot}[\alpha_5\beta_1]_{tot}}}{2[L]_{tot}} \cdot \left(FP_{\alpha_5\beta_1\cdot L} - FP_L\right) \tag{S16}$$

$$MFI_{obs} = \frac{[\alpha_5\beta_1\cdot L]}{[\alpha_5\beta_1]_{tot}} \cdot MFI_{max}$$

$$= \frac{[L]_{tot} + K_d^{app} + [\alpha_5\beta_1]_{tot} - \sqrt{\left([L]_{tot} + K_d^{app} + [\alpha_5\beta_1]_{tot}\right)^2 - 4[L]_{tot}[\alpha_5\beta_1]_{tot}}}{2[\alpha_5\beta_1]_{tot}} \cdot MFI_{max} \tag{S17}$$

where FP_L and $FP_{\alpha_5\beta_1\cdot L}$ are FP of free and $\alpha_5\beta_1$-bound FITC-cRGD or FITC-RGD, respectively, and MFI_{max} is the MFI when all $\alpha_5\beta_1$ on cell surface are bound with Alexa488-Fn3$_{9-10}$ or Alexa488-12G10.

Fitting the FP_{obs} and $[\alpha_5\beta_1]_{tot}$ data to Eq. S16 yielded K_d^{app}, FP_L and $FP_{\alpha_5\beta_1\cdot L}$. Fitting the MFI_{obs} and $[L]_{tot}$ data to Eq. S17 yielded K_d^{app} and MFI_{max}.

<u>Affinity of intact $\alpha_5\beta_1$ for Fn3$_{9-10}$ and Eqs. S18–S26</u>
K562 cells (2×10^6 cells/mL) were equilibrated with 1–10,000 nM Fn3$_{9-10}$ for 1.5 hr, followed by incubation with 0.4 nM Alexa488-12G10 Fab for 1.5 hr, and were subjected to flow cytometry. Both 12G10 and Fn3$_{9-10}$ stabilize the extended-open conformation. Alexa488-12G10 was used at a low concentration of 0.4 nM such that it did not show detectable binding to K562 cells in the absence of Fn3$_{9-10}$ and could be used to report stabilization by Fn3$_{9-10}$ of $\alpha_5\beta_1$ in the open conformation, which was only detectable at Fn3$_{9-10}$ concentrations above 100 nM. Therefore, we described reporting of the Fn3$_{9-10}$-stabilized conformation of $\alpha_5\beta_1$ by changes in mean fluorescence intensity (MFI) of Alexa488-12G10 using the following equations in which Fn3$_{9-10}$ is denoted as L and Alexa488-12G10 is denoted as Fab:

$$\alpha_5\beta_1 + L \rightleftharpoons \alpha_5\beta_1\cdot L \qquad K_d^{ens(Basal):L} = \frac{[\alpha_5\beta_1]'[L]}{[\alpha_5\beta_1\cdot L]} \tag{S18}$$

$$[\alpha_5\beta_1]_{tot} = [\alpha_5\beta_1] + [\alpha_5\beta_1\cdot L]' \tag{S19}$$

$$[L]_{tot} = [L] + [\alpha_5\beta_1\cdot L]' \tag{S20}$$

where $[\alpha_5\beta_1]_{tot}$ is the total amount of $\alpha_5\beta_1$ on cell surface, $[L]_{tot}$ is the total concentration of Fn3$_{9-10}$ in the assay, $[\alpha_5\beta_1\cdot L]'$ is the concentration of $\alpha_5\beta_1\cdot$Fn3$_{9-10}$ complex at equilibrium, and $K_d^{ens(Basal):L}$ is the affinity

for Fn3$_{9-10}$.

$$\alpha_5\beta_1 \cdot L + Fab \rightleftharpoons \alpha_5\beta_1 \cdot L \cdot Fab \qquad K_d^{EO:Fab} = \frac{[\alpha_5\beta_1 \cdot L][Fab]}{[\alpha_5\beta_1 \cdot L \cdot Fab]} \tag{S21}$$

$$[\alpha_5\beta_1 \cdot L]' = [\alpha_5\beta_1 \cdot L] + [\alpha_5\beta_1 \cdot L \cdot Fab] \tag{S22}$$

$$[Fab]_{tot} = [Fab] + [\alpha_5\beta_1 \cdot L \cdot Fab] \tag{S23}$$

where $[Fab]_{tot}$ is the total concentration of Alexa488-12G10 (0.4 nM); $[\alpha_5\beta_1 \cdot L]$ is the final concentration of Alexa488-12G10-free $\alpha_5\beta_1 \cdot Fn3_{9-10}$ complex in the final mixture, and $K_d^{EO:Fab}$ is the affinity of $\alpha_5\beta_1 \cdot Fn3_{9-10}$ complex (in the extended-open conformation) for Alexa488-12G10, which was measured separately in a saturation binding assay (previous section).

Solve Eq. S18–S23 for $[\alpha_5\beta_1 \cdot L \cdot Fab]$:

$$[\alpha_5\beta_1 \cdot L]' = \frac{[\alpha_5\beta_1]_{tot} + [L]_{tot} + K_d^{ens(Basal):L} - \sqrt{\left([\alpha_5\beta_1]_{tot} + [L]_{tot} + K_d^{ens(Basal):L}\right)^2 - 4[\alpha_5\beta_1]_{tot}[L]_{tot}}}{2} \tag{S24}$$

$$[\alpha_5\beta_1 \cdot L \cdot Fab] = \frac{[\alpha_5\beta_1 \cdot L]' + [Fab]_{tot} + K_d^{EO:Fab} - \sqrt{\left([\alpha_5\beta_1 \cdot L]' + [Fab]_{tot} + K_d^{EO:Fab}\right)^2 - 4[\alpha_5\beta_1 \cdot L]'[Fab]_{tot}}}{2} \tag{S25}$$

Therefore, the measured MFI (MFI_{obs}) is

$$MFI_{obs} = \frac{[\alpha_5\beta_1 \cdot L \cdot Fab]}{[\alpha_5\beta_1]_{tot}} \cdot MFI_{max}$$

$$= \frac{[\alpha_5\beta_1 \cdot L]' + [Fab]_{tot} + K_d^{EO:Fab} - \sqrt{\left([\alpha_5\beta_1 \cdot L]' + [Fab]_{tot} + K_d^{EO:Fab}\right)^2 - 4[\alpha_5\beta_1 \cdot L]'[Fab]_{tot}}}{2[\alpha_5\beta_1]_{tot}} \cdot MFI_{max} \tag{S26}$$

where MFI_{max} is the MFI when all $\alpha_5\beta_1$ on cell surface is bound to Alexa488-12G10.

Fitting the MFI_{obs} and $[L]_{tot}$ to Eq. S26 yielded $K_d^{ens(Basal):L}$ and MFI_{max}.

Affinity of $\alpha_5\beta_1$ ectodomain for Fn3$_{9-10}$ from competitive binding and Eqs. S27–S28

$\alpha_5\beta_1$ ectodomain affinities for Fn3$_{9-10}$ was measured by using Fn3$_{9-10}$ to compete binding of FITC-cRGD peptide ligand. $\alpha_5\beta_1$ ectodomain (270 nM in the absence of Fabs, 20 nM in the presence of HUTS4 Fab, 90 nM in the presence of 8E3 Fab, or 70–10,000 nM in the presence of mAb13 Fab or mAb13 plus 9EG7 Fabs) was equilibrated with 0–10,000 nM Fn3$_{9-10}$ (competitor) for 2 hr. The mixture was incubated with 5 nM FITC-cRGD (ligand) for 2 hr, and FP was measured.

Since only $\alpha_5\beta_1$ free of Fn3$_{9-10}$ could bind FITC-cRGD, the equations are identical to those for binding affinities for closure-stabilizing Fabs (Eq. S3–S11). Substituting Fab with C (for competitor) in Eq. S9 and S11:

$$[\alpha_5\beta_1]' = \frac{[\alpha_5\beta_1]_{tot} - [C]_{tot} - K_d^{app:C} + \sqrt{\left([\alpha_5\beta_1]_{tot} + [C]_{tot} + K_d^{app:C}\right)^2 - 4[\alpha_5\beta_1]_{tot}[C]_{tot}}}{2} \tag{S27}$$

$$FP_{obs} = FP_L + \frac{[\alpha_5\beta_1]' + [L]_{tot} + K_d^{app:L} - \sqrt{\left([\alpha_5\beta_1]' + [L]_{tot} + K_d^{app:L}\right)^2 - 4[\alpha_5\beta_1]'[L]_{tot}}}{2[L]_{tot}} \cdot \left(FP_{\alpha_5\beta_1 \cdot L} - FP_L\right) \tag{S28}$$

6

where FP_obs is the measured FP; FP_L and $FP_{\alpha_5\beta_1\cdot\text{L}}$ are FP of free FITC-cRGD and $\alpha_5\beta_1\cdot$FITC-cRGD complex, respectively; $[\alpha_5\beta_1]_\text{tot}$, $[\text{L}]_\text{tot}$ and $[\text{C}]_\text{tot}$ are total concentrations of $\alpha_5\beta_1$, FITC-cRGD ligand (5 nM) and Fn3$_{9-10}$ competitor in the assay, respectively; $[\alpha_5\beta_1]'$ is the concentration of Fn3$_{9-10}$-free $\alpha_5\beta_1$, either free of FITC-cRGD or with FITC-cRGD bound; $K_\text{d}^\text{app:C}$ and $K_\text{d}^\text{app:L}$ are apparent affinities of $\alpha_5\beta_1$ for Fn3$_{9-10}$ competitor and FITC-cRGD ligand, respectively.

For experiments in the absence of Fabs, or in the presence of HUTS4 or 8E3 Fab, fitting the FP_obs and $[\text{C}]_\text{tot}$ data to Eq. S28 using the $K_\text{d}^\text{app:L}$ value measured separately in a saturation binding assay yielded $K_\text{d}^\text{app:C}$, FP_L and $FP_{\alpha_5\beta_1\cdot\text{L}}$. For experiments in the presence of mAb13 Fab or mAb13 plus 9EG7 Fabs, global fitting of the FP_obs and $[\alpha_5\beta_1]_\text{tot}$ data at different fixed $[\text{C}]_\text{tot}$ to Eq. S28 yielded $K_\text{d}^\text{app:C}$, $K_\text{d}^\text{app:L}$, FP_L and $FP_{\alpha_5\beta_1\cdot\text{L}}$

Fab-binding affinities of $\alpha_5\beta_1$ conformational ensembles and Eqs. S29–S40
The basal ensemble (i.e., in the absence of Fabs) of intact $\alpha_5\beta_1$ on the cell surface or of its ectodomain fragment in solution comprises three overall conformational states—bent-closed (BC), extended-closed (EC), and extended-open (EO). Suppose a Fab binds (and thus stabilizes) one or more of the BC, EC and EO states in the basal ensemble to form BC·Fab, EC·Fab and/or EO·Fab complexes with intrinsic Fab-binding affinities K_a^BC, K_a^EC and/or K_a^EO, respectively:

$$\text{BC} + \text{Fab} \rightleftharpoons \text{BC·Fab} \qquad K_\text{a}^\text{BC} = \frac{[\text{BC·Fab}]}{[\text{BC}][\text{Fab}]} \tag{S29}$$

$$\text{EC} + \text{Fab} \rightleftharpoons \text{EC·Fab} \qquad K_\text{a}^\text{EC} = \frac{[\text{EC·Fab}]}{[\text{EC}][\text{Fab}]} \tag{S30}$$

$$\text{EO} + \text{Fab} \rightleftharpoons \text{EO·Fab} \qquad K_\text{a}^\text{EO} = \frac{[\text{EO·Fab}]}{[\text{EO}][\text{Fab}]} \tag{S31}$$

If the Fab does not bind a state i (i = BC, EC or EO), then $K_\text{a}^i = 0$ and $[i\cdot\text{Fab}] = 0$. For Fabs that bind two states i and j with equal affinities, i.e., $K_\text{a}^i = K_\text{a}^j$ (i = EC and j = EO for extension-stabilizing Fabs, i = BC and j = EC for closure-stabilizing Fabs), Fab-binding does not change the relative distribution of the two states:

$$\frac{[i\cdot\text{Fab}]}{[j\cdot\text{Fab}]} = \frac{K_\text{a}^i[i][\text{Fab}]}{K_\text{a}^j[j][\text{Fab}]} = \frac{[i]}{[j]} \tag{S32}$$

The experimentally measured affinity of the basal ensemble for Fab, $K_\text{a}^\text{ens(Basal)}$, is a probability-weighted average of K_a^BC, K_a^EC and K_a^EO:

$$
\begin{aligned}
K_\text{a}^\text{ens(Basal)} &= \frac{[\text{BC·Fab}] + [\text{EC·Fab}] + [\text{EO·Fab}]}{([\text{BC}] + [\text{EC}] + [\text{EO}])\,[\text{Fab}]} \\[2mm]
&= \frac{[\text{BC}]}{[\text{BC}] + [\text{EC}] + [\text{EO}]} \cdot \frac{[\text{BC·Fab}]}{[\text{BC}][\text{Fab}]} + \\[2mm]
&\quad \frac{[\text{EC}]}{[\text{BC}] + [\text{EC}] + [\text{EO}]} \cdot \frac{[\text{EC·Fab}]}{[\text{EC}][\text{Fab}]} + \\[2mm]
&\quad \frac{[\text{EO}]}{[\text{BC}] + [\text{EC}] + [\text{EO}]} \cdot \frac{[\text{EO·Fab}]}{[\text{EO}][\text{Fab}]} \\[2mm]
&= P^\text{BC} K_\text{a}^\text{BC} + P^\text{EC} K_\text{a}^\text{EC} + P^\text{EO} K_\text{a}^\text{EO}
\end{aligned}
\tag{S33}
$$

where P^{BC}, P^{EC} and P^{EO} are probabilities (populations) of the corresponding conformational states in the basal ensemble:

$$P^{BC} = \frac{[BC]}{[BC] + [EC] + [EO]} \tag{S34}$$

$$P^{EC} = \frac{[EC]}{[BC] + [EC] + [EO]} \tag{S35}$$

$$P^{EO} = \frac{[EO]}{[BC] + [EC] + [EO]} \tag{S36}$$

$$P^{BC} + P^{EC} + P^{EO} = 1 \tag{S37}$$

Because K_a^{BC}, K_a^{EC}, K_a^{EO}, P^{BC}, P^{EC} and P^{EO} are all constants of the equilibria in the ensemble, Eq. S33 shows that $K_a^{ens(Basal)}$ is a genuine equilibrium constant.

Binding affinity is often expressed as dissociation constant ($K_d = 1/K_a$) in the biological sciences to facilitate comparison to concentrations of the reactants. Following this convention, Eq. S33 can be rewritten as:

$$\frac{1}{K_d^{ens(Basal)}} = \frac{P^{BC}}{K_d^{BC}} + \frac{P^{EC}}{K_d^{EC}} + \frac{P^{EO}}{K_d^{EO}} \tag{S38}$$

The total probability (population) of all Fab-bound species in the ensemble is

$$\begin{aligned}
P^{\alpha_5\beta_1 \cdot Fab} &= \frac{[BC \cdot Fab] + [EC \cdot Fab] + [EO \cdot Fab]}{[BC] + [EC] + [EO] + [BC \cdot Fab] + [EC \cdot Fab] + [EO \cdot Fab]} \\
&= \frac{1}{\dfrac{[BC] + [EC] + [EO]}{[BC \cdot Fab] + [EC \cdot Fab] + [EO \cdot Fab]} + 1} \\
&= \frac{1}{K_d^{ens(Basal)} / [Fab] + 1} \tag{S39}
\end{aligned}$$

Eq. S39 shows that if the Fab concentration is sufficiently high such that $K_d^{ens(Basal)} / [Fab] \ll 1$, then $P^{\alpha_5\beta_1 \cdot Fab} \sim 1$ and the ensemble is dominated by the Fab-stabilized state(s).

For the $\alpha_5\beta_1$ headpiece, a similar analysis shows that at a sufficiently high concentration of Fab, the Fab-stabilized state dominates the ensemble.

In Eq. S39, [Fab] is the concentration of free Fab. In most experiments, Fabs are used at concentrations much higher than that of $\alpha_5\beta_1$; therefore, [Fab] can be approximated as the total Fab concentration minus the highest $\alpha_5\beta_1$ concentration used ($[Fab]_{tot} - [\alpha_5\beta_1]_{tot}$) in calculating $P^{\alpha_5\beta_1 \cdot Fab}$:
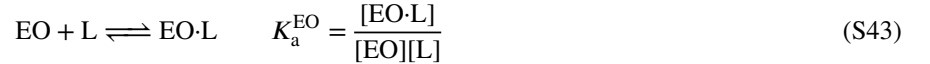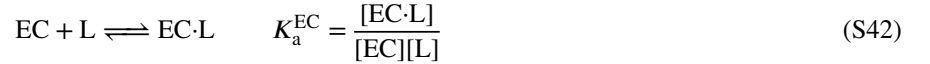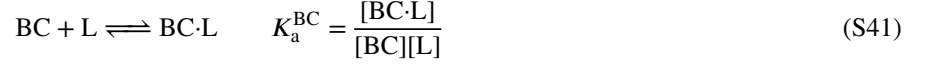
$$P^{\alpha_5\beta_1 \cdot Fab} = \frac{1}{K_d^{ens(Basal)} / \left([Fab]_{tot} - [\alpha_5\beta_1]_{tot}\right) + 1} \tag{S40}$$

<u>True ligand-binding affinities (K_d^{ens}) of $\alpha_5\beta_1$ conformational ensemble members and Eqs. S41–S72</u>
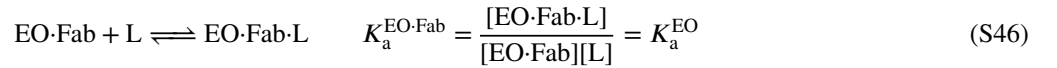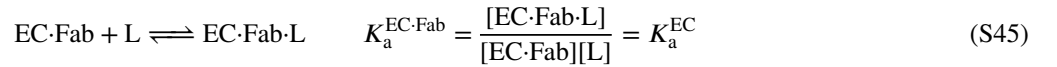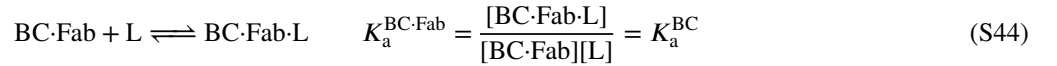
We now consider using Fabs to stabilize conformational ensembles in specific states. A complication is that in the absence of 100% binding of the Fab, unbound $\alpha_5\beta_1$ can exist in other states. We derive the equations for determining the contributions of both Fab-bound $\alpha_5\beta_1$ ($P^{\alpha_5\beta_1 \cdot Fab}$) and unbound $\alpha_5\beta_1$ ($1 - P^{\alpha_5\beta_1 \cdot Fab}$) to the measured apparent affinities (K_d^{app}). We show that under our experimental conditions, with open-stabilizing

and extension-stabilizing Fabs, $P^{\alpha_5\beta_1\cdot\mathrm{Fab}}$ is 95–99.6%, and $K_\mathrm{d}^\mathrm{app} \simeq K_\mathrm{d}^\mathrm{ens}$ (Fig. S2). With closure-stabilizing Fabs under our experimental conditions, $P^{\alpha_5\beta_1\cdot\mathrm{Fab}}$ is 99.8–99.9%, $K_\mathrm{d}^\mathrm{app}$ can differ from $K_\mathrm{d}^\mathrm{ens}$ (Fig. S2), and we use our derived equations to calculate true affinity, $K_\mathrm{d}^\mathrm{ens}$.

Intact $\alpha_5\beta_1$ or its ectodomain fragment contain three states in their conformational ensemble, BC, EC and EO. Suppose they bind a ligand, L, to form the BC·L, EC·L, and EO·L complexes with intrinsic ligand-binding affinity (association constants) K_a^BC, K_a^EC and K_a^EO, respectively:

$$\mathrm{BC} + \mathrm{L} \rightleftharpoons \mathrm{BC\cdot L} \qquad K_\mathrm{a}^\mathrm{BC} = \frac{[\mathrm{BC\cdot L}]}{[\mathrm{BC}][\mathrm{L}]} \tag{S41}$$

$$\mathrm{EC} + \mathrm{L} \rightleftharpoons \mathrm{EC\cdot L} \qquad K_\mathrm{a}^\mathrm{EC} = \frac{[\mathrm{EC\cdot L}]}{[\mathrm{EC}][\mathrm{L}]} \tag{S42}$$

$$\mathrm{EO} + \mathrm{L} \rightleftharpoons \mathrm{EO\cdot L} \qquad K_\mathrm{a}^\mathrm{EO} = \frac{[\mathrm{EO\cdot L}]}{[\mathrm{EO}][\mathrm{L}]} \tag{S43}$$

If a Fab is also present in the ensemble, then the Fab-bound state(s) BC·Fab, EC·Fab and/or EO·Fab can bind the ligand L to form BC·Fab·L, EC·Fab·L, and/or EO·Fab·L complexes with intrinsic ligand-binding affinity (association constants) $K_\mathrm{a}^\mathrm{BC\cdot Fab}$, $K_\mathrm{a}^\mathrm{EC\cdot Fab}$ and $K_\mathrm{a}^\mathrm{EO\cdot Fab}$, respectively. Suppose the Fab-bound $\alpha_5\beta_1$ states bind ligand with the same affinity as their corresponding native $\alpha_5\beta_1$ states (see main text for justification), then:

$$\mathrm{BC\cdot Fab} + \mathrm{L} \rightleftharpoons \mathrm{BC\cdot Fab\cdot L} \qquad K_\mathrm{a}^\mathrm{BC\cdot Fab} = \frac{[\mathrm{BC\cdot Fab\cdot L}]}{[\mathrm{BC\cdot Fab}][\mathrm{L}]} = K_\mathrm{a}^\mathrm{BC} \tag{S44}$$

$$\mathrm{EC\cdot Fab} + \mathrm{L} \rightleftharpoons \mathrm{EC\cdot Fab\cdot L} \qquad K_\mathrm{a}^\mathrm{EC\cdot Fab} = \frac{[\mathrm{EC\cdot Fab\cdot L}]}{[\mathrm{EC\cdot Fab}][\mathrm{L}]} = K_\mathrm{a}^\mathrm{EC} \tag{S45}$$

$$\mathrm{EO\cdot Fab} + \mathrm{L} \rightleftharpoons \mathrm{EO\cdot Fab\cdot L} \qquad K_\mathrm{a}^\mathrm{EO\cdot Fab} = \frac{[\mathrm{EO\cdot Fab\cdot L}]}{[\mathrm{EO\cdot Fab}][\mathrm{L}]} = K_\mathrm{a}^\mathrm{EO} \tag{S46}$$

If the Fab does not bind a state i (i = BC, EC or EO), then $[i\cdot\mathrm{Fab}] = 0$, $[i\cdot\mathrm{Fab\cdot L}] = 0$ and $K_\mathrm{a}^{i\cdot\mathrm{Fab}}$ is undefined.

Similarly to the earlier treatment of Fab-binding affinty (Eq. S33), it can be shown that the measured ligand-binding affinity of the ensemble, $K_\mathrm{a}^\mathrm{app}$, is ultimately a composite of intrinsic ligand-binding affinities:

$$\begin{aligned}
K_\mathrm{a}^\mathrm{app} &= \frac{[\mathrm{BC\cdot L}] + [\mathrm{EC\cdot L}] + [\mathrm{EO\cdot L}] + [\mathrm{BC\cdot Fab\cdot L}] + [\mathrm{EC\cdot Fab\cdot L}] + [\mathrm{EO\cdot Fab\cdot L}]}{([\mathrm{BC}] + [\mathrm{EC}] + [\mathrm{EO}] + [\mathrm{BC\cdot Fab}] + [\mathrm{EC\cdot Fab}] + [\mathrm{EO\cdot Fab}])\,[\mathrm{L}]} \\[2mm]
&= \frac{[\mathrm{BC}] + [\mathrm{EC}] + [\mathrm{EO}]}{[\mathrm{BC}] + [\mathrm{EC}] + [\mathrm{EO}] + [\mathrm{BC\cdot Fab}] + [\mathrm{EC\cdot Fab}] + [\mathrm{EO\cdot Fab}]} \cdot \frac{[\mathrm{BC\cdot L}] + [\mathrm{EC\cdot L}] + [\mathrm{EO\cdot L}]}{([\mathrm{BC}] + [\mathrm{EC}] + [\mathrm{EO}])\,[\mathrm{L}]} + \\[2mm]
&\quad \frac{[\mathrm{BC\cdot Fab}] + [\mathrm{EC\cdot Fab}] + [\mathrm{EO\cdot Fab}]}{[\mathrm{BC}] + [\mathrm{EC}] + [\mathrm{EO}] + [\mathrm{BC\cdot Fab}] + [\mathrm{EC\cdot Fab}] + [\mathrm{EO\cdot Fab}]} \cdot \frac{[\mathrm{BC\cdot Fab\cdot L}] + [\mathrm{EC\cdot Fab\cdot L}] + [\mathrm{EO\cdot Fab\cdot L}]}{([\mathrm{BC\cdot Fab}] + [\mathrm{EC\cdot Fab}] + [\mathrm{EO\cdot Fab}])\,[\mathrm{L}]} \\[2mm]
&= \left(1 - \frac{[\mathrm{BC\cdot Fab}] + [\mathrm{EC\cdot Fab}] + [\mathrm{EO\cdot Fab}]}{[\mathrm{BC}] + [\mathrm{EC}] + [\mathrm{EO}] + [\mathrm{BC\cdot Fab}] + [\mathrm{EC\cdot Fab}] + [\mathrm{EO\cdot Fab}]}\right) \cdot \frac{[\mathrm{BC\cdot L}] + [\mathrm{EC\cdot L}] + [\mathrm{EO\cdot L}]}{([\mathrm{BC}] + [\mathrm{EC}] + [\mathrm{EO}])\,[\mathrm{L}]} + \\[2mm]
&\quad \frac{[\mathrm{BC\cdot Fab}] + [\mathrm{EC\cdot Fab}] + [\mathrm{EO\cdot Fab}]}{[\mathrm{BC}] + [\mathrm{EC}] + [\mathrm{EO}] + [\mathrm{BC\cdot Fab}] + [\mathrm{EC\cdot Fab}] + [\mathrm{EO\cdot Fab}]} \cdot \frac{[\mathrm{BC\cdot Fab\cdot L}] + [\mathrm{EC\cdot Fab\cdot L}] + [\mathrm{EO\cdot Fab\cdot L}]}{([\mathrm{BC\cdot Fab}] + [\mathrm{EC\cdot Fab}] + [\mathrm{EO\cdot Fab}])\,[\mathrm{L}]} \\[2mm]
&= \left(1 - P^{\alpha_5\beta_1\cdot\mathrm{Fab}}\right) \cdot K_\mathrm{a}^\mathrm{ens(Basal)} + P^{\alpha_5\beta_1\cdot\mathrm{Fab}} \cdot K_\mathrm{a}^\mathrm{ens(Fab\text{-}stabilized\ states)}
\end{aligned} \tag{S47}$$

where $P^{\alpha_5\beta_1\cdot\text{Fab}}$ is defined in Eq. S39, $K_a^{\text{ens(Basal)}}$ and $K_a^{\text{ens(Fab-stabilized states)}}$, as follows, are ligand-binding affinities of the basal ensemble and the ensemble of all Fab-stabilized state(s), respectively:

$$K_a^{\text{ens(Basal)}} = \frac{[\text{BC·L}] + [\text{EC·L}] + [\text{EO·L}]}{([\text{BC}] + [\text{EC}] + [\text{EO}])\,[\text{L}]}$$

$$= \frac{[\text{BC}]}{[\text{BC}] + [\text{EC}] + [\text{EO}]} \cdot \frac{[\text{BC·L}]}{[\text{BC}][\text{L}]} +$$

$$\frac{[\text{EC}]}{[\text{BC}] + [\text{EC}] + [\text{EO}]} \cdot \frac{[\text{EC·L}]}{[\text{EC}][\text{L}]} +$$

$$\frac{[\text{EO}]}{[\text{BC}] + [\text{EC}] + [\text{EO}]} \cdot \frac{[\text{EO·L}]}{[\text{EO}][\text{L}]}$$

$$= P^{\text{BC}} K_a^{\text{BC}} + P^{\text{EC}} K_a^{\text{EC}} + P^{\text{EO}} K_a^{\text{EO}} \tag{S48}$$

$$K_a^{\text{ens(Fab-stabilized states)}} = \frac{[\text{BC·Fab·L}] + [\text{EC·Fab·L}] + [\text{EO·Fab·L}]}{([\text{BC·Fab}] + [\text{EC·Fab}] + [\text{EO·Fab}])\,[\text{L}]}$$

$$= \frac{[\text{BC·Fab}]}{[\text{BC·Fab}] + [\text{EC·Fab}] + [\text{EO·Fab}]} \cdot \frac{[\text{BC·Fab·L}]}{[\text{BC·Fab}][\text{L}]} +$$

$$\frac{[\text{EC·Fab}]}{[\text{BC·Fab}] + [\text{EC·Fab}] + [\text{EO·Fab}]} \cdot \frac{[\text{EC·Fab·L}]}{[\text{EC·Fab}][\text{L}]} +$$

$$\frac{[\text{EO·Fab}]}{[\text{BC·Fab}] + [\text{EC·Fab}] + [\text{EO·Fab}]} \cdot \frac{[\text{EO·Fab·L}]}{[\text{EO·Fab}][\text{L}]}$$

$$= P^{\text{BC·Fab}} K_a^{\text{BC}} + P^{\text{EC·Fab}} K_a^{\text{EC}} + P^{\text{EO·Fab}} K_a^{\text{EO}} \tag{S49}$$

where the probabilities P^{BC}, P^{EC} and P^{EO} are defined in Eq. S34–S36, the intrinsic ligand-binding affinities K_a^{BC}, K_a^{EC} and K_a^{EO} are defined in Eq. S41–S43, and the probabilities $P^{\text{BC·Fab}}$, $P^{\text{EC·Fab}}$ and $P^{\text{EO·Fab}}$ are as follows:

$$P^{\text{BC·Fab}} = \frac{[\text{BC·Fab}]}{[\text{BC·Fab}] + [\text{EC·Fab}] + [\text{EO·Fab}]} \tag{S50}$$

$$P^{\text{EC·Fab}} = \frac{[\text{EC·Fab}]}{[\text{BC·Fab}] + [\text{EC·Fab}] + [\text{EO·Fab}]} \tag{S51}$$

$$P^{\text{EO·Fab}} = \frac{[\text{EO·Fab}]}{[\text{BC·Fab}] + [\text{EC·Fab}] + [\text{EO·Fab}]} \tag{S52}$$

$$P^{\text{BC·Fab}} + P^{\text{EC·Fab}} + P^{\text{EO·Fab}} = 1 \tag{S53}$$

Eq. S47 can be rewritten using dissociation constants:

$$\frac{1}{K_d^{\text{app}}} = \frac{1 - P^{\alpha_5\beta_1\cdot\text{Fab}}}{K_d^{\text{ens(Basal)}}} + \frac{P^{\alpha_5\beta_1\cdot\text{Fab}}}{K_d^{\text{ens(Fab-stabilized states)}}} \tag{S54}$$

In the absence of Fabs (i.e., $P^{\alpha_5\beta_1\cdot\text{Fab}} = 0$), Eq. S54 degenerates to $K_d^{\text{app}} = K_d^{\text{ens(Basal)}}$, which confirms the obvious fact that, in the absence of Fabs, the basal ensemble's ligand-binding affinity $K_d^{\text{ens(Basal)}}$ is

10

determined experimentally. By separately accounting for the contributions to K_d^app of $\alpha_5\beta_1$ both bound to Fab ($P^{\alpha_5\beta_1\cdot\text{Fab}}$) and not bound to Fab ($1 - P^{\alpha_5\beta_1\cdot\text{Fab}}$), we may calculate true affinities of Fab-stabilized individual states (K_d^EC and K_d^EO) or ensembles of two states ($K_\text{d}^\text{ens(BC+EC)}$ and $K_\text{d}^\text{ens(EC+EO)}$). In other words, K_d^app determined in the presence of Fabs, together with $K_\text{d}^\text{ens(Basal)}$ and $P^{\alpha_5\beta_1\cdot\text{Fab}}$ (see previous section and Table S1), can be used to calculate $K_\text{d}^\text{ens(Fab-stabilized states)}$ by solving Eq. S54:

$$K_\text{d}^\text{ens(Fab-stabilized states)} = \frac{P^{\alpha_5\beta_1\cdot\text{Fab}} K_\text{d}^\text{ens(Basal)} K_\text{d}^\text{app}}{K_\text{d}^\text{ens(Basal)} - \left(1 - P^{\alpha_5\beta_1\cdot\text{Fab}}\right) K_\text{d}^\text{app}} \tag{S55}$$

Eq. S48–S49 can be rewritten using dissociation constants:

$$\frac{1}{K_\text{d}^\text{ens(Basal)}} = \frac{P^\text{BC}}{K_\text{d}^\text{BC}} + \frac{P^\text{EC}}{K_\text{d}^\text{EC}} + \frac{P^\text{EO}}{K_\text{d}^\text{EO}} \tag{S56}$$

$$\frac{1}{K_\text{d}^\text{ens(Fab-stabilized states)}} = \frac{P^\text{BC·Fab}}{K_\text{d}^\text{BC}} + \frac{P^\text{EC·Fab}}{K_\text{d}^\text{EC}} + \frac{P^\text{EO·Fab}}{K_\text{d}^\text{EO}} \tag{S57}$$

Eq. S56–S57 relate the measurables $K_\text{d}^\text{ens(Basal)}$ and $K_\text{d}^\text{ens(Fab-stabilized states)}$ to the probabilities (populations) and intrinsic ligand-binding affinities of each state in the basal ensemble, forming the basis for their calculation described in the next section. The rest of this section will examine specific cases of $K_\text{d}^\text{ens(Fab-stabilized states)}$ determined with different Fabs (Eq. S55).

Three-state ensembles
Open-stabilizing Fabs (O Fab) selectively stabilize the EO state, i.e., [BC·Fab] = 0 and [EC·Fab] = 0, hence $P^\text{BC·Fab} = 0$, $P^\text{EC·Fab} = 0$ and $P^\text{EO·Fab} = 1$ (from Eq. S50–S52). Therefore, $K_\text{d}^\text{ens(Fab-stabilized states)} = K_\text{d}^\text{EO}$ (from Eq. S57), and Eq. S55 becomes:

$$K_\text{d}^\text{EO} = \frac{P^{\alpha_5\beta_1\cdot\text{Fab}} K_\text{d}^\text{ens(Basal)} K_\text{d}^\text{app(O Fab)}}{K_\text{d}^\text{ens(Basal)} - \left(1 - P^{\alpha_5\beta_1\cdot\text{Fab}}\right) K_\text{d}^\text{app(O Fab)}} \approx K_\text{d}^\text{app(O Fab)} \tag{S58}$$

Fig. S2 shows that $P^{\alpha_5\beta_1\cdot\text{Fab}}$ was > 95% for all open-stabilizing Fab used here at concentrations shown in Table S1, and that $K_\text{d}^\text{app(O Fab)}$ is indistinguishable from K_d^EO; i.e., the difference between these quantities is smaller than the experimental error in K_d^EO.

Extension-stabilizing Fabs (E Fab) stabilize both EC and EO states, i.e., [BC·Fab] = 0. Denoting $K_\text{d}^\text{ens(Fab-stabilized states)}$ as $K_\text{d}^\text{ens(EC+EO)}$, Eq. S55 becomes:

$$K_\text{d}^\text{ens(EC+EO)} = \frac{P^{\alpha_5\beta_1\cdot\text{Fab}} K_\text{d}^\text{ens(Basal)} K_\text{d}^\text{app(E Fab)}}{K_\text{d}^\text{ens(Basal)} - \left(1 - P^{\alpha_5\beta_1\cdot\text{Fab}}\right) K_\text{d}^\text{app(E Fab)}} \approx K_\text{d}^\text{app(E Fab)} \tag{S59}$$

As in the case of open-stabilizing Fabs, Fig. S2 shows that $P^{\alpha_5\beta_1\cdot\text{Fab}}$ was > 95% for all extension-stabilizing Fab used here at concentrations shown in Table S1, and that $K_\text{d}^\text{app(E Fab)}$ is indistinguishable from $K_\text{d}^\text{ens(EC+EO)}$; i.e., the difference between these quantities is smaller than the experimental error in $K_\text{d}^\text{ens(EC+EO)}$.

From Eq. S50–S52, S32 and S35–S36:

$$P^\text{BC·Fab} = 0 \tag{S60}$$

$$P^{\text{EC·Fab}} = \frac{[\text{EC·Fab}]}{[\text{EC·Fab}] + [\text{EO·Fab}]} = \frac{[\text{EC}]}{[\text{EC}] + [\text{EO}]} = \frac{P^{\text{EC}}}{P^{\text{EC}} + P^{\text{EO}}} \tag{S61}$$

$$P^{\text{EO·Fab}} = \frac{[\text{EO·Fab}]}{[\text{EC·Fab}] + [\text{EO·Fab}]} = \frac{[\text{EO}]}{[\text{EC}] + [\text{EO}]} = \frac{P^{\text{EO}}}{P^{\text{EC}} + P^{\text{EO}}} \tag{S62}$$

Thus, from Eq. S57:

$$\frac{1}{K_d^{\text{ens(EC+EO)}}} = \frac{P^{\text{EC}}}{P^{\text{EC}} + P^{\text{EO}}} \cdot \frac{1}{K_d^{\text{EC}}} + \frac{P^{\text{EO}}}{P^{\text{EC}} + P^{\text{EO}}} \cdot \frac{1}{K_d^{\text{EO}}} \tag{S63}$$

Closure-stabilizing Fabs (C Fab) stabilize both BC and EC states, i.e., [EO·Fab] = 0. Denoting $K_d^{\text{ens(Fab-stabilized states)}}$ as $K_d^{\text{ens(BC+EC)}}$, Eq. S55 becomes:

$$K_d^{\text{ens(BC+EC)}} = \frac{P^{\alpha_5\beta_1\cdot\text{Fab}} K_d^{\text{ens(Basal)}} K_d^{\text{app(C Fab)}}}{K_d^{\text{ens(Basal)}} - \left(1 - P^{\alpha_5\beta_1\cdot\text{Fab}}\right) K_d^{\text{app(C Fab)}}} \tag{S64}$$

Fig. S2 shows that $P^{\alpha_5\beta_1\cdot\text{Fab}}$ was around 99.8–99.9% for all closure-stabilizing Fab used here at concentrations shown in Table S1, and that $K_d^{\text{app(C Fab)}}$ is appreciably different from $K_d^{\text{ens(BC+EC)}}$. Therefore, $K_d^{\text{ens(BC+EC)}}$ was calculated from $P^{\alpha_5\beta_1\cdot\text{Fab}}$, $K_d^{\text{ens(Basal)}}$ and $K_d^{\text{app(C Fab)}}$ using Eq. S64.

From Eq. S50–S52, S32 and S34–S35:

$$P^{\text{BC·Fab}} = \frac{[\text{BC·Fab}]}{[\text{BC·Fab}] + [\text{EC·Fab}]} = \frac{[\text{BC}]}{[\text{BC}] + [\text{EC}]} = \frac{P^{\text{BC}}}{P^{\text{BC}} + P^{\text{EC}}} \tag{S65}$$

$$P^{\text{EC·Fab}} = \frac{[\text{EC·Fab}]}{[\text{BC·Fab}] + [\text{EC·Fab}]} = \frac{[\text{EC}]}{[\text{BC}] + [\text{EC}]} = \frac{P^{\text{EC}}}{P^{\text{BC}} + P^{\text{EC}}} \tag{S66}$$

$$P^{\text{EO·Fab}} = 0 \tag{S67}$$

Thus, from Eq. S57:

$$\frac{1}{K_d^{\text{ens(BC+EC)}}} = \frac{P^{\text{BC}}}{P^{\text{BC}} + P^{\text{EC}}} \cdot \frac{1}{K_d^{\text{BC}}} + \frac{P^{\text{EC}}}{P^{\text{BC}} + P^{\text{EC}}} \cdot \frac{1}{K_d^{\text{EC}}} \tag{S68}$$

Extension-stabilizing Fab plus closure-stabilizing Fab (E+C Fabs) selectively stabilize the EC state, i.e., [BC·Fab] = 0 and [EO·Fab] = 0, hence $P^{\text{BC·Fab}} = 0$, $P^{\text{EC·Fab}} = 1$ and $P^{\text{EO·Fab}} = 0$ (from Eq. S50–S52). Therefore, $K_d^{\text{ens(Fab-stabilized states)}} = K_d^{\text{EC}}$ (from Eq. S57), and Eq. S55 becomes:

$$K_d^{\text{EC}} = \frac{P^{\alpha_5\beta_1\cdot\text{Fab}} K_d^{\text{ens(Basal)}} K_d^{\text{app(E+C Fabs)}}}{K_d^{\text{ens(Basal)}} - \left(1 - P^{\alpha_5\beta_1\cdot\text{Fab}}\right) K_d^{\text{app(E+C Fabs)}}} \tag{S69}$$

Two-state ensembles

For $\alpha_5\beta_1$ headpiece, the basal ensemble comprises only two overall conformational states: closed (C) and open (O). Similar analysis shows that the ensemble's ligand-binding affinity is (using dissociation constants):

$$\frac{1}{K_d^{\text{ens(Basal; HP)}}} = \frac{P^{\text{C}}}{K_d^{\text{C}}} + \frac{P^{\text{O}}}{K_d^{\text{O}}} \tag{S70}$$

where K_d^{C}, K_d^{O}, P^{C} and P^{O} are intrinsic ligand-binding affinities and probabilities (populations) of the closed and open headpiece conformations, respectively.

Open-stabilizing Fabs (O Fab) selectively stabilize the open headpiece. Therefore,

12

$$K_\text{d}^\text{ens(Fab-stabilized states)} = K_\text{d}^\text{O} \text{ and}$$

$$K_\text{d}^\text{O} = \frac{P^{\alpha_5\beta_1\cdot\text{Fab}} K_\text{d}^\text{ens(Basal; HP)} K_\text{d}^\text{app(O Fab)}}{K_\text{d}^\text{ens(Basal; HP)} - \left(1 - P^{\alpha_5\beta_1\cdot\text{Fab}}\right) K_\text{d}^\text{app(O Fab)}} \approx K_\text{d}^\text{app(O Fab)} \tag{S71}$$

$P^{\alpha_5\beta_1\cdot\text{Fab}}$ was 98.2% for the open-stabilizing Fab 12G10 used here at 2000 nM (Table S1), and Fig. S2 shows that $K_\text{d}^\text{app(O Fab)}$ is indistinguishable from K_d^O; i.e., the difference between these quantities is smaller than the experimental error in K_d^O.

Closure-stabilizing Fabs (C Fab) selectively stabilize the closed headpiece. Therefore, $K_\text{d}^\text{ens(Fab-stabilized states)} = K_\text{d}^\text{C}$ and

$$K_\text{d}^\text{C} = \frac{P^{\alpha_5\beta_1\cdot\text{Fab}} K_\text{d}^\text{ens(Basal; HP)} K_\text{d}^\text{app(C Fab)}}{K_\text{d}^\text{ens(Basal; HP)} - \left(1 - P^{\alpha_5\beta_1\cdot\text{Fab}}\right) K_\text{d}^\text{app(C Fab)}} \approx K_\text{d}^\text{app(C Fab)} \tag{S72}$$

Fig. S2 shows that $P^{\alpha_5\beta_1\cdot\text{Fab}}$ was > 99.8% for all closure-stabilizing Fab used here at concentrations shown in Table S1, and that $K_\text{d}^\text{app(C Fab)}$ is indistinguishable from K_d^C; i.e., the difference between these quantities is smaller than the experimental error in K_d^C.

Calculation of probability of each conformational state and Eqs. S73–S77

The experimentally determined ligand-binding affinities $K_\text{d}^\text{ens(Basal)}$ (measured in the absence of Fab), K_d^EO (Eq. S58), $K_\text{d}^\text{ens(EC+EO)}$ (Eq. S59) and K_d^EC (Eq. S69) relate to the probabilities P^BC, P^EC and P^EO through Eq. S56 and S63, which are repeated here for convenience:

$$\frac{1}{K_\text{d}^\text{ens(Basal)}} = \frac{P^\text{BC}}{K_\text{d}^\text{BC}} + \frac{P^\text{EC}}{K_\text{d}^\text{EC}} + \frac{P^\text{EO}}{K_\text{d}^\text{EO}} \tag{S56 revisited}$$

$$\frac{1}{K_\text{d}^\text{ens(EC+EO)}} = \frac{P^\text{EC}}{P^\text{EC} + P^\text{EO}} \cdot \frac{1}{K_\text{d}^\text{EC}} + \frac{P^\text{EO}}{P^\text{EC} + P^\text{EO}} \cdot \frac{1}{K_\text{d}^\text{EO}} \tag{S63 revisited}$$

In addition, the measured $K_\text{d}^\text{ens(BC+EC)}$ (Eq. S64) and K_d^EC are virtually indistinguishable, suggesting that $K_\text{d}^\text{BC} \simeq K_\text{d}^\text{EC} \simeq K_\text{d}^\text{ens(BC+EC)}$. Therefore, K_d^BC and K_d^EC are approximated by $K_\text{d}^\text{ens(BC+EC)}$. Since $K_\text{d}^\text{ens(BC+EC)}$ is much larger than $K_\text{d}^\text{ens(Basal)}$, $K_\text{d}^\text{ens(EC+EO)}$ and K_d^EO, this approximation and the relatively large uncertainty in $K_\text{d}^\text{ens(BC+EC)}$ have no impact on the calculated probabilities (Fig. S2).

Solve these equations for the probabilities, noting that $P^\text{BC} + P^\text{EC} + P^\text{EO} = 1$ (Eq. S37):

$$P^\text{EO} = \frac{K_\text{d}^\text{EO}\left(K_\text{d}^\text{ens(BC+EC)} - K_\text{d}^\text{ens(Basal)}\right)}{K_\text{d}^\text{ens(Basal)}\left(K_\text{d}^\text{ens(BC+EC)} - K_\text{d}^\text{EO}\right)} \tag{S73}$$

$$P^\text{EC} = \frac{K_\text{d}^\text{ens(BC+EC)}\left(K_\text{d}^\text{ens(BC+EC)} - K_\text{d}^\text{ens(Basal)}\right)\left(K_\text{d}^\text{ens(EC+EO)} - K_\text{d}^\text{EO}\right)}{K_\text{d}^\text{ens(Basal)}\left(K_\text{d}^\text{ens(BC+EC)} - K_\text{d}^\text{EO}\right)\left(K_\text{d}^\text{ens(BC+EC)} - K_\text{d}^\text{ens(EC+EO)}\right)} \tag{S74}$$

$$P^{\text{BC}} = \frac{K_d^{\text{ens(BC+EC)}}\left(K_d^{\text{ens(Basal)}} - K_d^{\text{ens(EC+EO)}}\right)}{K_d^{\text{ens(Basal)}}\left(K_d^{\text{ens(BC+EC)}} - K_d^{\text{ens(EC+EO)}}\right)} \tag{S75}$$

Likewise, for $\alpha_5\beta_1$ headpiece

$$P^{\text{O}} = \frac{K_d^{\text{O}}\left(K_d^{\text{C}} - K_d^{\text{ens(Basal; HP)}}\right)}{K_d^{\text{ens(Basal; HP)}}\left(K_d^{\text{C}} - K_d^{\text{O}}\right)} \tag{S76}$$

$$P^{\text{C}} = \frac{K_d^{\text{C}}\left(K_d^{\text{ens(Basal; HP)}} - K_d^{\text{O}}\right)}{K_d^{\text{ens(Basal; HP)}}\left(K_d^{\text{C}} - K_d^{\text{O}}\right)} \tag{S77}$$

Calculation of free energy of each conformational state and Eqs. S78–S84

Using EO as the reference state ($\Delta G^{\text{EO}} = 0$), the relative free energies of the BC and EC states, ΔG^{BC} and ΔG^{EC}, are related to the probabilities (populations) P^{BC}, P^{EC} and P^{EO} through the Boltzmann distribution (as also shown in Fig. 1C):

$$P^{\text{BC}} = \frac{1}{Q}\exp\left(-\frac{\Delta G^{\text{BC}}}{RT}\right) \tag{S78}$$

$$P^{\text{EC}} = \frac{1}{Q}\exp\left(-\frac{\Delta G^{\text{EC}}}{RT}\right) \tag{S79}$$

$$P^{\text{EO}} = \frac{1}{Q} \tag{S80}$$

$$Q = 1 + \exp\left(-\frac{\Delta G^{\text{BC}}}{RT}\right) + \exp\left(-\frac{\Delta G^{\text{EC}}}{RT}\right) \tag{S81}$$

where Q is known as the partition function.

Solve Eq. S78–S81 for ΔG^{BC} and ΔG^{EC}, and substituting P^{BC}, P^{EC} and P^{EO} with Eq. S73–S75:

$$\Delta G^{\text{BC}} = -RT \ln\left(\frac{P^{\text{BC}}}{P^{\text{EO}}}\right) = -RT \ln \frac{K_d^{\text{ens(BC+EC)}}\left(K_d^{\text{ens(BC+EC)}} - K_d^{\text{EO}}\right)\left(K_d^{\text{ens(Basal)}} - K_d^{\text{ens(EC+EO)}}\right)}{K_d^{\text{EO}}\left(K_d^{\text{ens(BC+EC)}} - K_d^{\text{ens(Basal)}}\right)\left(K_d^{\text{ens(BC+EC)}} - K_d^{\text{ens(EC+EO)}}\right)} \tag{S82}$$

$$\Delta G^{\text{EC}} = -RT \ln\left(\frac{P^{\text{EC}}}{P^{\text{EO}}}\right) = -RT \ln \frac{K_d^{\text{ens(BC+EC)}}\left(K_d^{\text{ens(EC+EO)}} - K_d^{\text{EO}}\right)}{K_d^{\text{EO}}\left(K_d^{\text{ens(BC+EC)}} - K_d^{\text{ens(EC+EO)}}\right)} \tag{S83}$$

Likewise, for $\alpha_5\beta_1$ headpiece, using O as the reference state ($\Delta G^{\text{O}} = 0$)

$$\Delta G^{\text{C}} = -RT \ln\left(\frac{P^{\text{C}}}{P^{\text{O}}}\right) = -RT \ln \frac{K_d^{\text{C}}\left(K_d^{\text{ens(Basal; HP)}} - K_d^{\text{O}}\right)}{K_d^{\text{O}}\left(K_d^{\text{C}} - K_d^{\text{ens(Basal; HP)}}\right)} \tag{S84}$$

14

Calculation of free energies associated with conformational changes and Eqs. S85–S94

$\alpha_5\beta_1$ activation is associated with ectodomain extension and headpiece opening. These two types of conformational changes are not necessarily separate, independent steps; nor must they occur in a predefined order, allowing the conformational change among the three integrin states to be defined as from one state to another, or as interchange between one state and two other states. Indeed, we have previously described scenarios for different orders of steps [7], and movies show how headpiece opening may either follow or precede extension (Supplemental Movies EV1–EV3). States such as bent-open may also be possible (Movie EV3); however, since these states have never been visualized by electron microscopy or small-angle X-ray scattering, their populations must be small, and thus the presence of their populations in the numerator or denominator of K_{conf} (defined below) has little effect on K_{conf} values.

Extension from BC to EC defines $K_{\text{conf}}^{\text{E}}$ and its associated free energy $\Delta G_{\text{conf}}^{\text{E}}$:

$$\text{BC} \rightleftharpoons \text{EC} \qquad K_{\text{conf}}^{\text{E}} = \frac{[\text{EC}]}{[\text{BC}]} = \frac{P^{\text{EC}}}{P^{\text{BC}}} \tag{S85}$$

$$\Delta G_{\text{conf}}^{\text{E}} = -RT \ln K_{\text{conf}}^{\text{E}} = -RT \ln \frac{P^{\text{EC}}}{P^{\text{BC}}} = -RT \ln \frac{\left(K_{\text{d}}^{\text{ens(BC+EC)}} - K_{\text{d}}^{\text{ens(Basal)}}\right)\left(K_{\text{d}}^{\text{ens(EC+EO)}} - K_{\text{d}}^{\text{EO}}\right)}{\left(K_{\text{d}}^{\text{ens(BC+EC)}} - K_{\text{d}}^{\text{EO}}\right)\left(K_{\text{d}}^{\text{ens(Basal)}} - K_{\text{d}}^{\text{ens(EC+EO)}}\right)} \tag{S86}$$

Opening from EC to EO defines $K_{\text{conf}}^{\text{O}}$ and its associated free energy $\Delta G_{\text{conf}}^{\text{O}}$:

$$\text{EC} \rightleftharpoons \text{EO} \qquad K_{\text{conf}}^{\text{O}} = \frac{[\text{EO}]}{[\text{EC}]} = \frac{P^{\text{EO}}}{P^{\text{EC}}} \tag{S87}$$

$$\Delta G_{\text{conf}}^{\text{O}} = -RT \ln K_{\text{conf}}^{\text{O}} = -RT \ln \frac{P^{\text{EO}}}{P^{\text{EC}}} = -RT \ln \frac{K_{\text{d}}^{\text{ens(BC+EC)}} - K_{\text{d}}^{\text{EO}}}{K_{\text{d}}^{\text{EO}}\left(K_{\text{d}}^{\text{ens(BC+EC)}} - K_{\text{d}}^{\text{ens(EC+EO)}}\right)} \tag{S88}$$

With these definitions, $\Delta G_{\text{conf}}^{\text{E}}$ and $\Delta G_{\text{conf}}^{\text{O}}$ sum to $-\Delta G^{\text{BC}}$.

Alternatively, extension from BC to either EC or EO defines $K_{\text{conf}}^{\text{E tot}}$ and its associated free energy $\Delta G_{\text{conf}}^{\text{E tot}}$:

$$\left.\begin{array}{c} \text{BC} \rightleftharpoons \text{EC} \\[1em] \text{BC} \rightleftharpoons \text{EO} \end{array}\right\} \quad K_{\text{conf}}^{\text{E tot}} = \frac{[\text{EC}] + [\text{EO}]}{[\text{BC}]} = \frac{P^{\text{EC}} + P^{\text{EO}}}{P^{\text{BC}}} \tag{S89}$$

$$\Delta G_{\text{conf}}^{\text{E tot}} = -RT \ln K_{\text{conf}}^{\text{E tot}} = -RT \ln \frac{P^{\text{EC}} + P^{\text{EO}}}{P^{\text{BC}}} = -RT \ln \frac{K_{\text{d}}^{\text{ens(BC+EC)}}\left(K_{\text{d}}^{\text{ens(Basal)}} - K_{\text{d}}^{\text{ens(EC+EO)}}\right)}{K_{\text{d}}^{\text{ens(EC+EO)}}\left(K_{\text{d}}^{\text{ens(BC+EC)}} - K_{\text{d}}^{\text{ens(Basal)}}\right)} \tag{S90}$$

Extension-and-opening from either BC or EC to EO defines $K_{\text{conf}}^{\text{Activation}}$ and its associated free energy $\Delta G_{\text{conf}}^{\text{Activation}}$:

$$\left.\begin{array}{c} \text{BC} \rightleftharpoons \text{EO} \\[1em] \text{EC} \rightleftharpoons \text{EO} \end{array}\right\} \quad K_{\text{conf}}^{\text{Activation}} = \frac{[\text{EO}]}{[\text{BC}] + [\text{EC}]} = \frac{P^{\text{EO}}}{P^{\text{BC}} + P^{\text{EC}}} \tag{S91}$$

$$\Delta G_{\text{conf}}^{\text{Activation}} = -RT \ln K_{\text{conf}}^{\text{Activation}} = -RT \ln \frac{P^{\text{EO}}}{P^{\text{BC}} + P^{\text{EC}}} = -RT \ln \frac{K_{\text{d}}^{\text{EO}}\left(K_{\text{d}}^{\text{ens(BC+EC)}} - K_{\text{d}}^{\text{ens(Basal)}}\right)}{K_{\text{d}}^{\text{ens(BC+EC)}}\left(K_{\text{d}}^{\text{ens(Basal)}} - K_{\text{d}}^{\text{EO}}\right)} \tag{S92}$$

For $\alpha_5\beta_1$ headpiece, the only conformational change is opening from C to O, which defines $K_{\text{conf}}^{\text{O; HP}}$ and its associated free energy $\Delta G_{\text{conf}}^{\text{O; HP}}$:

$$\text{C} \rightleftharpoons \text{O} \qquad K_{\text{conf}}^{\text{O; HP}} = \frac{[\text{O}]}{[\text{C}]} = \frac{P^{\text{O}}}{P^{\text{C}}} \tag{S93}$$

$$\Delta G_{\text{conf}}^{\text{O; HP}} = -RT \ln K_{\text{conf}}^{\text{O; HP}} = -RT \ln \frac{P^{\text{O}}}{P^{\text{C}}} = -RT \ln \frac{K_{\text{d}}^{\text{O}}\left(K_{\text{d}}^{\text{C}} - K_{\text{d}}^{\text{ens(Basal; HP)}}\right)}{K_{\text{d}}^{\text{C}}\left(K_{\text{d}}^{\text{ens(Basal; HP)}} - K_{\text{d}}^{\text{O}}\right)} \tag{S94}$$

Supplemental References

1. Huang, C., and Springer, T.A. (1997). Folding of the β-propeller domain of the integrin α_L subunit is independent of the I domain and dependent on the β_2 subunit. Proc Natl Acad Sci U S A *94*, 3162–3167.

2. Su, Y., Xia, W., Li, J., Walz, T., Humphries, M.J., Vestweber, D., Cabañas, C., Lu, C., and Springer, T.A. (2016). Relating conformation to function in integrin $\alpha_5\beta_1$. Proc Natl Acad Sci U S A. 3. Freyer, M.W., and Lewis, E.A. (2008). Isothermal titration calorimetry: experimental design, data analysis, and probing macromolecule/ligand binding and kinetic interactions. Methods Cell Biol *84*, 79–113.

4. Babul, J., and Stellwagen, E. (1969). Measurement of protein concentration with interferences optics. Anal Biochem *28*, 216–221.

5. Mohri, H. (1996). Fibronectin and integrins interactions. J Investig Med *44*, 429-441.

6. Rossi, A.M., and Taylor, C.W. (2011). Analysis of protein-ligand interactions by fluorescence polarization. Nat Protoc *6*, 365–387.

7. Takagi, J., Petre, B.M., Walz, T. and Springer, T.A. (2002). Global conformational rearrangements in integrin extracellular domains in outside-in and inside-out signaling. Cell *110*, 5, 599–611.
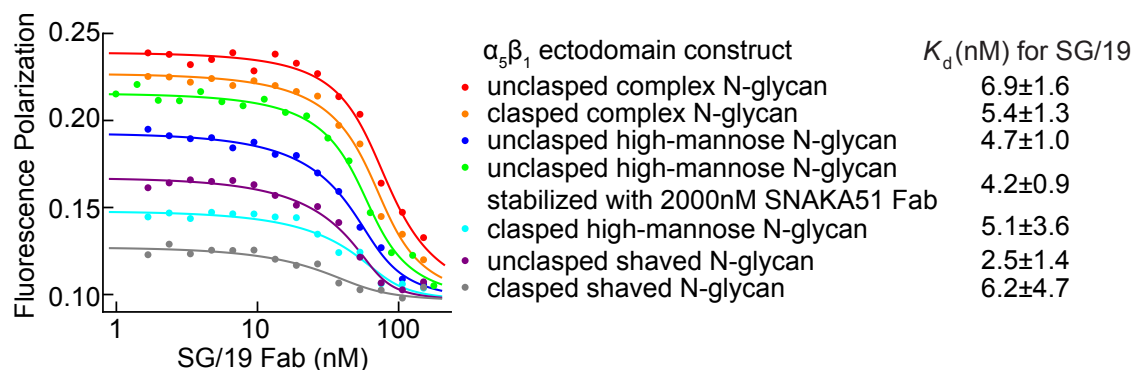
Supplemental Figures

Fig. S1. Affinities of SG/19 Fab for $\alpha_5\beta_1$ ectodomain preparations.

Binding of closure-stabilizing Fab SG/19 to $\alpha_5\beta_1$ (100 nM) influenced binding of FITC-cRGD (5 nM) to $\alpha_5\beta_1$ as monitored by FP. K_d values were obtained from fitting the FP data to Eq. S11. Errors are fitting errors from triplicates.
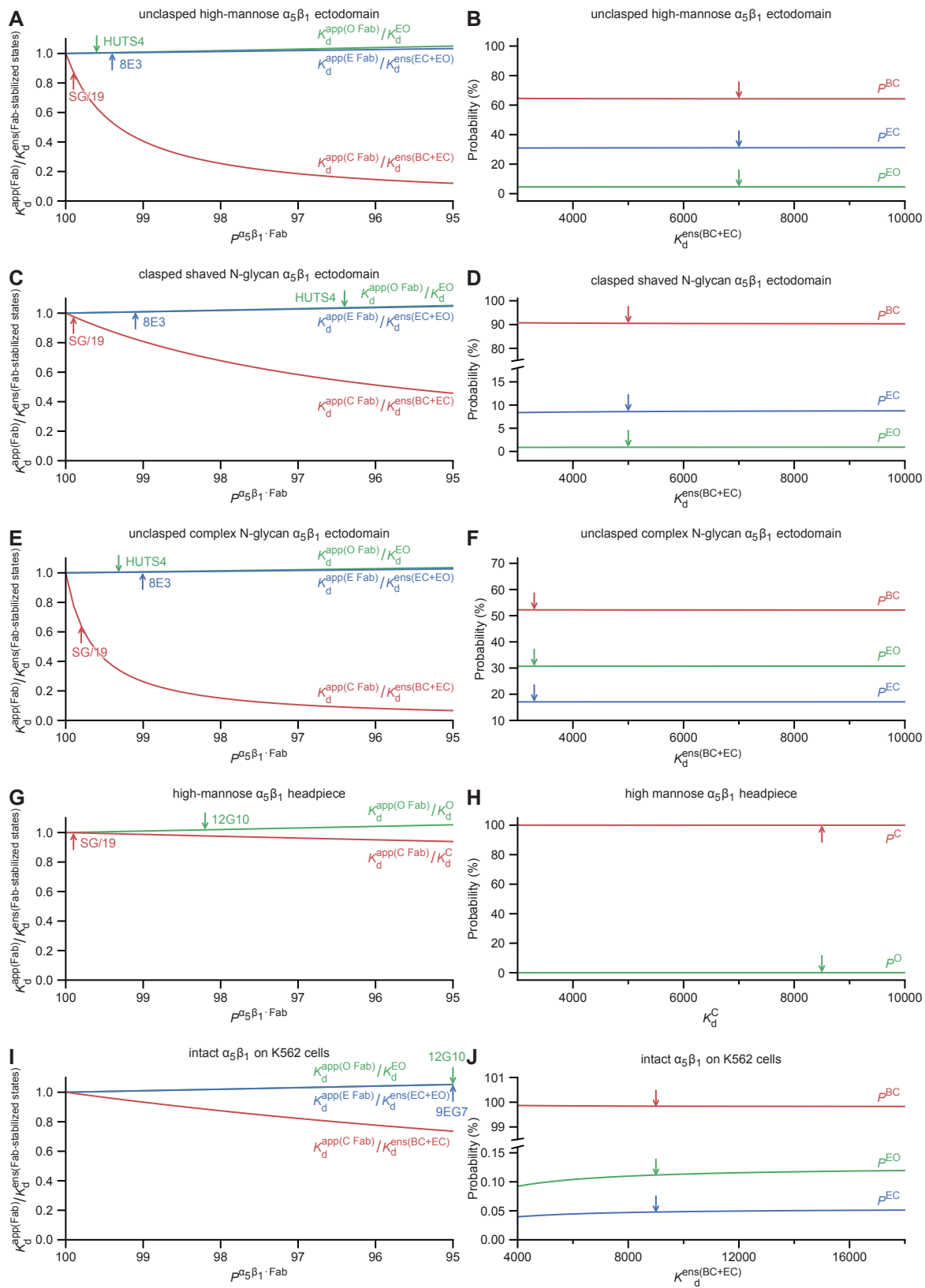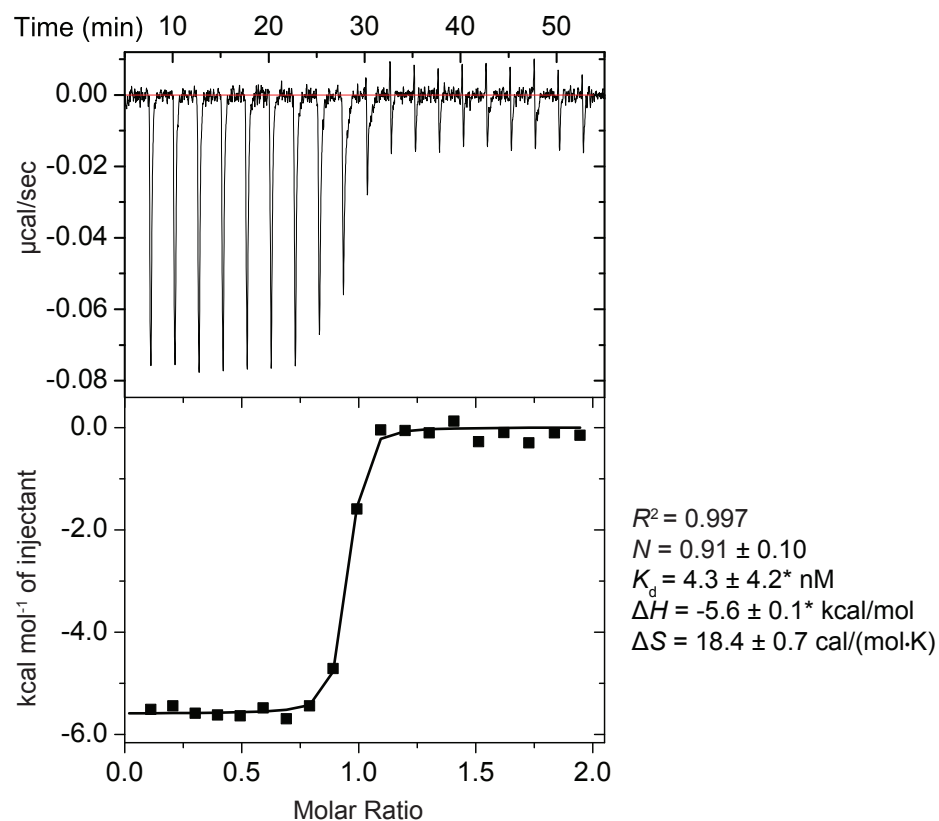
Fig. S2. Accuracy in determination of the thermodynamic parameters in α₅β₁ ensembles.
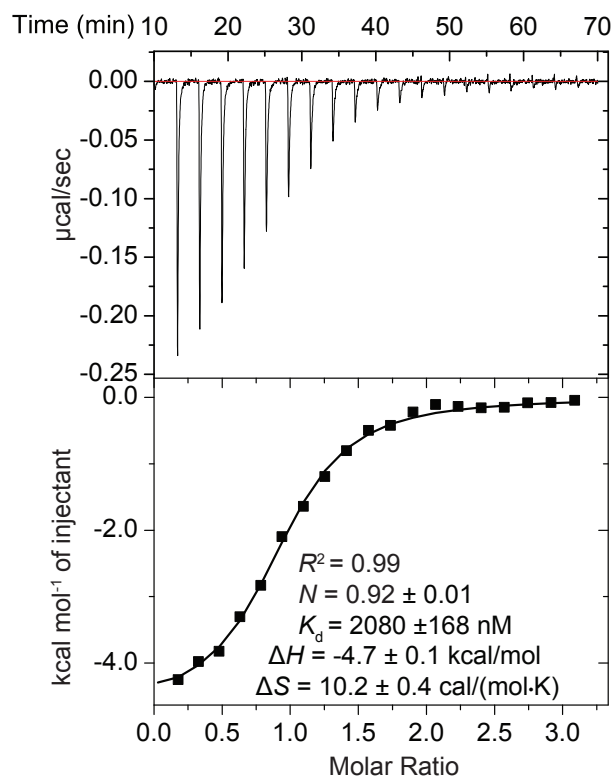(A, C, E, G and I) The ratio of apparent ligand-binding affinity in the presence of Fabs ($K_\mathrm{d}^{\mathrm{app(Fab)}}$) to that

of the ensemble comprising Fab-stabilized states only ($K_d^{\text{ens(Fab-stabilized states)}}$, Eq. S55) plotted against the fraction of Fab-bound $\alpha_5\beta_1$ ($P^{\alpha_5\beta_1 \cdot \text{Fab}}$). The plots were made with experimental values of $K_d^{\text{ens(Basal)}}$ and $K_d^{\text{ens(Fab-stabilized states)}}$, except $K_d^{\text{ens(BC+EC)}}$ for intact $\alpha_5\beta_1$ on K562 cells is estimated from K_d^{EO} using the same fold-difference as found with Fn3$_{9-10}$ for the $\alpha_5\beta_1$ ectodomain (Fig. 4D). Arrows show $P^{\alpha_5\beta_1 \cdot \text{Fab}}$ values under the experimental conditions used with the indicated Fabs (Table S1). (B, D, F, H and J) Lack of sensitivity of the probability of each conformational state on the ensemble affinity of closed states ($K_d^{\text{ens(BC+EC)}}$). Plots were made from Eq. S73–S75, using experimental values of K_d^{EO}, $K_d^{\text{ens(EC+EO)}}$ and $K_d^{\text{ens(Basal)}}$. Arrows show experimental values of $K_d^{\text{ens(BC+EC)}}$ (or K_d^{C} for the headpiece). (A and B) Unclasped high-mannose N-glycan $\alpha_5\beta_1$ ectodomain. (C and D) Clasped shaved N-glycan $\alpha_5\beta_1$ ectodomain. (E and F) Unclasped complex N-glycan $\alpha_5\beta_1$ ectodomain. (G and H) High-mannose $\alpha_5\beta_1$ headpiece. (I and J) Intact $\alpha_5\beta_1$ on K562 cells. Although curves are not shown for all $\alpha_5\beta_1$ ectodomain, headpiece, and semi-truncated constructs, their curves are identical or intermediate between the examples shown here. Thus, the headpiece and semi-truncated construct have identical curves, and require the highest Fab concentrations for opening. Among ectodomains, the clasped shaved and the unclasped complex N-glycan ectodomains require the most and least energy to activate ($\Delta G_{\text{conf}}^{\text{Activation}}$), respectively.

A   8E3 Fab titrate high-mannose $\alpha_5\beta_1$ headpiece

R^2 = 0.997
N = 0.91 ± 0.10
K_d = 4.3 ± 4.2* nM
ΔH = -5.6 ± 0.1* kcal/mol
ΔS = 18.4 ± 0.7 cal/(mol·K)

B
RGD titrate unclasped high-mannose $\alpha_5\beta_1$ ectodomain

R^2 = 0.99
N = 0.92 ± 0.01
K_d = 2080 ±168 nM
ΔH = -4.7 ± 0.1 kcal/mol
ΔS = 10.2 ± 0.4 cal/(mol·K)

C
RGD titrate unclasped high-mannose $\alpha_5\beta_1$ ecto-
domain in the presence of open-stabilizing Fab

R^2 = 0.99
N = 1.1 ± 0.1
K_d = 68 ± 25 nM
ΔH = -5.2 ± 0.4 kcal/mol
ΔS = 15.3 ± 1.5 cal/(mol·K)

20

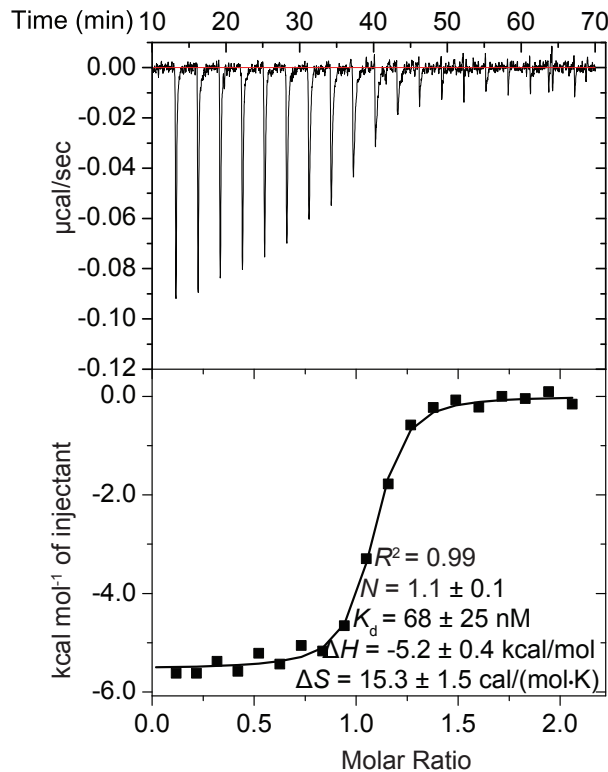**Fig. S3. Affinity of 8E3 Fab and RGD peptide for $\alpha_5\beta_1$ preparations by ITC.**
(A) $10\,\mu$M $\alpha_5\beta_1$ titrated with $100\,\mu$M 8E3 Fab. (B) $25\,\mu$M $\alpha_5\beta_1$ titrated with $375\,\mu$M RGD peptide. (C) $10\,\mu$M $\alpha_5\beta_1$ titrated with $100\,\mu$M RGD peptide in the presence of $20\,\mu$M open-stabilizing Fab HUTS4. Data were fit to the one-site binding model (Freyer and Lewis, 2008) in OriginPro 7. Errors with "*" are s.d. from three independent measurements. Binding entropy ΔS was calculated from $\Delta G = RT \ln K_\mathrm{d} = \Delta H - T\Delta S$ and errors were propagated. Other errors without "*" are fitting errors.
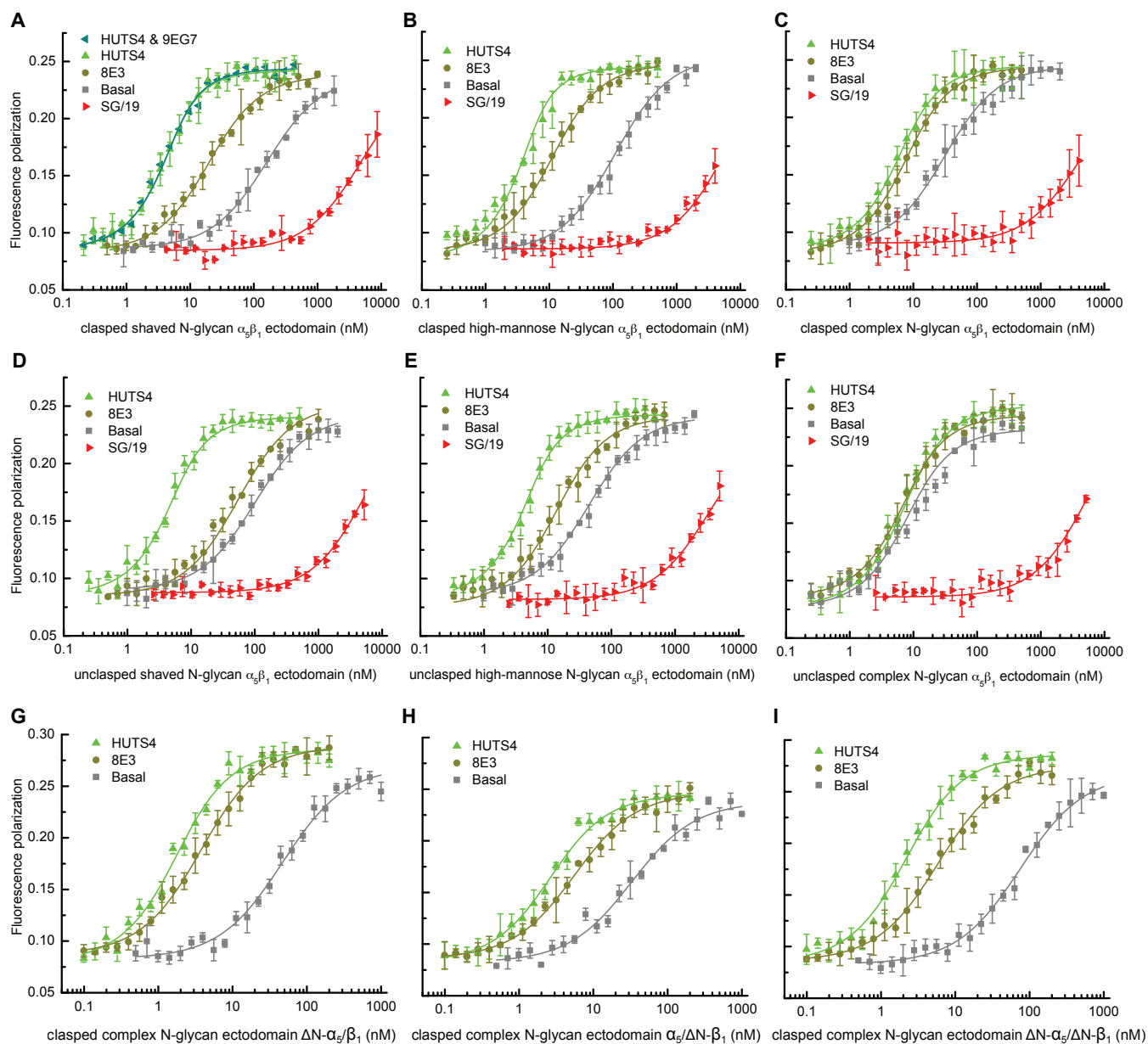
Fig. S4. Intrinsic and ensemble affinities of $\alpha_5\beta_1$ preparations for cRGD.
Clasped (A–C) and unclasped (D–F) $\alpha_5\beta_1$ ectodomain with shaved (A and D), high-mannose (B and E) and complex (C and F) N-glycans. (G–I) Clasped complex N-glycan $\alpha_5\beta_1$ ectodomain glycosylation site mutants ΔN-α_5/β_1 (G), α_5/ΔN-β_1 (H) and ΔN-α_5/ΔN-β_1 (I). Binding was measured in the absence of Fabs, or in the presence of 5 µM open-stabilizing Fab HUTS4, 2 µM extension-stabilizing Fab 8E3, or 10 µM closure-stabilizing Fab SG/19. Data were fit to Eq. S16. Error bars in the plots are s.d. of triplicates.

A
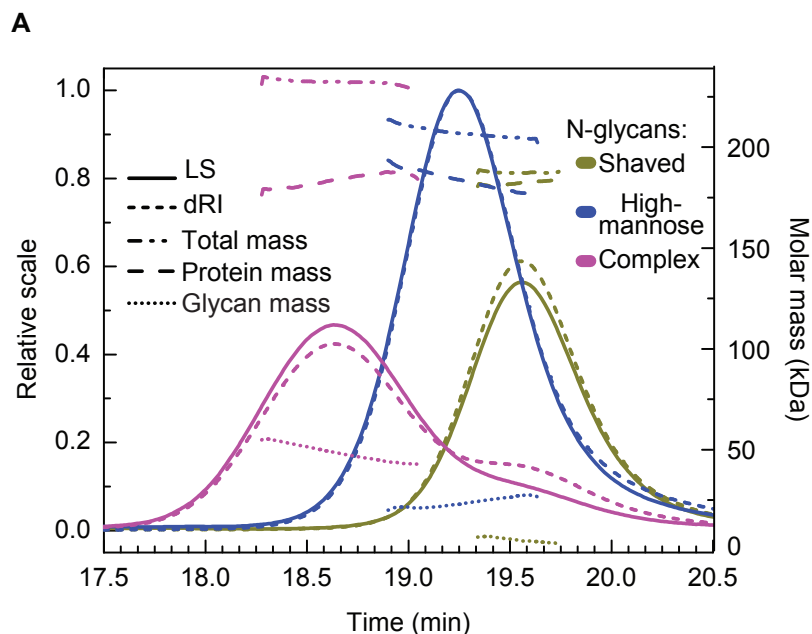
B Unclasped $\alpha_5\beta_1$ ectodomain
(protein molar mass from sequence: 184.7kDa)

	Complex N-glycan	High-mannose N-glycan	Shaved N-glycan
Total molar mass	232.2 kDa	207.2 kDa	187.5 kDa
Fitting error	(±0.236%)	(±0.245%)	(±0.196%)
Protein molar mass	183.6KDa	183.4kDa	182.2 kDa
Fitting error	(±0.235%)	(±0.246%)	(±0.196%)
Glycan molar mass	48.6 kDa	23.5kDa	5.0 kDa
Fitting error	(±1.199%)	(±2.105%)	(±8.283%)
Protein	79%	89%	97%
Glycan	21%	11%	3%

Fig. S5. Protein/carbohydrate composition of unclasped $\alpha_5\beta_1$ ectodomain with shaved, high-mannose and complex N-glycans.
(A) Gel filtration profile and molar mass analysis. Light scattering (LS) intensity and differential refractive index (dRI) were normalized to their maximum values. (B) Calculated protein, glycan, and total molar masses according to (A) using the protein conjugate model. Errors are fitting errors.

23

A Clasped complex N-glycan α$_5$β$_1$ ectodomain (5130 particles)
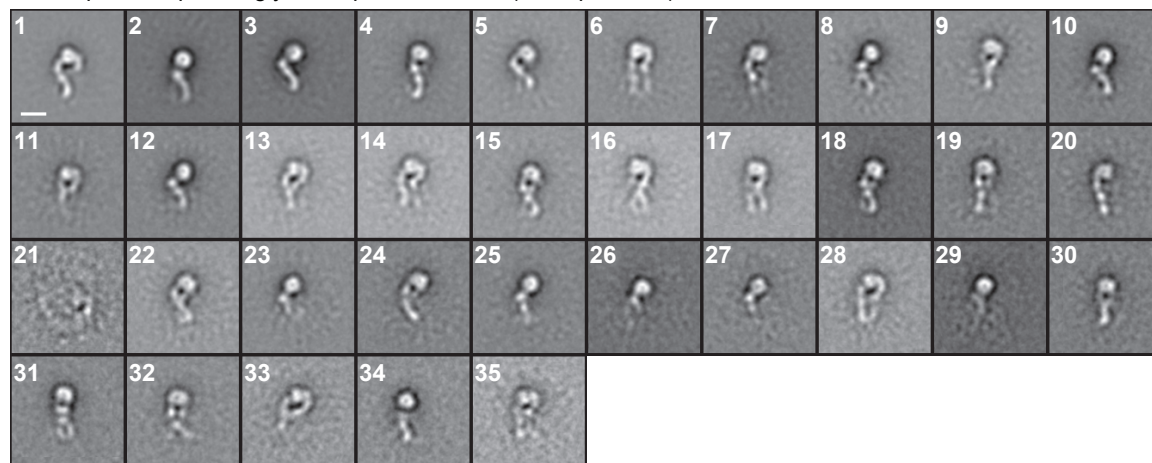
B Clasped shaved N-glycan α$_5$β$_1$ ectodomain (5185 particles)

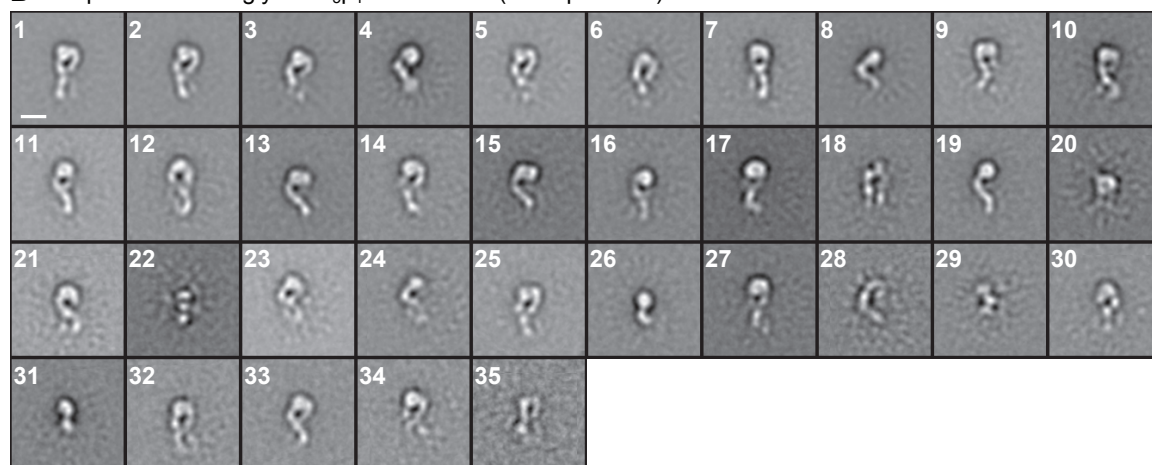## Fig. S6. EM of clasped α$_5$β$_1$ ectodomains.

All class averages of clasped α$_5$β$_1$ ectodomain with complex (A) and shaved (B) N-glycans. Scale bar is 10 nm.
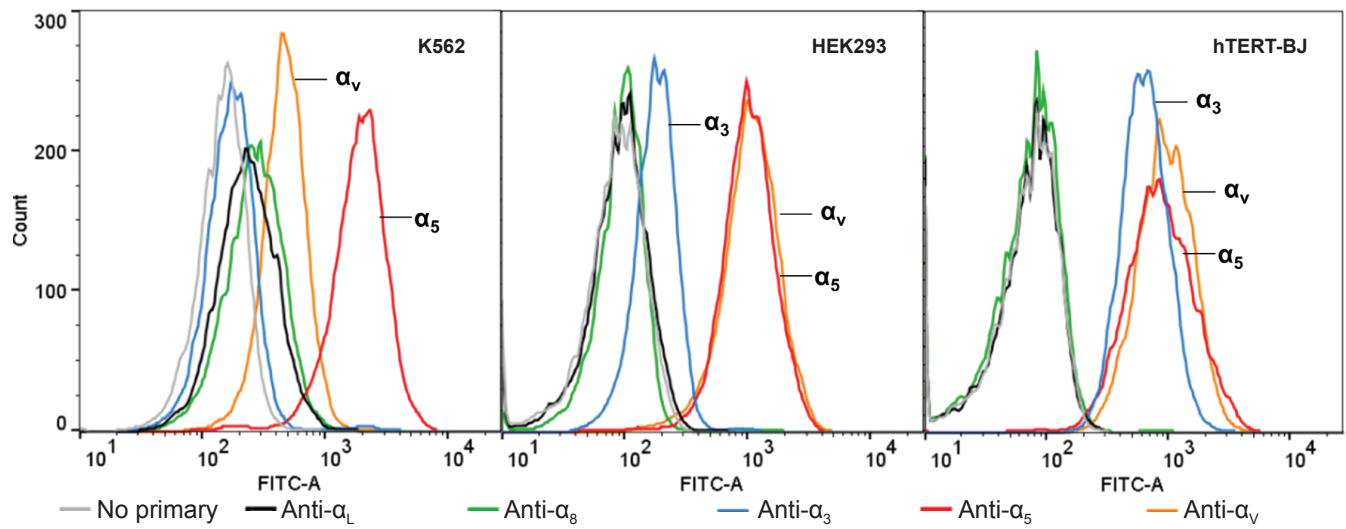
Fig. S7. Immuno-fluorescent staining of integrin α subunits on K562, HEK293 and hTERT-BJ cells analyzed by flow cytometry.

Cells were stained with 2.5 μg/mL primary antibody, followed by 2 μg/mL FITC-conjugated secondary antibody. Anti-α_L serves as negative control.
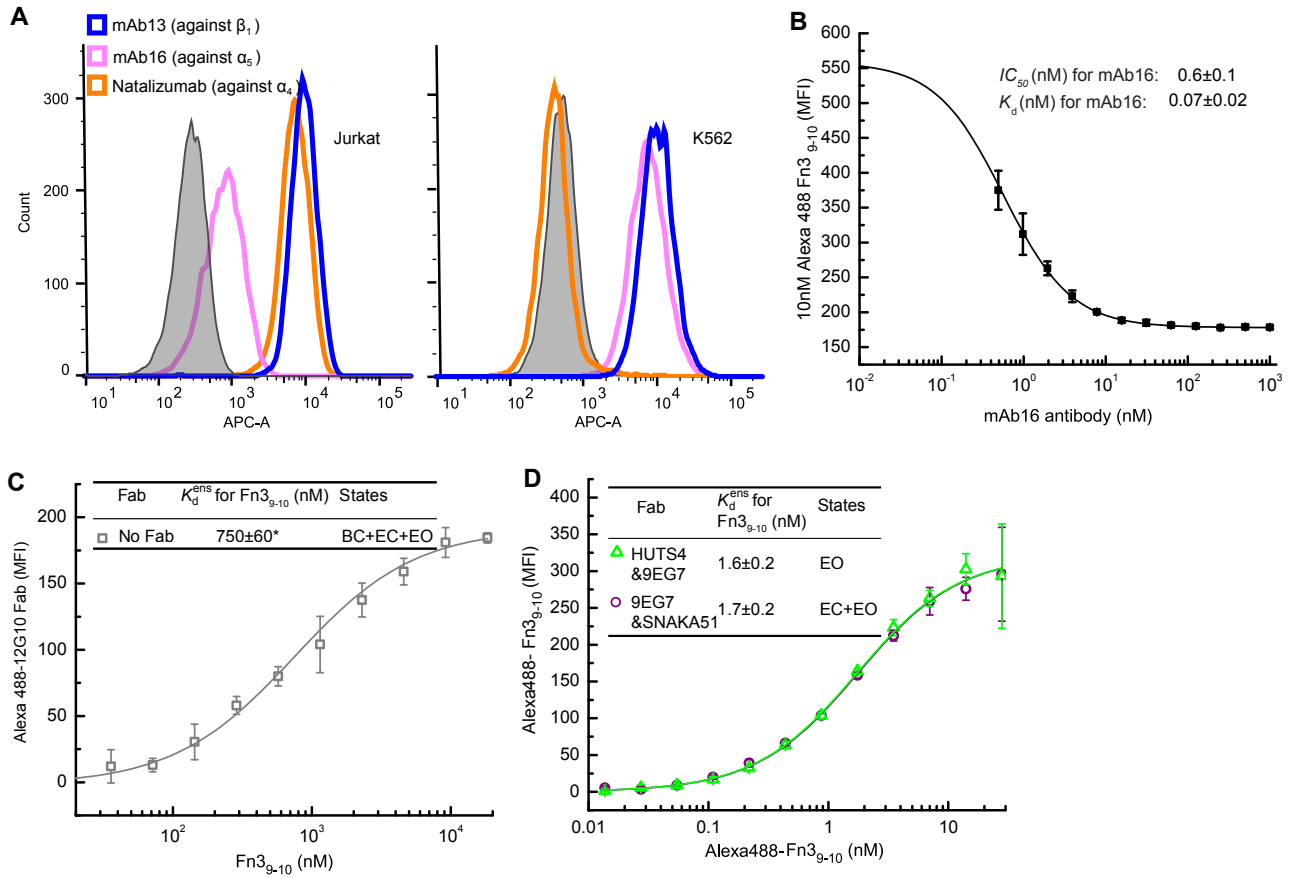
Fig. S8. Conformational equilibria and intrinsic affinity of intact $\alpha_5\beta_1$ on Jurkat cells.
(A) Immuno-fluorescent staining of integrin α_5, α_4 and β_1 subunits with Alexa647 labeled detection antibodies on Jurkat and K562 cells analyzed by flow cytometry. Anti-mouse IgG serves as negative control. (B) Affinities of mAb16, α_5-specific blocking antibody, for $\alpha_5\beta_1$. Binding of mAb16 to $\alpha_5\beta_1$ influenced binding of Alexa488-Fn$_{9-10}$ (10 nM) to $\alpha_5\beta_1$ on K562 cells under saturating open-stabilizing Fab 9EG7 and HUTS4 as monitored by FACS. IC_{50} value was fitted to Eq. S2, errors are fitting errors from triplicates. K_d values were obtained by $K_d = \dfrac{IC_{50}}{K_d^{\text{EO:Fn}_{9-10}} + 1}$, where $K_d^{\text{EO:Fn}_{9-10}} = 1.4$ nM as determined in Fig.7B. Errors in K_d are propagated from errors in IC_{50} and $K_d^{\text{EO:Fn}_{9-10}}$. (C)Affinity of $\alpha_5\beta_1$ on Jurkat cells for Fn$_{9-10}$ by enhancement of 0.4 nM Alexa488-12G10 Fab binding. (D) Affinity of $\alpha_5\beta_1$ on Jurkat cells for Alexa488-Fn$_{9-10}$ in presence of indicated Fabs.

Table S1. Fab EC_{50} or K_d values, concentrations used in ligand-binding affinity measurements ([Fab]$_{tot}$), and probabilities of Fab-bound $\alpha_5\beta_1$ states ($P^{\alpha_5\beta_1\cdot\text{Fab}}$).

	Fab Stabilized states	HUTS4 EO	12G10 EO	8E3 EC+EO	9EG7 EC+EO	N29 EC+EO	SNAKA51 EC+EO	SG/19 BC+EC	mAb13 BC+EC
high-mannose headpiece	EC_{50} (nM)	2800±600	28±3	4.3±4.2[1]				< 4.7[2]	< 2.3[2]
	[Fab]$_{tot}$ (nM)	unused	2000	20000	epitope not present			20000	20000
	$P^{\alpha_5\beta_1\cdot\text{Fab}}$ (%)		98.2	99.8				> 99.8	> 99.9
clasped complex N-glycan ectodomain	EC_{50} (nM)	34±4		15±3				5.4±1.3[3]	
	[Fab]$_{tot}$ (nM)	5000	unused	2000	unused	unused	unused	10000	unused
	$P^{\alpha_5\beta_1\cdot\text{Fab}}$ (%)	99.3		99.0				99.9	
unclasped complex N-glycan ectodomain	EC_{50} (nM)	< 34[4]		< 15[4]				6.9±1.6[3]	
	[Fab]$_{tot}$ (nM)	5000	unused	2000	unused	unused	unused	10000	unused
	$P^{\alpha_5\beta_1\cdot\text{Fab}}$ (%)	> 99.3		> 99.0				99.8	
clasped high-mannose ectodomain	EC_{50} (nM)	80±6		15±3				5.1±3.6[3]	
	[Fab]$_{tot}$ (nM)	5000	unused	2000	unused	unused	unused	10000	unused
	$P^{\alpha_5\beta_1\cdot\text{Fab}}$ (%)	98.3		99.0				99.9	
unclasped high-mannose ectodomain	EC_{50} (nM)	20±3	1.1±0.2	9±4	3.1±1.4	5.0±2.4	8.1±3.1	4.7±1.0[3]	2.3±1.0
	[Fab]$_{tot}$ (nM)	5000	1000	2000	2000	2000	2000	10000	15000
	$P^{\alpha_5\beta_1\cdot\text{Fab}}$ (%)	99.6	99.8	99.4	99.8	99.7	99.5	99.9	99.9
clasped shaved N-glycan ectodomain	EC_{50} (nM)	167±23		14±5				6.2±4.7[3]	
	[Fab]$_{tot}$ (nM)	5000	unused	2000	unused	unused	unused	10000	unused
	$P^{\alpha_5\beta_1\cdot\text{Fab}}$ (%)	96.4		99.1				99.9	
unclasped shaved N-glycan ectodomain	EC_{50} (nM)	49±6		6±5				2.5±1.4[3]	
	[Fab]$_{tot}$ (nM)	5000	unused	2000	unused	unused	unused	10000	unused
	$P^{\alpha_5\beta_1\cdot\text{Fab}}$ (%)	98.9		99.6				99.9	
intact $\alpha_5\beta_1$ on K562 cells	EC_{50} (nM)	2900±300	107±5		690±30				
	[Fab]$_{tot}$ (nM)	unused	2000	unused	13000	unused	unused	unused	unused
	$P^{\alpha_5\beta_1\cdot\text{Fab}}$ (%)		95.0		95.0				

	Fabs Stabilized states	HUTS4+9EG7 EO	Fn3$_{9–10}$+9EG7 EO	9EG7+SNAKA51 EC+EO	mAb13+9EG7 EC	SG/19+SNAKA51 EC
unclasped high-mannose ectodomain	EC_{50} (nM)	< 20			1.8±0.6[5]	3.0±0.7[5]
	[Fab]$_{tot}$ (nM)	5000+2000	unused	unused	15000+10000	15000+10000
	$P^{\alpha_5\beta_1\cdot\text{Fab}}$ (%)	> 99.6			99.9	99.9
intact $\alpha_5\beta_1$ on K562 cells	EC_{50} (nM)	21±2[6]	2.1±0.1[7]	< 690±30[8]		
	[Fab/Fn3$_{9–10}$]$_{tot}$ (nM)	2000+6000	2000+13000	13000+2000	unused	unused
	$P^{\alpha_5\beta_1\cdot\text{Fab}}$ (%)	99.0	99.9	> 95.0		

[1]K_d value determined by ITC (Fig. S3A).

[2]K_d and EC_{50} values are shown as lower than those determined for the unclasped high-mannose ectodomain; they must be so based on Eq. S33, because the ~100-fold lower basal affinity of the high-mannose headpiece compared to the unclasped high-mannose ectodomain (Fig. 3) demonstrates a higher proportion of the closed conformation in the headpiece ensemble than in the unclasped high-mannose ectodomain ensemble.

[3]K_d value determined for SG/19 in the presence of 100 nM $\alpha_5\beta_1$ ectodomain (Fig. S1).

[4]EC_{50} values are shown as lower than those determined for the clasped complex N-glycan ectodomain; they must be so based on Eq. S33, because the ~2-fold higher basal affinity of the unclasped complex N-glycan ectodomain compared to the clasped complex N-glycan ectodomain (Fig. 5B) demonstrates a higher proportion of the EO conformation in the unclasped complex N-glycan ectodomain ensemble than in the clasped complex N-glycan ectodomain ensemble.

[5]K_d value for mAb13 or SG/19, measured in the presence of 100 nM unclasped high-mannose $\alpha_5\beta_1$ ectodomain and 2000 nM 9EG7 or SNAKA51 (representative data in Fig. S1).

[6]Measured for HUTS4 in the presence of 6000 nM 9EG7 (Fig. 7A).

[7]K_d value is determined for Fn3$_{9–10}$ in the presence of 13000 nM 9EG7 on K562 cells (Fig. 7B).

[8]EC_{50} value for 9EG7 in the presence of its synergic Fab SNAKA51 (Su et al., 2016), inferred from 9EG7 Fab's EC_{50} value under basal condition.